

Use of the sub-structuring method in the analysis of vibrating structures with layered damping technologies



A thesis submitted to the University of Sheffield
for the degree of Doctor of Philosophy in the Faculty of Engineering

by

Ameer Tofan Shafiq Al-juboory

Supervisors

Dr. Jem Rongong

Dr. Charles Lord

Department of Mechanical Engineering

University of Sheffield

December 2020

Abstract

This research focuses on a composite constructed from a polymer matrix reinforced with stiff platelets. The platelets are relatively large and are located within the matrix in three layers, where individual platelets are staggered relative to those in adjacent layers. This composite is interesting because it combines the damping ability of the polymer with the rigidity created by the structured assembly of platelets. When loaded, the high difference in elastic modulus between the stiff platelets and soft polymer results in a zigzag strain field. This work presents an analytical model that can estimate the equivalent flexural modulus of the soft-stiff staggered system and evaluates the effectiveness of such a construction in reducing vibration.

The analytical model estimates the bending angle of a unit cell of the composite involving a region around the middle of the central platelets. The estimation is achieved by a method called the “Effective Bending Moment Method” (EBMM) which obtains the bending deflection from the contributions of parts through the cross section.

The suitability of the model is evaluated experimentally using a beam constructed from an epoxy matrix and reinforced using steel platelets. Predicted system loss factors and flexural modulus values are compared with results measured using free vibration and cyclic 3-point bend tests. Also, digital image correlation (DIC) is used to examine the real zigzag strain distribution through the cross-section during flexure and therefore to validate the assumptions made when developing the model.

The final part of the work considers the effectiveness of the staggered platelet composite in vibration reduction. A simplified model, representing the swing-modes of an automotive oil pan, is used to demonstrate the reductions in vibration level than can be achieved using the same epoxy-steel combination employed during the model validation stage.

Acknowledgement

First of all, I would like to express my sincere gratitude to my supervisor Dr. Jem Rongong for the continuous support of my PhD study and the related subjects, for his motivation, patience, guidance and immense knowledge. Besides my supervisor, I would like warmly to thank my second supervisor Dr. Charles Lord, for his encouragement and enthusiastic. My especially thank extended to my sponsor the Ministry of Higher Education and Scientific Research thanks are, for the cooperation and financial support. I also would like to thank the Mechanical Engineering Department – University of Sheffield, for providing the appropriate research work environment. Last but not least, I would like to thank my family: my son, lovely boy, Mohannad, for his future to be an intellectual man, and to my parents, brothers and sister for pursuing me during the study journey.

Publication from this work

[1] A.T. Al-juboory, J.A. Rongong, C.E Lord, Modelling of combined stiff-soft damping material using an effective bending moment method, in: PGEM. Conf., Imperial College, London, 16-17 Nov 2017.

Contents

Abstract.....	i
Acknowledgement.....	ii
Publication from this work.....	iii
Contents.....	iv
List of figures.....	vii
List of tables.....	x
Nomenclature.....	xi
Chapter 1 Introduction.....	1
1.1 Background.....	1
1.2 The staggered structure.....	2
1.3 Work motivation.....	2
1.4 Aims and objectives.....	3
1.5 Thesis layout.....	4
Chapter 2 Literature Review.....	5
2.1 Introduction.....	5
2.2 Equivalent properties of the composite structures.....	6
2.2.1 Equivalent properties of laminated beams under flexure.....	6
2.2.2 Platelet-based composites.....	10
2.2.3 Staggered composite materials.....	14
2.2.4 Zigzag strain behaviour.....	16
2.3 Modelling of a viscoelastically-damped structure.....	22
2.3.1 Viscoelastic layered damping.....	23
2.3.2 Flexural viscoelastic loss factor.....	27
2.3.3 Temperature and frequency dependence.....	34

2.3.4 Poisson’s ratio for polymeric materials.....	37
2.4 Summary.....	43
Chapter 3 Effective flexural rigidity for a staggered unit cell.....	46
3.1 Introduction.....	46
3.2 Dynamic analysis of unit cell.....	47
3.2.1 Analytical effective rigidity.....	47
3.2.2 Numerical model of the unit cell.....	50
3.3 Strain behaviour analysis.....	52
3.3.1 Normal strain analysis.....	53
3.3.2 Shear strain analysis.....	55
3.3.3 The forces flow mechanism.....	57
3.4 The Effective Bending Moment Method (EBMM).....	58
3.4.1 Bending angle mechanism.....	58
3.4.2 The analytical model.....	59
3.4.3 Numerical model.....	65
3.5 Conclusions.....	68
Chapter 4 Experimental studies of the staggered composite.....	69
4.1 Introduction.....	69
4.2 Methodology.....	70
4.3 Specimen manufacture.....	71
4.4 Three point bending test.....	76
4.5 Digital Image Correlation experiment (DIC).....	78
4.6 Free vibration test.....	82
4.7 Temperature and frequency dependency test.....	84
4.7.1 Methodology.....	85

4.7.2 The temperature domain.....	86
4.7.3 The frequency domain.....	86
4.7.4 The results of the experiment	86
4.8 DMA numerical simulation.....	92
4.8.1 Boundary conditions and loading.....	93
4.8.2 Simulation results	95
4.9 Comparison of analytical model with experiment	98
4.10 Conclusions	100
Chapter 5 Case study: vibration suppression of the swing mode of a fluid-filled tank...	101
5.1 Introduction	101
5.2 Selection of the tank structure for the study.....	103
5.3 Finite element model.....	103
5.4 Natural frequencies and mode shape.....	104
5.4.1 Boundary conditions.....	104
5.4.2 Numerical results.....	106
5.5 Harmonic response numerical analysis	107
5.6 FE results and discussion	110
5.7 Conclusions from the case study	111
Chapter 6 Conclusions and future work	112
6.1 Findings by chapter	112
6.2 Main conclusions of the research	113
6.3 Limitations of the work	114
6.4 Novelty.....	115
6.5 Recommendations for future work.....	115
Bibliography.....	117

List of figures

Figure 1.1: Configuration of the staggered composite	2
Figure 2.1: Symmetric layered sandwich composite [1]	6
Figure 2.2: Laminated unit cell composite	7
Figure 2.3: Kirchhoff hypothesis [3] (a) bimaterial beam (b) deformed element	7
Figure 2.4: Two laminated beam [6]	10
Figure 2.5: Voigt and Reuss model [8] (a) laminate Voigt (b) fibrous Voigt (c) laminate Reuss	11
Figure 2.6: Short fibre composite [9] (a) parallel pattern (b) staggered pattern	12
Figure 2.7: Platelets reinforced composites (a) circular platelets [10] (b) rectangular platelets [11]	12
Figure 2.8: Rectangular platelet reinforced composites materials [13]	13
Figure 2.9: Staggered steel platelets [15] (a) rectangular (b) circular (c) volume fraction	14
Figure 2.10: Discrete composite materials [17]	15
Figure 2.11: Staggered structure [19] (a) bone-like structures (b) load transfer path (c) tension region (d) stresses distribution on hard platelet	15
Figure 2.12: Collagen, parallel and staggered arrays [21]	16
Figure 2.13: Zigzag displacement development [25] (a) MZZF (b) MZZF into first order approach (c) MZZF into higher-order approach	18
Figure 2.14: Transverse displacement [29] (a) layerwise (b) equivalent single layer	19
Figure 2.15: The zigzag deformation corresponding function $u(i)$ [46]	21
Figure 2.16: Three layer flexural deformation [54]	23
Figure 2.17: Model with an ideal damper [80]	28

Figure 2.18: Comparison of ideal loss factor with the experimental(a) with frequency ratio [81] (b) with length-thickness ratio [82].....	29
Figure 2.19: Response spectrum (real part) [86]	30
Figure 2.20: Adhesively bonded double containment cantilever joint [88]	31
Figure 2.21: Thin plate viscoelastic joints [93]	32
Figure 2.22: Storage modulus with respect to the temperature [98]	34
Figure 2.23: Master curve of soybean oil with epoxy resin [99].....	35
Figure 2.24: Reduced frequency nomogram for Butyl Rubber [107]	37
Figure 2.25: Poisson's ratio time scales [109].....	38
Figure 2.26: First natural frequencies and loss factors with Poisson's ratio	39
Figure 2.27: Longitudinal deformation to the normal load [110]	40
Figure 2.28: Poisson's ratio from FEA for a large shape factor specimen [110] where $R=E^*/E$	40
Figure 2.29: The complex plane [115]	42
Figure 2.30: Extensometer setup for Poisson's ratio measurement [116].....	43
Figure 3.1: Staggered unit cell composite	47
Figure 3.2: Staggered composite (a) unit cell (b) assumed slices	48
Figure 3.3: Cantilever boundary conditions (a) first natural frequency versus modulus ratio (b) effective rigidity versus modulus ratio	50
Figure 3.4: Cantilever of staggered composite.....	51
Figure 3.5: Comparison of analytic and numerical result for (a) first natural frequency versus modulus ratio (b) effective rigidity versus modulus ratio	51
Figure 3.6: Analytical and numerical comparison (a) first natural frequency versus modulus ratio (b) effective rigidity versus modulus ratio	52

Figure 3.7: Strain behaviour (a) selected sections (b) modulus ratio 1 (c) modulus ratio 0.7 (d) modulus ratio 0.4 (e) modulus ratio 0.1 (f) modulus ratio 0.01.....	54
Figure 3.8: Shear strain behaviour (a) modulus ratio 0.4 (b) modulus ratio 0.1 (c) modulus ratio 0.01.....	55
Figure 3.9: Timoshenko shear strain behaviour (a) modulus ratio 0.4 (b) modulus ratio 0.1 (c) modulus ratio 0.01.....	56
Figure 3.10: Effective forces flow.....	57
Figure 3.11: Effective bending guide regions.....	58
Figure 3.12: Resultant bending angle mechanism (upper half of unit cell).....	59
where ε_p , ε_v , τ_{xy} and τ_t are, respectively, platelet strain, matrix strain, XY shear strain and Timoshenko shear strain.....	59
Figure 3.13: Diagram of unit cell deformation.....	60
Figure 4.1: Drawing of Specimen mould (a) aluminium elements (b) plastic straps.....	72
Figure 4.2: Steel upper holder drawing.....	73
Figure 4.3: The mould elements (a) platelets holder (b) mould (c) platelets into matrix.....	74
Figure 4.4: The casting (a) platelets-matrix (b) matrix (c) specimens.....	75
Figure 4.5: Three-point bending beam test (a) epoxy (b) platelets-epoxy (c) steel.....	76
Figure 4.6: Three point bending test (a) epoxy beam (b) steel beam specimens (c) platelets-epoxy beam.....	78
Figure 4.7: The painted and sprayed composite specimen.....	79
Figure 4.8: The monitored painted surface of specimen.....	79
Figure 4.9: Three point bending test (a) monitored composite region (b) Poisson;s ratio results.....	80
Figure 4.10: DIC normal strain result of three point bending test (a) at 2 mm deflection (b) at 4 mm deflection.....	81

Figure 4.11: Free vibration test (a) epoxy specimen (b) staggered epoxy-steel specimen	82
Figure 4.12: Frequency response function test (a) epoxy specimen (b) staggered epoxy-steel specimen.....	83
Figure 4.13: DMA specimens.....	84
Figure 4.14: Specimen test setup.....	85
Figure 4.15: Loss factor behaviour with respect to the temperature	87
Figure 4.16: Loss factor behaviour with respect to the frequency	88
Figure 4.17: Loss modulus behaviour with respect to the temperature.....	89
Figure 4.18: Loss modulus behaviour with respect to the frequency	90
Figure 4.19: Elastic modulus behaviour with respect to the temperature	91
Figure 4.20: Elastic modulus behaviour with respect to the temperature	92
Figure 4.21: FE design, (B and C) sinusoidal displacement edges (A) face fixed support	93
Figure 4.22: FE model (a) staggered model (b) dynamic three point bending deformation	94
Figure 4.23: FE model (a) FE design (b) dynamic deformation for face fixed support.	97
Figure 5.1: FE model for tank (a) undeformed model mesh (b) shape mode of the lateral swinging	105
Figure 5.2: Frequency-Amplitude response for the epoxy model (a) without fluid load (b) with fluid load.....	108
Figure 5.3: Frequency-Amplitude response for the staggered composite (a) without fluid load (b) with fluid load	108
Figure 5.4: Amplitude-Frequency response for the composite and homogeneous model (a) $T=25^{\circ}\text{C}$ without fluid load (b) $T=25^{\circ}\text{C}$ with fluid load (c) $T=40^{\circ}\text{C}$ without fluid load (d) $T=40^{\circ}\text{C}$ with fluid load	109

List of tables

Table 3.1: Materials properties	50
Table 3.2: Equivalent modulus of composite at $E_p=200$, $E_v=2$ GPa, $\rho_p=7850$ $\rho_v=950$ kg/m ³ , $\nu_p=0.3$	66
Table 3.3: Equivalent modulus of composite at $E_p=200$, $E_v=1$, GPa, $\rho_p=7850$ $\rho_v=950$ kg/m ³ , $\nu_p=0.3$	66
Table 3.4: Equivalent modulus of composite at $E_p=200$, $E_v=0.1$ GPa, $\rho_p=7850$ $\rho_v=950$ kg/m ³ , $\nu_p=0.3$	67
Table 4.1: Epoxy ingredient mass fraction.....	71
Table 4.2: Dimensions and density of specimens	77
Table 4.3: Modulus results for the epoxy-steel specimen from three point bend test....	77
Table 4.4: Flexural modulus results for epoxy-steel specimen	83
Table 4.5: Comparison of the dynamic reaction.....	95
Table 4.6: Comparison of the dynamic reaction.....	96
Table 4.7: Comparison of experimental and analytic equivalent modulus	99
Table 5.1: Natural frequency of tank swing	106

Nomenclature

A	Unit cell cross-section area
A_t	Timoshenko shear area
a	Amplitude
D	Formulated variable
dev	Standard deviation
c	Damping factor
E_p	Platelet elastic modulus
E_v	Matrix elastic modulus
E_e	Equivalent elastic modulus
E^*	Loss modulus
E_e	Effective modulus
E_r	Modulus ratio
EI	Rigidity
EI_p	Platelets rigidity
EI_v	Matrix rigidity
EI_e	Effective rigidity
f	Frequency
G	Shear modulus
G_v	Matrix shear modulus
H	Height of composite
h	Height of layer
h_e	Effective height
I	Second moment of area
k	System stiffness
k_e	Effective stiffness
k_t	Timoshenko shear coefficient

L	Length of unit cell
L_p	Length of platelets
M	Bending moment
M_p	Platelets bending moment
M_v	Matrix bending moment
M_z	Murakami zigzag function
m	mass
n	Number of results
N	Axial force
P	Normal force
Q_x	Shear force
r_p	Platelets volume fraction
r_v	Matrix volume fraction
R_x	local beam curvature
s	Matrix space
T	Temperature
t	Time
U	Strain energy
V	Potential energy
q	Layer number
W	Period damping energy
X, Y, Z	Cartesian coordinates
u, w	Local displacement
i	Accounting number
ε	Normal strain
ε_p	Platelets normal strain
ε_v	Matrix normal strain
ε_e	Effective normal strain

σ	Normal stress
σ_p	Platelets normal stress
σ_v	Matrix normal stress
τ	Shear stress
τ_{xy}	XY shear stress
τ_t	Timoshenko shear stress
γ	Shear strain angle
θ	Bending angle
ϕ	Phase angle
η	Loss factor
η_r	Damping ratio
ν	Poisson's ratio
ν_h	Homogeneous Poisson's ratio
ν_p	Platelet Poisson's ratio
ν_v	Matrix Poisson's ratio
ω	Frequency
ω_n	Natural frequency
λ	Dimensionless parameter
ζ	Damping ratio
δ	Bending deflection
ψ	Local section angle
ρ	Density
ρ_h	Homogeneous density
ρ_p	Platelet density
ρ_v	Matrix density

Chapter 1

Introduction

1.1 Background

The suppression of vibration through passive energy dissipation is widely used in the design of mechanical appliances and structures. Viscoelastic polymers are among the most widely used passive damping materials and are often incorporated into vibrating structures in the form of layered dampers to provide energy dissipation when subjected to flexural deformations. Viscoelasticity in polymers arises from the mobility of flexible segments of the molecular structure which provide fixing of temporary shape and recovery of permanent shape. This feature enables there to be a delayed response to dynamic loading, which causes energy dissipation. However, introducing viscoelastic materials into structures generally reduces their overall stiffness which is usually a critical design constraint.

Conventional mechanical devices, such as the components in cars and aircraft, should be optimised in terms of stiffness and damping. This is because the dynamic response is the principal factor affecting the design criteria such as improved reliability, extended life and reduced noise. This research deals with the design of a layered damping technology based on platelets to generate engineering structures that provide a compromise between energy dissipation and stiffness.

1.2 The staggered structure

This thesis focuses on a staggered structure where stiff platelets are embedded within a viscoelastic matrix, as shown in Figure 1.1. This composite combines the low modulus of a viscoelastic polymer with platelets made of a high modulus material such as steel. The strain is concentrated in the viscoelastic material during flexural deformation, especially between the ends of platelets.

One of the benefits of this composite is that it can be implemented as a plate or shell to control the dissipation of vibrational energy by concentrating strain in the viscoelastic matrix.

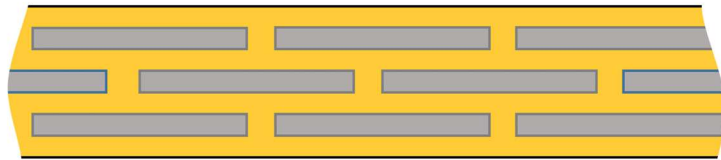


Figure 1.1: Configuration of the staggered composite

The challenge in this structure is that the configuration concentrates strain in the matrix which gives a zigzag distribution of strain through the thickness. Additionally, the flexural rigidity changes along the in-plane direction. To understand this composite, the equivalent flexural stiffness of the structure should be formulated accurately. The ability to describe this effective stiffness analytically is desirable in order to provide an insight into the parameters affecting the dynamic response.

1.3 Work motivation

The move towards lightweight components in machinery has increased their susceptibility to vibration. This is particularly severe in the components traditionally constructed from a metal plate. Designers can address this by reducing the plate thickness

and then applying vibration damping or replacing the metal components with polymer-based ones.

Polymers usually have adequate inherent damping but lack rigidity. Normal reinforcements such as the addition of long glass or carbon fibres transfers load to the reinforcement and reduces damping effectiveness. For damping metal plate subjected to flexural vibrations, layered dampers incorporating viscoelastic materials have been studied extensively. However, the use of layered dampers is still limited because of concerns about added mass, durability, simulation complexity and manufacturability. The embedded platelet approach that is considered in this work aims to address these problems by creating a reinforcement that can be incorporated locally within the host structure at the design stage. This avoids the need for low-durability damping materials and complicated retrofit procedures. Additionally, the use of segmented reinforcement greatly simplifies manufacturability as one of the limitations of full layer technologies such as a three-layer steel sheet, is that it cannot easily be pressed into shape.

The concept under consideration in this work is a segmented reinforcement that can be evaluated and deployed as a series of sub-structure units that retain the host material's inherent damping by transferring load through it. There is currently a lack of work that deals with such configurations subjected to flexural loading. As this is the most common deformation mode in lightweight structures, the value of research into this topic becomes clear.

1.4 Aims and objectives

This work aims to: a) examine the sub-structured composites constructed by reinforcing soft viscoelastic materials with layers of high stiffness platelets located in a staggered arrangement and b) formulate an analytical model that is suitable for analysing the dynamic characteristics of the composite when it is subjected to flexural vibrations.

The main objectives set in order to achieve these aims are defined below.

- Develop an analytic model that can represent the equivalent flexural behaviour of the composite.

- Compare the behaviour predicted by the analytic model with that obtained from finite element analysis.
- Compare predictions from modelling with experimental work, including behaviour at different temperatures.
- Investigate the performance of the sub-structured composite in a numerical study of a representative structure.

1.5 Thesis layout

This thesis is divided into six chapters, as described below.

Chapter 2 is a literature review which describes existing approaches for obtaining a) the equivalent mechanical properties of axially-loaded, staggered composites and b) flexural layered sandwich beams. The effects of temperature and frequency on the modulus and damping behaviour of the viscoelastic polymers is also discussed. A summary is provided at the end of this chapter to identify key knowledge gaps.

Chapter 3 introduces new analytical and numerical models that describe the zig-zag strain behaviour of a heterogeneous staggered unit cell. A comparison between the two approaches shows the validity of the assumptions made in the analytical model.

Chapter 4 deals with experimental work carried out to validate the models. This includes a static and dynamic response to loading, evaluation of local strains using digital image correlation and investigation of behaviour at different temperatures.

Chapter 5 reports a case study in which the suitability of the staggered composite is evaluated in a more realistic application – the construction of a tank (based on an engine oil pan) that contains a fluid whose sloshing generates significant dynamic loading on the structure.

Finally, Chapter 6 summarises the work, defines the novel contributions of this thesis and provides recommendations for future work.

Chapter 2

Literature Review

2.1 Introduction

This thesis focuses on the flexural vibration of a particular type of sub-structured composite: a viscoelastic polymer matrix reinforced with layers of stiff platelets. Such a composite can simultaneously provide high levels of flexural rigidity and damping if optimised appropriately for the relevant application. An important goal of this work is to develop an efficient model that describes the dynamic behaviour of this type of composite to enable theoretical design and optimisation studies to be conducted.

Models of composites often aim to find the properties of a homogeneous material that provides equivalent behaviour when subjected to particular loading conditions. The defining features of the type of composite considered in this work include the presence of viscoelastic and the abrupt and enormous change in the elastic modulus between the polymer matrix and platelets. Under load, these features generate a zigzag strain distribution through the thickness of the composite that is sensitive to temperature and the loading rate (or frequency). The literature review therefore concentrates on two main topics in the modelling of composite structures, namely:

- a) obtaining equivalent properties of layered and plate-reinforced systems
- b) representing viscoelastic behaviour in layered plates and beams.

2.2 Equivalent properties of the composite structures

Composites are widely used to combine the desirable properties of different materials. This section reviews the publications that have developed approaches to obtain equivalent properties for layered and plate-reinforced composites.

2.2.1 Equivalent properties of laminated beams under flexure

Many research papers have presented the concept of effective bending characteristics for the design of a multi-layered composite.

Gryzgoridis et al [1] introduced a simple direct approach to formulating the equivalent flexural rigidity of a symmetric sandwich composite, as shown in Figure 2.1. Noting that the layers deflect the same amount in flexure, they modelled the composite as a set of parallel springs. In this way, the equivalent rigidity was formulated as a sum of the core rigidity and sandwich plates as

$$EI_e = E_c I_c + 2E_f I_f \quad 2.1$$

where EI_e , $E_c I_c$ and $E_f I_f$ are the equivalent flexural rigidity, core rigidity and sandwich plate rigidity, respectively. This formula was validated numerically and experimentally under static and dynamic conditions for the following specimen dimensions: length 254 mm, core thickness 8.95 mm and face laminate 1.49 mm. However, this simple method was only used to obtain the properties of symmetric sandwich structures where the modulus of the core was close to that of the face plates.

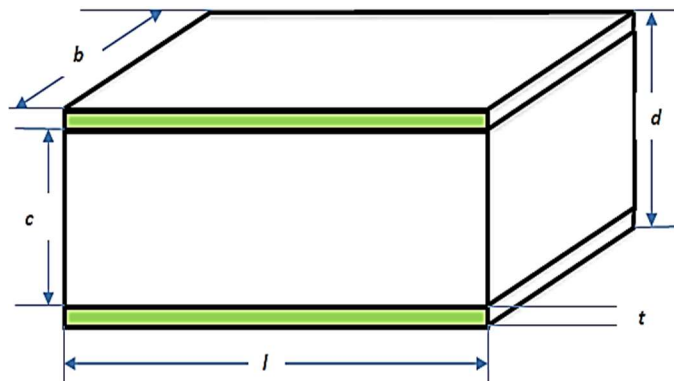


Figure 2.1: Symmetric layered sandwich composite [1]

Hajianmaleki and Qatu [2] presented a different model to account for the effect of shear force and element rotary inertia in order to estimate the equivalent stiffness and modulus of the thick laminated beams, as shown in Figure 2.2. They proposed two approaches: first, the beam Bernoulli equation and second, the matrices approach. This work mentioned that the effective modulus formulation can also involve the shear deformation effect for the laminated composite materials.

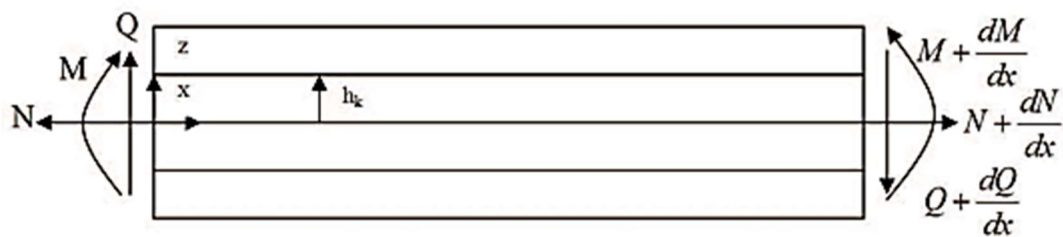


Figure 2.2: Laminated unit cell composite

where M , N and Q are the bending moment, axial force, and shear force respectively

As an additional development, Dominguez [3] used an analysis of the local displacement element during the bending deformation of a bimaterial beam, as shown in Figure 2.3a. He simplified an analytical model based on Kirchhoff's hypothesis, which was based on the assumption that the transverse section remains straight and perpendicular to the neutral axis during bending deformation, as shown in Figure 2.3b, to estimate the bending stiffness.

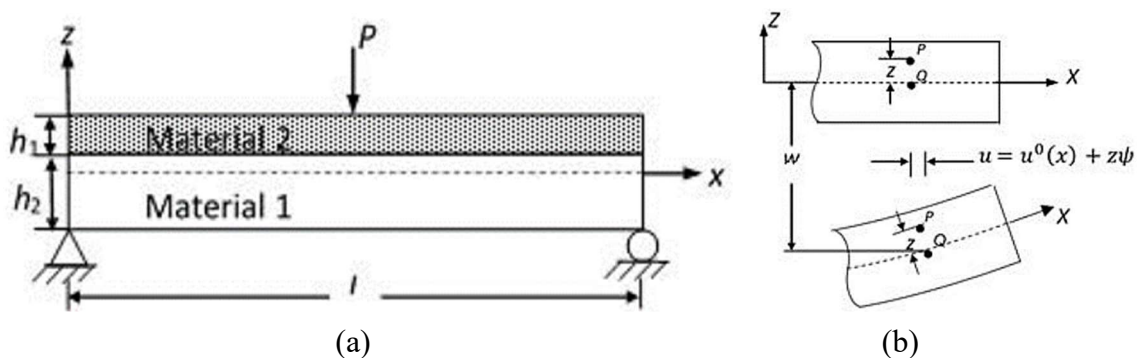


Figure 2.3: Kirchhoff hypothesis [3] (a) bimaterial beam (b) deformed element where u and w are, respectively, the local displacement in x and z axes, and ψ is the cross-section angle

The strain and stress through the thickness are given as

$$\varepsilon = \varepsilon_x^\circ + zR_x \quad 2.2$$

$$\sigma_{xi} = E_i \varepsilon_{xi} \quad 2.3$$

where ε°, i are the mid-plane strain and material number, and R_x is the local beam curvature given as,

$$R_x = \frac{d\psi}{dx} \quad 2.4$$

The net axial force and bending moment are defined as

$$N = \int_{-h/2}^{h/2} \sigma_x dz \quad 2.5$$

$$M = \int_{-h/2}^{h/2} \sigma_x z dz \quad 2.6$$

upon substituting Equation 2.2 into 2.3 into 2.5 and 2.6, the formulation becomes

$$N = A\varepsilon^\circ + BR_x \quad 2.7$$

$$M = B\varepsilon^\circ + DR_x \quad 2.8$$

where A , B , and D are the extensional, coupling and bending stiffness which can be simplified as

$$A = E_1 h_1 + E_2 h_2 \quad 2.9$$

$$B = \frac{1}{2} h_1 h_2 (E_2 - E_1) \quad 2.10$$

$$D = \frac{1}{12} [E_1 (h_1^3 + 3h_1 h_2^2) + E_2 (h_2^3 + 3h_1^2 h_2)] \quad 2.11$$

The finite element simulation conducted three-point bending to detect the flexural response of the bimaterial beam. The analytical results were validated using the

simulation results. Although he expanded the formulation to involve Kirchhoff's hypothesis, he also attempted to utilise this theorem in the laminated systems only.

Sayyad et al [4] developed the bending analysis of laminated composite using trigonometric shear deformation theory considering the effects of transverse shear and normal strain for the bending analysis of laminated composite beams. The displacement field equations of the theory were stated as,

$$u(x, z) = u_o(x) - z \frac{dw_o}{dx} + \frac{h}{\pi} \sin \frac{\pi z}{h} \alpha(x) \quad 2.12$$

$$w(x, z) = w_o(x) + \frac{h}{\pi} \cos \frac{\pi z}{h} \mu(x) \quad 2.13$$

where α and μ are the displacement field functions.

In this approach, the displacement behaviour allows the curvature strain distribution to vary through the composite thickness. However, the disadvantage of this theory was the assumption of the shear behaviour as a sine/cosine shape, which means that the behaviour could not predict shear deformation when the real values are not like the sine/cosine functions.

Vest and Darlow [5] studied a continuous system considering the mass and inertia elements used for evaluating equivalent beam stiffness, including the effects of transverse inertia and shear deformation. This analytical approach applied the Euler-Bernoulli beam equation to determine the bending stiffness while Lenci and Clementi [6] used Timoshenko kinematics and the lateral rotary inertia two-layer beam. The Timoshenko effect involves the shear deformation and rotational bending effects. This approach can describe the bending deformation behaviour of thick beams. Each layer was modelled by considering the axial and rotational inertia of the shear stiffness and normal interface stiffness, as shown in Figure 2.4. They observed that the natural frequencies were almost independent of the normal interface stiffness of the two-layer beam. In a subsequent publication, Lenci et al [7] addressed the free vibration of the non-uniform cables and beam. They used an asymptotic development method to achieve a simple formula to detect the natural frequencies.

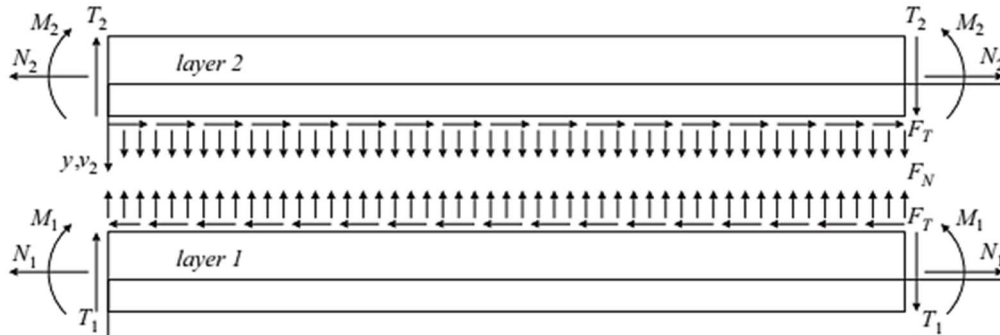


Figure 2.4: Two laminated beam [6]

As mentioned above, the laminated beams were modelled using various theories and approaches. However, the basic concept was to make the laminated beam as an equivalent beam with uniform properties. Although these theories and approaches targeted the laminated beam, the current work retains the basic idea that is to be applied in the staggered beam structure according to the deformation mechanism inside the unit cell. However, the approaches in this section can be adapted to estimate the local flexural modulus. Then, the effective flexural modulus can be calculated by parallel/series spring theory for the staggered unit cell.

2.2.2 Platelet-based composites

A number of different approaches have been used to obtain equivalent properties for composites comprising a flexible matrix reinforced with platelets. Some of the approaches have been described below.

Chen and Lakes [8] studied the parallel and series bending unit cells model, as shown in Figure 2.5, to evaluate the stiffness and loss factor of composite materials. They applied parallel bending relation to obtain the equivalent storage modulus as

$$E_e = r_p E_p + r_m E_m \quad 2.14$$

and series bending relation as

$$\frac{1}{E_e} = \frac{1}{r_p E_p} + \frac{1}{r_m E_m} \quad 2.15$$

where E_e , E_p , E_m , r_p and r_m are the equivalent storage modulus, platelet storage modulus, matrix storage modulus, platelet volume fraction and matrix volume fraction, respectively. They used the approximate models to define the upper and lower bounds of the resulting equivalent modulus. However, they introduced the equivalent properties for these composite system under tension deformation only.

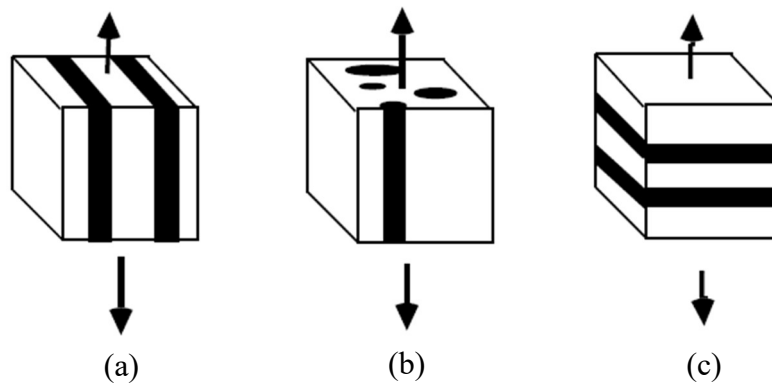


Figure 2.5: Voigt and Reuss model [8] (a) laminate Voigt (b) fibrous Voigt (c) laminate Reuss

Agarwal et al [9] used a numerical simulation to determine the equivalent mechanical properties for two short fibre arrangements parallel and staggered, as shown in Figure 2.6. They indicated the equivalent properties under axial load. The composite stress-strain behaviour was validated using experimental results. Here the composite system involved the staggered configuration, but they also introduced the equivalent properties under tension load.

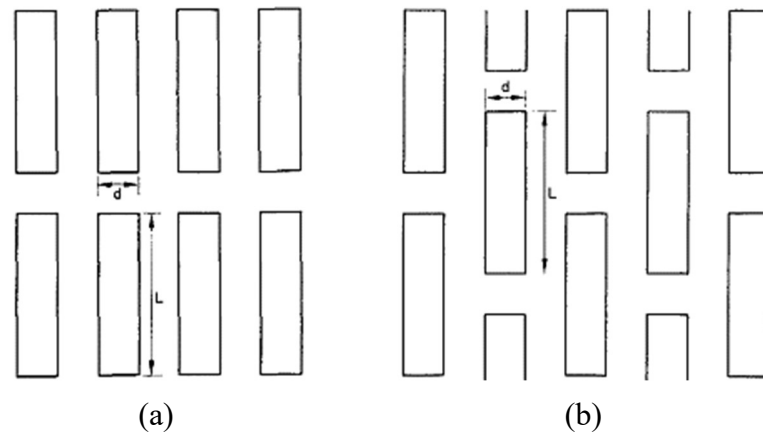


Figure 2.6: Short fibre composite [9] (a) parallel pattern (b) staggered pattern

Chou and Green [10] studied the two-dimensional stiffening of silicon carbide circular platelets reinforcing an alumina matrix, as shown in Figure 2.7a. They found that the predicted stiffness of the composite increases with the increase in the platelet volume fraction. Hsueh [11] created an analytical model for stress transfer in two dimensions for rectangular platelets bonded and debonded ends under tension load, as shown in Figure 2.7b. Hsueh et al [12] validated the previous analytical model using a numerical simulation.

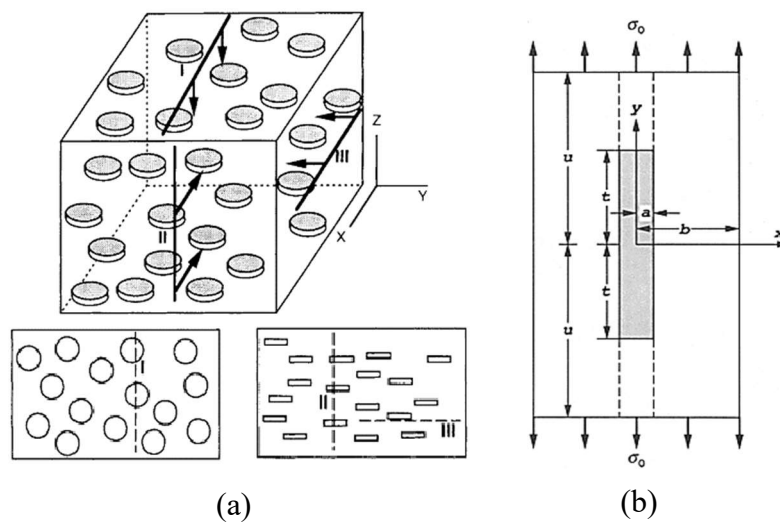


Figure 2.7: Platelets reinforced composites (a) circular platelets [10] (b) rectangular platelets [11]

Fattahi and Mondali [13] applied equilibrium forces under plane stresses, as shown in Figure 2.8, according to the Timoshenko and Goodier formula as,

$$\frac{\partial \sigma_x}{\partial x} + \frac{\partial \tau_{xy}}{\partial y} = 0 \quad 2.16$$

$$\frac{\partial \sigma_y}{\partial y} + \frac{\partial \tau_{xy}}{\partial x} = 0 \quad 2.17$$

They derived the displacement formulation for both matrix and platelets and validated it using finite element simulation. As a result, they estimated the displacement with respect to the normal stress for the parallel platelets reinforced matrix.

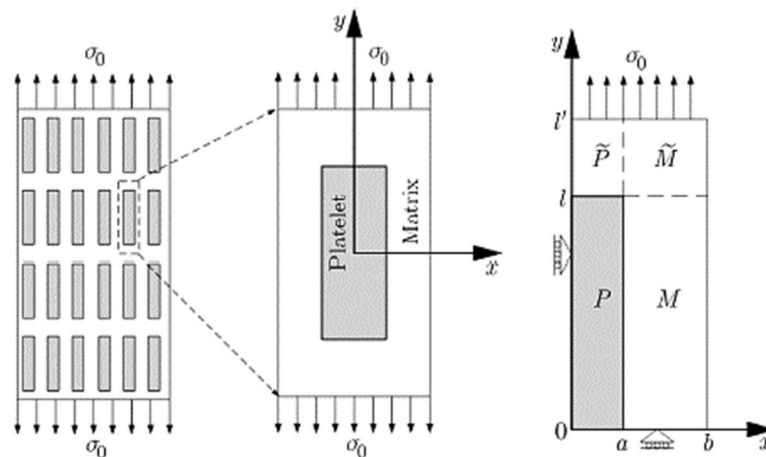


Figure 2.8: Rectangular platelet reinforced composites materials [13]

Regarding the platelets' orientation, Norris [14] derived an effective moduli formula for aligned and randomly oriented circular platelets within the matrix.

The above publications have considered platelet reinforcement of the matrix under tensile deformation in one-dimensional and two-dimensional configurations. In both cases, the stress transfer was analysed to determine the deformation mechanism for setting the equivalent properties of the composite. As a result, it is applicable for staggered systems under tension condition, not bending.

2.2.3 Staggered composite materials

The properties of a platelet-reinforced composite depend on the location and orientation of the platelets and if the platelets are of a similar length scale to the structure in question. This section discusses staggered arrangements.

Initially, Glavinchevski and Piggott in 1973 [15] tested staggered steel platelets embedded in polycarbonate under axial tension deformation. They used rectangular and circular platelets, as shown in Figure 2.9. The volume fraction approach was used to indicate the equivalent modulus improvement. The tensile test indicated an increase in strength, as shown in Figure 2.9c. Although this approach targeted the staggered composite using fraction ratio, the current work targets modulus ratio to address resultant bending angle for small value of modulus ratio.

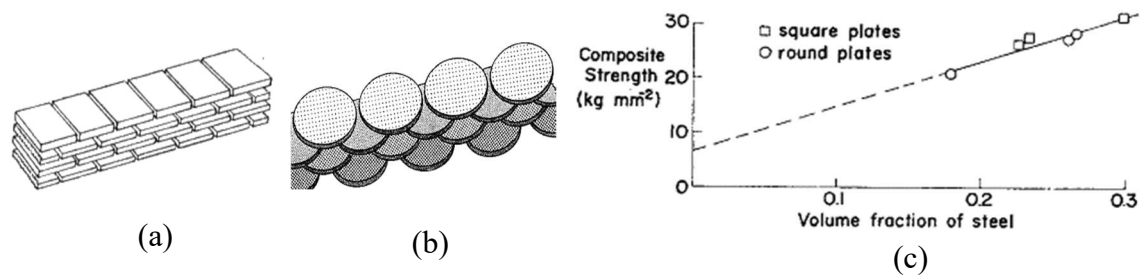


Figure 2.9: Staggered steel platelets [15] (a) rectangular (b) circular (c) volume fraction

Based on the Voigt and Reuss model, Brodt and Lakes [16] studied the stiffness-loss for laminated microstructure materials. Numerically, they explored the structure of the Voigt and Reuss unit cells. The study showed that Reuss's structure was more optimised than Voigt's regarding the characteristics of the damping response. However, the equivalent properties of the staggered composite under tension differed from the staggered under bending load.

Verbeek and Focke [17] predicted the equivalent Young's modulus of staggered composite materials, as shown in Figure 2.10, assuming that the load transferred to the platelets via a shear force. They considered a repetitive unit to represent the composite where the rectangular platelets aligned parallel to the applied force. The advantage of this prediction was that it depended on unit cell analysis. This advantage allowed the analysis

of the deformation and load for the sub-structured unit cell and application of the equivalent properties for the structure.

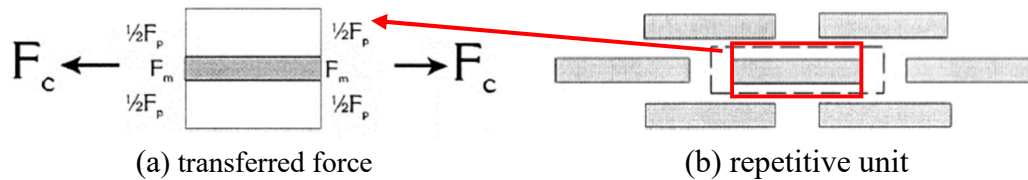


Figure 2.10: Discrete composite materials [17]

Kotha et al [18] analysed a staggered structure assuming an axial and shear stress transfer between the fibre and matrix based on shear-lag theory. He found that the reactions between the overlapped platelets result in a stress concentration at the centre of the platelets.

Zhang and To [19] expanded a theoretical analysis for a staggered unit cell in the hierarchical composite structure, as shown in Figure 2.11, based on strain in the matrix. As shown in Figure 2.11b, the soft matrix transfers the tension load to the platelet structure. This tension load results in a deformation concentration in the soft region between the platelets, as shown in Figure 2.11c. The shear deformation region occurred in the soft layer between the platelets, which results in peak tension stress in the middle of the platelets, as shown in Figure 2.11d. Although this analysis applied for tension load, it highlighted the importance of accounting for the strain concentrations between platelets.

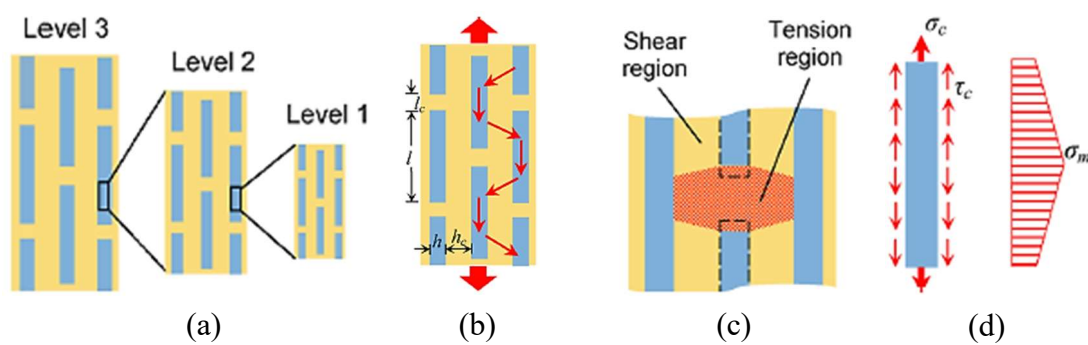


Figure 2.11: Staggered structure [19] (a) bone-like structures (b) load transfer path (c) tension region (d) stresses distribution on hard platelet

Upon observing the similarity of the platelet composites to biological materials, Lakes [20] presented a review article covering biological tissue with a small-scale microstructure hierarchy such as bone, bamboo, tendon and wood, and artificial staggered hierarchy composite materials. He found that the staggered hierarchy composite enhanced the damping of the composite. In the same area, Jager and Fartzl [21] compared parallel and staggered platelets, as shown in Figure 2.12. They used different layer thicknesses and lengths in both platelet configurations. It was found that the staggered arrays increased the modulus.

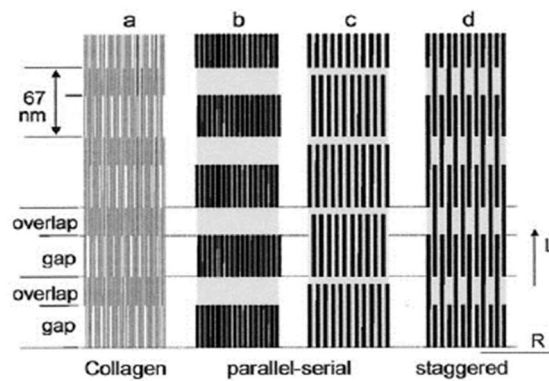


Figure 2.12: Collagen, parallel and staggered arrays [21]

While it is clear that the analysis of staggered platelet composites has been considered previously, in these studies, the loading has been applied uniformly. The models used would thus not be directly applicable for flexural loading where the force-deformation behaviour varies throughout the thickness of the structure.

2.2.4 Zigzag strain behaviour

The bending deformation of a laminated beam made from heterogeneous layers results in strain refraction across the composite thickness. The abrupt change in strain slope between the bonded adjacent layers generates zigzag displacement behaviour during bending deformation. Many studies have presented theories and approaches addressing the zigzag strain behaviour.

Carrera [22] presented a historical review of the zigzag theories developed to analyse multi-layered structures. The zigzag theory for a single equivalent layer was first analytically introduced by Lekhnitskii in 1935. He obtained the zigzag theory by addressing a layered cantilever beam problem. In 1958, Ambartsumian extended the zigzag theory to multi-layer plates and shells. Later in 1984, Reissner proposed a variational theory formulating both displacements and transverse stress assumptions. Based on these three historical theories, Murakami [23] was the first author who developed the Reissner-Mindlin refinement approach to enable shear deformation analysis through the laminated composite thickness.

Murakami presented a formulation named “Murakami Zig Zag Function” (MZZF), as shown in Figure 2.13a, describing the zigzag displacement profile as,

$$M_z(z_i) = (-1)^i \frac{z_i}{2h_i} \quad 2.18$$

where M_z , z , h and i are MZZF, coordinate through the local layer axis, local layer thickness and layer number, respectively. Toledano and Murakami [24] developed the MZZF based on a high-order polynomial incorporating the zigzag function, as shown in Figure 2.13b. Next, Carrera [25] investigated the previous work using a numerical simulation. He designed simulation models to evaluate the first-order through to fourth-order incorporating MZZF, as shown in Figure 2.13c, under both static and dynamic conditions. The simulation evaluation revealed that the developed higher-order zigzag enhanced the accuracy of the results. Kant and Swaminathan [26] also applied a higher-order approach using shear and normal stress across the multi-layer thickness.

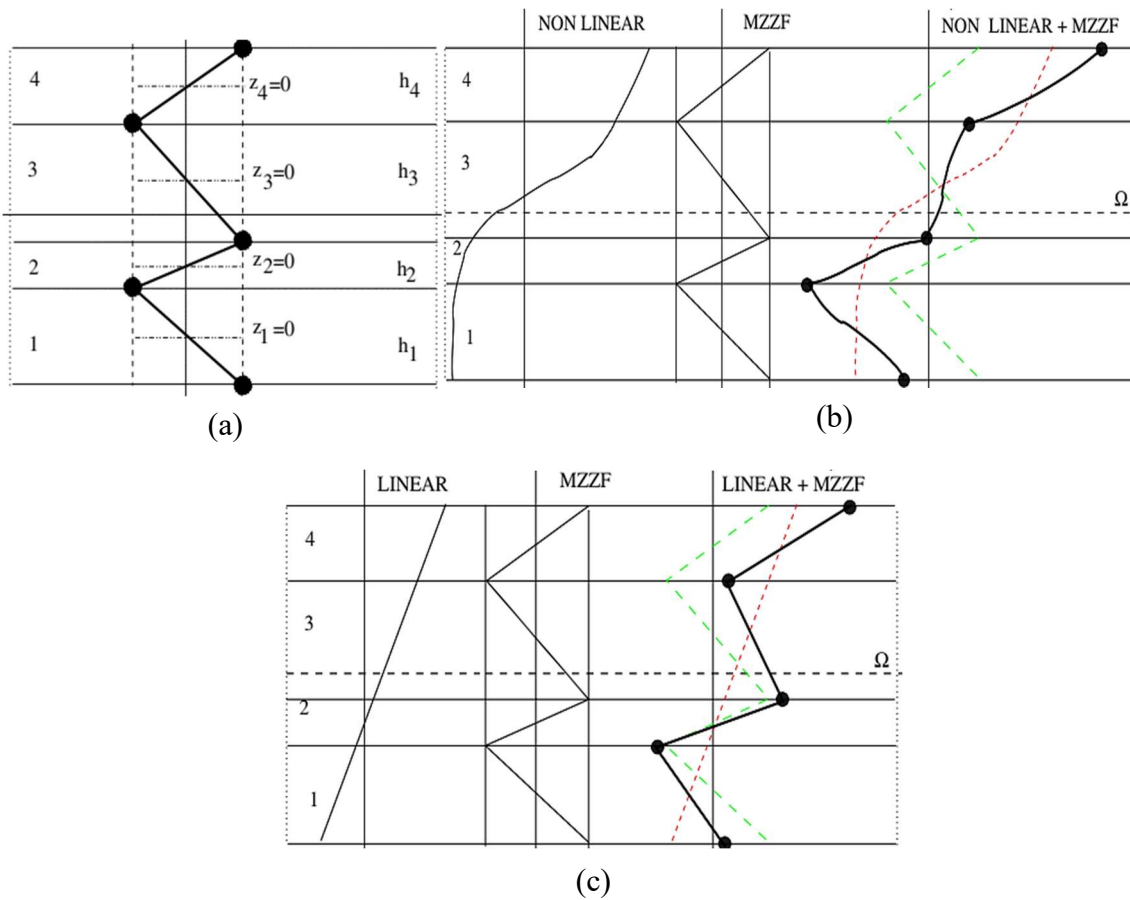


Figure 2.13: Zigzag displacement development [25] (a) MZZF (b) MZZF into first order approach (c) MZZF into higher-order approach

Vidal and Polit [27] improved the analytical model using MZZF in a sinusoidal strain function through the thickness. This model used a confirmed FE approach using Lagrange and Hermite interpolations. They aimed to examine the influence of a zigzag function in the sinusoidal model in both static and vibration conditions. Mechanical tests for thin/thick laminated and sandwich beams validated the FE model in order to evaluate the capability of the finite element. The results were compared with elasticity or finite element reference solutions. Their finite element model was shown to yield satisfactory results at a low computational cost.

Demasi introduced a unified formulation of laminated beams in a series of publications. First [28], he formulated governing equations independently addressing the displacement

variables and out-of-plane stresses. These equations freely enable the displacements and stresses. Second [29], based on the governing equations, the composite multi-layered structure was unified to become one equivalent layer, as shown in Figure 2.14. The generated layer matrices from the fundamentals were assembled.

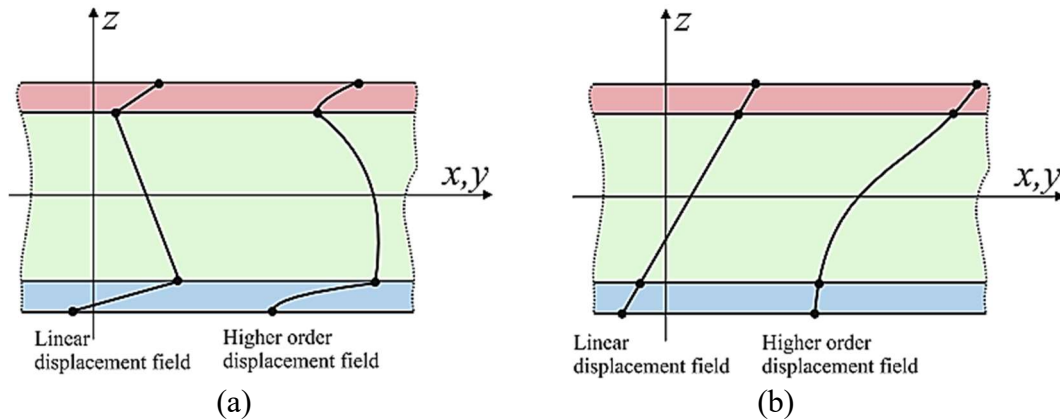


Figure 2.14: Transverse displacement [29] (a) layerwise (b) equivalent single layer

Third [30], the unified layer allowed for the compatibility of the displacements and equilibrium between the layers. This part made the generation of the unified layer effective and easy, in addition to the same for implementing the laminated beam. Fourth [31], in this part, the unified formulation was applied to the higher-order Murakami's zigzag function [24]. Finally, Santarpia and Demasi [32] modified Murakami's zigzag function for a thick laminated beam. They formulated a combination of displacement behaviour and transverse stresses along the thickness.

As mentioned above, The MZZF was established and improved mathematically. It can solve the zigzag which has opposite by opposite line along the element thickness. However, the MZZF cannot describe the zigzag behaviour having multiple slopes.

Departing from equivalent single-layer model theories, layer-wise theories are represented by a set of bonded interlaminar layers. These theories enable the interlaminar stress continuity conditions and the modelling of the zigzag displacement through a laminated composite thickness

Icadri and Urraci [33] adapted the zigzag theory addressing the normal deformability and transverse shear. The results showed that the fixed kinematic theories were often

more accurate than a layer function approach. As an additional improvement, Icardi and Urraci [34] developed the previous work by generalising the zigzag theory from an arbitrary representation to simplification in order to determine the transverse shear and normal deformation effects on a soft sandwiched core. Icardi [35] modified a zigzag approach to analyse a thick composite beam. He used a third-order layer-wise function for in-plane displacement and fourth-order for transverse displacement for gradient continues at the layers contact faces.

Kapurja et al [36] introduced an analytical formulation for a one-dimensional zigzag theory of laminated beams. They assessed the theory using two-dimensional elasticity solutions for a simply supported beam under a static load and harmonic transverse load. They evaluated the effect of the thickness-length ratio on the accuracy of the results. The observed zigzag theory solutions were more accurate than the shear deformation theories.

Di Sciuva [37] proposed an analytical approach using a zigzag displacement field with shear deformation effects in a multi-layer plate. This zigzag displacement behaviour enhanced the layer-wise linear distribution across the thickness and allowed the transverse shearing stresses to be accountable. The analytical approach was validated using numerical tests for the bending, buckling and vibration of a simple supported three-layer square plate. Numerically, Averill [38] used a two-node finite element based on the zigzag laminate approach of DiSciuva [37]. He improved the element accuracy using interdependent element interpolation in thin and thick laminated plates. Averill and Yip [39] developed a high-order zigzag to enable a finite element model for thick beams and a laminated composite. The element included a single zigzag sub-laminate to accurately formulate the bending and transverse shear kinematics in thick laminates.

Coda et al [40] proposed an approach enhancing the transverse strain behaviour for the plates without introducing new degrees of freedom for modelling the zigzag displacement behaviour in thick plates. This approach enhanced the possibility of solving the extreme geometric nonlinear problem of orthotropic laminated shells, considering the results in terms of displacements and stresses.

The research discussed above has dealt with the incorporation of the deformation of the laminated beams in different material layers, depending on the MZZF, as shown in Equation 2.18. The aim is to allow the zigzag strain behaviour due to the change in slope

at the interlaminar continuity point of transverse stresses at each layer interface. The incorporation of the MZZF can describe the single equivalent layer strain behaviour mathematically, but it cannot determine the resultant bending angle of the different local layer angles.

Later, a study of the zigzag theories revealed some finite element implementation problems. To solve these problems, many studies have developed a new Refined Zigzag Theory (RZT) to make it amenable for finite element implementation.

Tessler et al [41], [42] determined the RZT by refining the concepts of Timoshenko, Di Sciuva, and Averill. The key points of this work were first that the assumed zigzag function vanished at the top and bottom surfaces of the composite beam. Second, the theory requires only continuous kinematics for finite element modelling where these elements are based on the theories of Timoshenko [43], Mindlin [44], and Reissner [45]. This work improved the computational efficiency for beams, plates, and finite shell elements.

Tessler et al [46] applied RZT to sandwiched beams under kinematic Timoshenko Beam Theory. This theory was formulated for the zero displacement boundary conditions at the top and bottom surfaces, as shown in Figure 2.15. They compared the refined theory with the finite element analysis and found a high level of correlation.

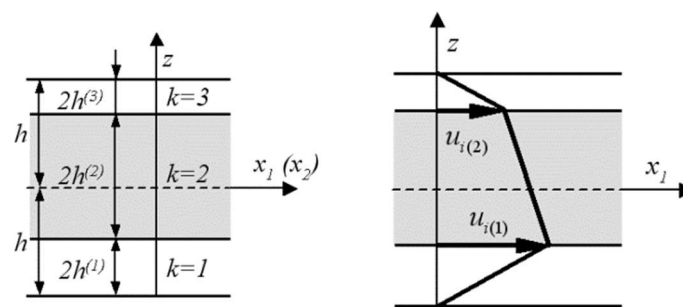


Figure 2.15: The zigzag deformation corresponding function $u(i)$ [46]

Next, Tessler et al [47] improved the previous zigzag theory. This work was devoid of shear force inconsistency when the force result does not correspond to the integral transverse shear stress. Tessler et al [48] also developed RZT for a sandwiched beam

based on a superposition multi-scale formulation of displacement expression. He then derived four zigzag functions using the condition of the homogenous transverse shear properties. Pagani et al [49] also used refined theory analysis but for only one-dimensional laminated beams to detect the global and local mechanical behaviours. Numerically, they applied the hierarchal refined model to the symmetric, antisymmetric, eight-layer, single-cell and multi-cell beams. According to the obtained results, the local behaviour of a single layer was represented accurately.

Iurlaro et al [50] formulated a third-order RZT for sandwiched and multi-layered beams. They modelled a continuous element using an isoparametric interpolation that adopted the formulation of nine nodes/fifteen degrees of freedom element to reduce the computational work.

Patni et al [51] employed equivalent single-layer models. Computationally, this approach implemented Murakami's zigzag function and RZT for the constant stiffness of the sandwiched beams. They achieved accurate gains in terms of computational efficiency through a three-dimensional finite element using the equivalent single-layer approach with RZT functions.

Numerically, Versino et al [52] developed the RZT using a zero-order function with three-nodes and six-nodes. They assessed the new element using laminated and sandwiched plates with simply supported and cantilever boundary conditions. This work targeted a balance between accuracy and computational efficiency.

In most of the above analyses of RZT, the approaches targeted the simplification of the finite element calculations to adapt the global and local relations to the heterogeneous laminated structure. However, RZT does not deal with real zigzag phenomena when it comes to evaluating the equivalent mechanical properties. In addition, RZT does not deal with the effective bending angle along the zigzag strain.

2.3 Modelling of a viscoelastically-damped structure

Viscoelastic materials dissipate vibrational energy as heat when subjected to cyclic strain. Viscoelasticity involves a combination of elastic and viscous effects. Therefore

under cyclic loading, significant frequency dependence can be observed. As the viscoelastic materials used in damping are typically polymers, the temperature-frequency superposition principle holds and therefore the temperature dependence is also significant.

Viscoelastic materials have been used for many years as vibration dampers and information about the fundamental considerations is available in textbooks such as those by Nashif [53]. This review focuses on two specific areas in the literature about viscoelastic materials. These particular areas are sandwiched viscoelastic layer dampers and Poisson's ratio for viscoelastic polymers.

2.3.1 Viscoelastic layered damping

There have been many studies conducted looking into the flexural vibration of beams that are damped using constrained layers of viscoelastic polymers. Initially, in 1959, Ross, Kerwin and Ungar (RKU) [54] presented an analytical method used to compute the effective flexural rigidity and damping loss factor for three-layered beams in which the central "constrained" layer is viscoelastic. The damping mechanism based on the shear and tension deformation in the viscoelastic core is shown in Figure 2.16. This work addressed the flexural viscoelastic shear and tension deformation in order to formulate the equivalent rigidity, loss factor and natural frequency.

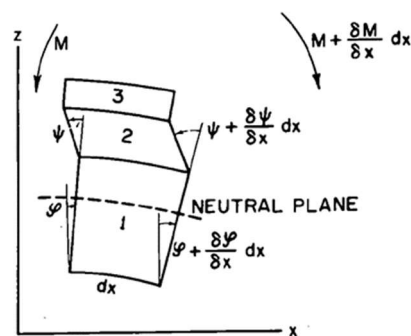


Figure 2.16: Three layer flexural deformation [54]

Bateman [55] extended the RKU equations for a five-layer laminated beam, base layer and double constraining layers. The RKU equations computed the stiffness of the three layers as one equivalent layer. The RKU equations were then used again to calculate

the loss factor for the entire composite. This design presented a higher loss factor for damping than the familiar three-layer beam. Runyon [56] extended the analysis to investigate the effectiveness of RKU for beams and plates. He investigated the effectiveness of extended RKU for a cantilever and clamped-clamped boundary conditions and aspect ratio in addition to different layered thickness.

Nakanishi [57] improved sound isolation using laminated plates. It was shown that the RKU model estimated the transmission loss using the treated homogeneous laminated panels. In this work, the contact faces between the layers were considered to be a thin layer equivalent to the friction effect. The RKU equations were applied by considering the assumed frictional thin layer as a viscoelastic layer.

Torvik and Runyon [58] validated an approximate analytical approach to determine the frequencies and loss factors of rectangular constrained plates. They applied the RKU analysis to predict the loss factors for the beams with simply supported ends and other options. Sasikumar [59] tested the effect of constrained layer stiffness on the damping of beam structures. The results showed that the loss factor increased due to the higher stiffness of the constrained layer. Huang et al [60] investigated the thickness of the constrained viscoelastic material. They detected that the viscoelastic layer thickness can improve the loss factor.

Marsh [61] developed a viscoelastic damping system for balancing the stiffness of a structure. The RKU equation was used to optimise the thickness of the base, viscoelastic and constrained layers to achieve the maximum system loss factor without compromising the stiffness of the structure.

Belbute [62] applied an analytic approach to the sandwich beams under bending deformation. He used Higher-Order Shear Deformation Theory to represent the viscoelastic displacement and a First-Order Shear Deformation Theory to represent the face layers. He found that the shear theories results were close to the finite element simulation results.

Di Taranto [63] showed that a beam with a constrained layer damping needs a sixth-order differential equation. Mead and Markus [64] derived a sixth-order equation of

motion in terms of the displacements of a beam with a single constrained layer damping under different conditions. Next, Mead and Markus [65] provided exact solutions for a clamped-clamped beam. Additional improvements were provided by Rao [66] who developed a sixth-order model by applying Hamilton's principle to the system energies. A comparative finite element simulation validated the sandwich beam model under clamped-clamped, free-free, simply-supported, clamped-pinned, and cantilever boundary conditions. Although the Higher-Order Shear Deformation Theory dealt with polynomial shear behaviour in a different order, this approach cannot deal with zigzag behaviour, whether shear or normal strain.

Regarding the discontinuous system, Uppal [67] characterised the structural damping of the discontinuous surface treatment under different excitations. This treatment optimised the surface usage experimentally. The analysis was based on DiTaranto to extend the RKU equations. They noted that the discontinuous surface increased the energy dissipation.

Lifshitz and Leibowitz [68] designed a computational program to optimise the dimensions of sandwich beams for maximising the damping. This programme covered an extended variety of boundary conditions. They applied the programme to two design concepts to introduce a computational tool for improving the damping. Hamdaoui et al [69] also applied the optimal design to reduce the noise and vibrations using viscoelastic materials. Also, as a staggered composite, the dimensions optimisation can be used to improve the damping.

Kumar et al [70] improved the loss factor of a viscoelastic damper plate and validated it using the finite element method based on the cantilever boundary conditions. Power series expanding was used to express the loss factor and Young's modulus in the finite element using an iterative method. They used harmonic analysis to calculate the loss factor and natural frequencies under different boundary conditions and in the various dimensions of the constrained layer thicknesses. The results showed that the loss factor was increased as the shear force increased in the higher mode.

Rao and Nakra [71] analysed the passive viscoelastic damping of unsymmetrical sandwich plates and beams. This study also included the effect of transverse inertia and

longitudinal, translatory and rotary inertia. Rao [72] also studied three forms of passive viscoelastic damping to use in the aerospace and automotive industry. He used the viscoelastic damper, constrained layer treatment and free layer damping treatment. The results of the constrained layer showed a maximum shear deformation. This work covered the temperature and frequency effects that were found to be suitable for the passive damping requirements. He concluded that the damping variation with temperature and frequency is very important in the aerospace and automotive industry.

Lewandowski et al [73] applied Maxwell and Kelvin's models, the complex modulus model, and the fractional-derivative Kelvin model for viscoelastic dampers. They used finite element analysis to derive the equation of motion and energy dissipation. Models were presented to compare the frequency as a solution for the eigenvalue. The results agree with the dynamic characteristics of the viscoelastic damper of the presented frame. This work of the damping application was to improve the damping in outlet vane using the internal viscoelastic fillers. Syed et al [74] investigated the effect of damping material thickness on the vibration of the gearbox cover. They concluded that the thickness of the damping materials is the main factor in reducing the gearbox noise. This work mentioned that the constrained layer damping thickness changes the behaviour of the damping itself. Concerning a 2D model, it can be used as it has a minimal computational time and storage needs. Cortes and Elejabarrieta [75] investigated the dynamic behaviour of a thick viscoelastic layer with free damping beams. They formulated the stiffness to be applicable in each layer. This work showed that the thick model presented accurate results, and it can be used in applications to describe the free layer damping beam. The low order vibration mode was studied by Nayfeh [76] to induce the damping of an elastic-viscoelastic sandwich beam vibration. This model showed that the damping depends on the stiffness to mass ratio of the base layer. He used a sandwiched cantilever beam. This composite produced high damping.

Meaud et al [77] investigated the loss factor and effective dynamic modulus of the parallel layers loaded in an arbitrary direction. The finite element model analysed the constrained and free parallel layer. The models showed that the behaviour softened in compression while stiffening under tension. They created a strain formula for the composite material. This formulation was compromised of the stiffness and loss factor combination.

Although the above studies estimated the frequencies and loss factor of the constrained damped beams, there were only a limited number of studies on the influence of segmented damped beams as presented in this section. Therefore, this thesis targeted the segmented multilayers beam to estimate the natural frequency and loss factor.

2.3.2 Flexural viscoelastic loss factor

For a structure subjected to periodic loading, the loss factor is defined as the ratio of the average energy dissipated per radian to the maximum energy stored [54]. This parameter was used widely in damping investigations. It can be obtained experimentally. Many researchers have investigated the loss factor using different experimental methods and mathematical expressions. Grootenhuis [78] optimised the loss factor for the bending of laminated beam made from three, four and five layers by comparing a resonance magnification factor. In this study, different thicknesses for the viscoelastic cores and plates were used. Regarding non-metallic materials, he used the force-displacement equation to express the hysteresis diagram based on the observation of the phase angle and energy dissipation per cycle under a harmonic load. This work also introduced a resonance magnification to measure the loss factor. Carfagni et al [79] introduced an experimental work to find and express the loss factor. They classified the loss factor measurement according to the oscillation, inertia, resonance method, and the direct measurement of stress and strain. Moreover, the work revealed an analysis of the hysteresis loop diagram in order to recognise the loss factor when the value is less than 0.1.

Crandall [80] compared the actual cantilever loss factor with the ideal loss factor due to the damping coefficient of the ideal dashpot in a single degree of freedom damped forced vibration, as shown in Figure 2.17. For the ideal case, the energy dissipation over one cycle is given by,

$$W = \int_0^{\pi/\omega} \left(c \frac{dx}{dt} \right) \frac{dx}{dt} dt = \pi c a^2 |\omega| \quad 2.19$$

The maximum potential energy as,

$$V = \frac{1}{2}Ka^2 \quad 2.20$$

The loss factor of the ideal damper as,

$$\eta = \frac{c|\omega|}{K} \quad 2.21$$

where W , V , K and a is the period damping energy, maximum potential energy, spring stiffness and amplitude, respectively.

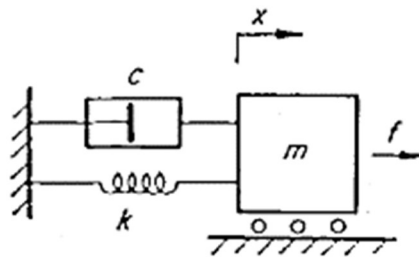


Figure 2.17: Model with an ideal damper [80]

He indicated that the ideal loss factor was close to the experimental loss factor which was adopted from Heine [81] with respect to the natural frequency domain as shown in Figure 2.18a as well as with respect to the length-thickness ratio domain adopted from Baker et al [82] as shown in Figure 2.18b for aluminium alloy 2024-T4.

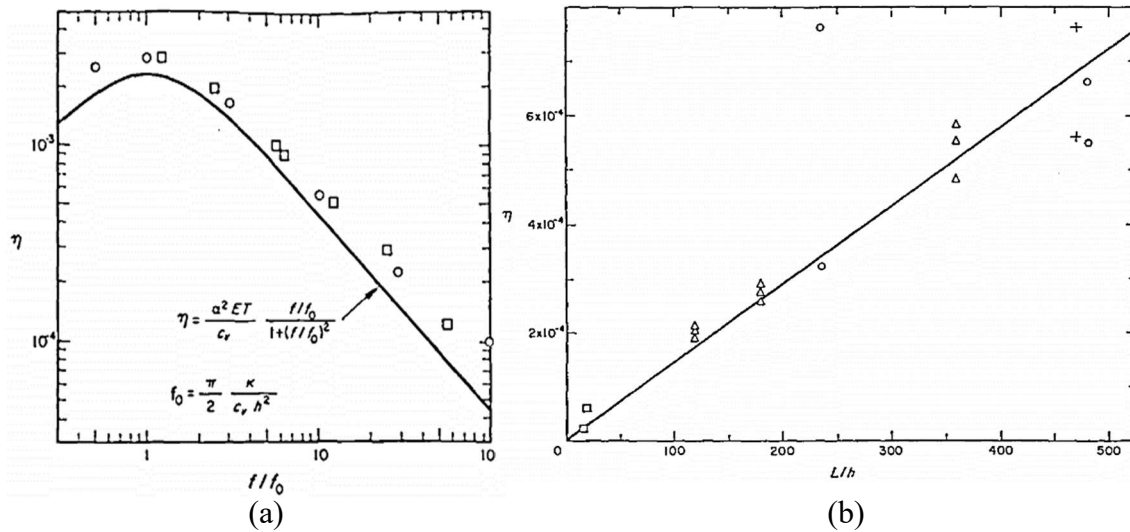


Figure 2.18: Comparison of ideal loss factor with the experimental (a) with frequency ratio [81] (b) with length-thickness ratio [82]

This work described the small amount of energy lost in elastic materials where transmitted from the system by sound wave radiation, dissipated within the material.

A two-dimensional orthotropic structure was investigated by Cherif et al [83] based on the damping loss factor estimation. Several angles were chosen to analyse the wave propagation. The finite element model was designed to investigate the proposed plate. The experimental test applied an isotropic aluminium panel and two orthotropic composite sandwich panels with a honeycomb core. This work introduced the Inverse Wave Method to estimate the loss factor for the plates.

Lima et al [84] measured the flexural resonance frequencies and used an inverse methodology to evaluate the mechanical properties of sandwich beams. The physical parameters were the loss factor and Young's modulus. They designed an FE simulation to validate a mathematical model. The results showed that the inverse methodology could effectively determine the loss factor optimisation of the sandwich beam. Mandal et al [85] investigated the loss factor of orthotropic plates. They adopted a single degree of freedom system under very low-frequency values in order to measure the damping loss factor of the different plates pasted with self-adhesive and high-density bitumen pads with coated aluminium. It was found that the high value of the loss factor results from the high amount

of bending rigidity of the plates. They also observed an increase in the loss factor of the corrugated plates that was higher than that of the isotropic plates.

Turning to the free vibration decay, Sun et al [86] applied a free oscillation response to display the frequency spectrum. They calculated the loss factor using direct peak wave formulas

$$\eta = \frac{1 - (f_b/f_a)^2}{[1 + (f_b/f_a)]^2} \quad 2.22$$

where f_a and f_b are the frequencies at the peaks of the real part as shown in Figure 2.19,

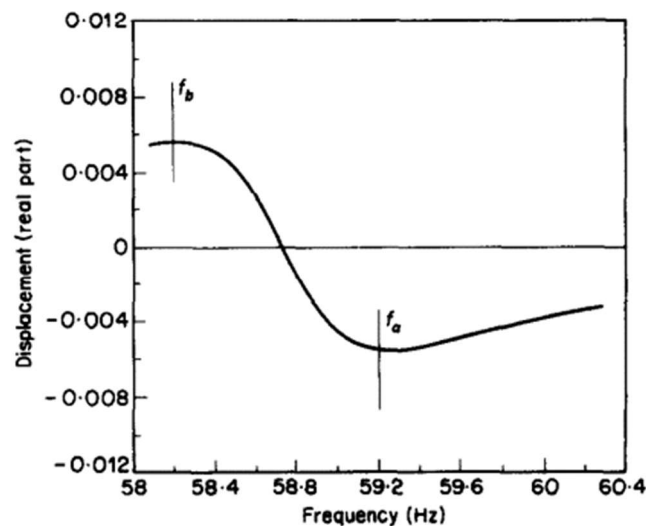


Figure 2.19: Response spectrum (real part) [86]

This real part formula is usually used with a free vibration decay method to investigate the loss factor. In the same context, Berthelot et al [87] investigated the free damping vibration in order to study the damping coefficient based on the loss factor.

Apalak et al [88] studied the cantilever joint of double containment that was adhesively bonded under transverse force, as shown in Figure 2.20. They used a contactless sensor to detect the adhesive joint response subjected to a transverse load. The

first natural frequency under bending was calculated experimentally. The loss factor was estimated for different specimen lengths. In this work, the force location was optimised to reduce the attenuation time.

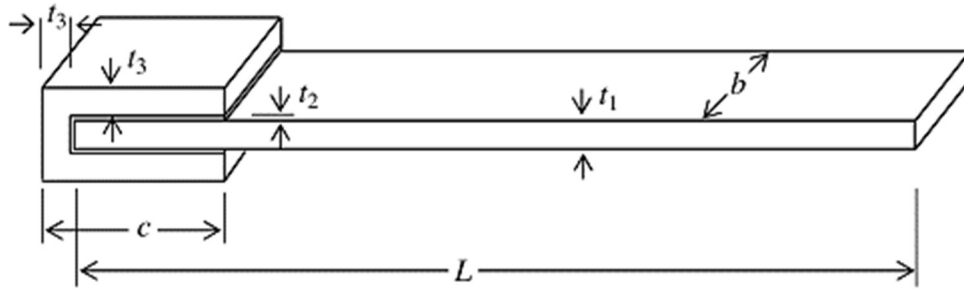


Figure 2.20: Adhesively bonded double containment cantilever joint [88]

Regarding computational model algorithms, Ewing et al [89] validated the estimation of the loss factor for panel damping using a finite element model for a rectangular plate mechanically loaded at a single point. The plate analysed the free-response decay covering a loss factor range from 0.001 to 0.1. The simulation agreed with the results between the known values of the loss factor and those obtained from the simulated accelerations. This work validated the simulation approach for plates and it can also be used in beams.

Depending on the Modal Strain Energy method (MSE), many studies have estimated the loss factor. In 1982, Johnson and Kienholz [90] used the modal strain energy method to estimate the damping under vibration condition of a three-layer viscoelastic core according to the following formula,

$$\eta_i = \frac{\sum_{k=1}^q \eta_r U_r^k}{\sum_{k=1}^q U_r^k} \quad 2.23$$

where η , U , i and q are loss factor, strain energy, mode number account and layer number.

The finite element model was designed to predict the loss factor of the elastic layer. This formula was validated using the finite element model and experimental results. Next, Tsai and Chang [91] modified Johnson and Kienholz's model to estimate the modal damping ratio. The analytical results show that the modified MSE became more accurate when the damping ratio was greater than 20%.

Kim and Griffin [92] used a finite element approach to represent the joint element. In this approach, they assumed the modes shape to be the same as the elastic modes, and then the damping ratio was estimated from a fraction of the strain energy. As a result, they concluded that the value of the strain energy stored in viscoelastic material could be calculated at each mod shape deformation. Rongong [93] also used MSE to optimise the viscoelastic joints to reduce the vibration and noise in thin plate structures. A numerical method using the finite element technique was developed to compute the loss factor. The numerical results were validated at different boundary conditions as shown in Figure 2.21. The results show that the vibration reduction level in the thin plate was effectively dropped.



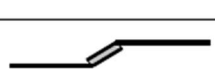



Single Lap	
Supported Lap	
Angled Lap	
Butt	
Potted	
Interlock	

Figure 2.21: Thin plate viscoelastic joints [93]

Lepoittevin and Kress [94] enhanced the damping of a constrained viscoelastic beam by segmenting the constrained layer. He observed that the cutting of the constrained layer increased the shear deformation at that position. The modal strain energy method was used to estimate the damping efficiency. As an optimisation, MSE was applied in each mode to locate the segmentation positions.

Koruk and Sanliturk [95] presented two steps for the optimisation of passive damping which can be used for different structures. First, there is a procedure based on the big bang–big crunch method for damping optimisation. According to the big bang–big crunch, the algorithm addressed random selections in the big bang phase and then shrunk to a single selection through the minimum cost approach. Second, the approach was based on the modal strain energy method that predicted the damping levels of structures with selected damping treatments.

Lisitano et al [96] proposed an approach revealing the relation between the modal damping ratio and modal strain energy. They assumed that the strain energy became concentrated at the nodal area of each mode shape during beam vibration. The Bernoulli–Euler beam formulated the theoretical model and validated using experimental results. They confirmed that the damping ratio could be theoretically predicted correctly using the arbitrary mode shape of the Euler–Bernoulli beam.

Pan and Zhang [97] investigated the damping of the viscoelastic layer using modal strain energy and the superposition approach. They evaluated the loss factor for a simply supported beam under a sinusoidal load with a temperature range. This approach was validated to be useful in the layer damping area.

This section has outlined the estimation of the loss factor for a damped beam numerically and experimentally. As previously mentioned, the loss factor is affected by the composite structure, dimensions, and frequency under dynamic conditions. Also, the damping ratio is evaluated by the static numerical finite element approach employing the MSE. However, the loss factor value can be obtained experimentally only therefore it is clear that this thesis should plan to estimate the damping experimentally.

2.3.3 Temperature and frequency dependence

Viscoelastic materials are generally polymers. Therefore there is enormous variability in their composition regarding the complex modulus and loss factor. Unlike metals, the polymers have a high sensitivity due to the strain rate, temperature, and cyclic strain amplitude. The temperature and frequency dependency of polymer materials have been studied extensively due to the complex modulus and loss factor.

Goyanes et al [98] investigated the damping of epoxy matrix filled with quartz powder. They measured the loss tangent and storage modulus at a frequency ranging from 7.8 to 323 Hz between room temperature and 187 °C. The damping with quartz as a polymer-particle interaction was obtained, as shown in Figure 2.22.

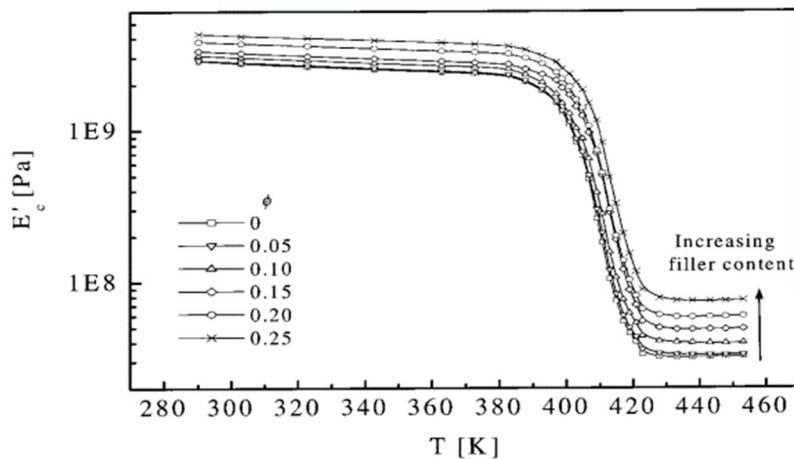


Figure 2.22: Storage modulus with respect to the temperature [98]

The plotted curves that were obtained show that the storage modulus increases with respect to the increase of the quartz filler content. This behaviour is maintained where there is an increase in the quartz filler.

Shabeer et al [99] used soybean oil with epoxy resin to investigate natural viscoelastic materials. The storage modulus and loss tangent were plotted using temperature in order to discover the mechanical behaviour of the composite. The master curve was also generated, as shown in Figure 2.23, to predict the storage modulus with respect to time

and temperature. As shown, the storage has a linear behaviour with respect to the logarithm frequency. They found that the mixture of epoxy resin and a certain amount of soybean oil indicates quite a good potential material for suppressing noise and vibration as an alternative polymer.

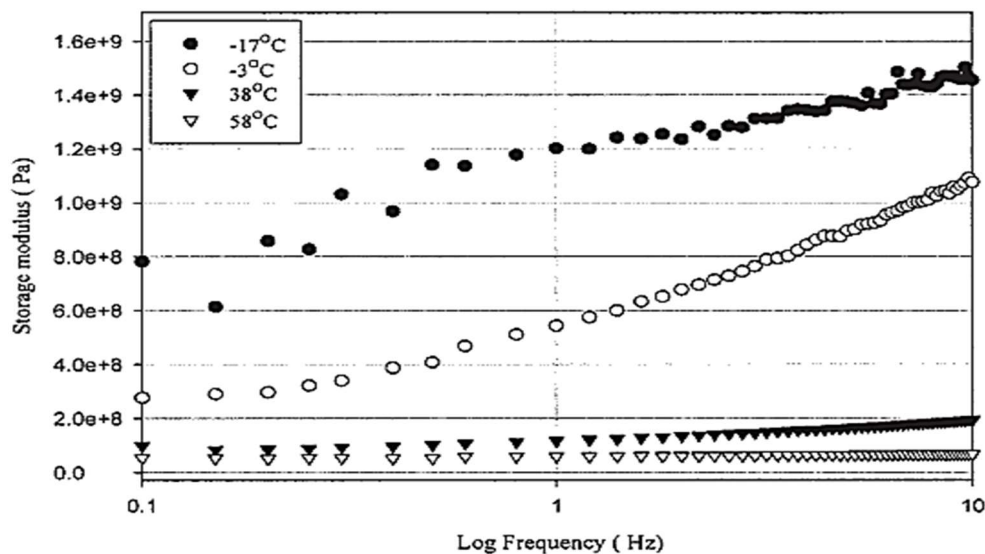


Figure 2.23: Master curve of soybean oil with epoxy resin [99]

Saseendran et al [100] conducted two experimental works to develop a methodology analysing the curing effect on the viscoelastic storage modulus. They used LY5052 epoxy resin for plotting the storage modulus in the logarithmic frequency domain at various temperatures. The results showed that the thermo-viscoelastic properties could be assumed to be independent of the curing time.

Martinez et al [101] studied the thermal and rheological gelation and vitrification times. They found that the isothermal curing master curve was controlled by shifting the glass transition temperature due to logarithm time. Ratna et al [102] developed a three epoxy composition. The composition attained low transition temperatures contrary to normal epoxies. Furthermore, the time-temperature analysis indicated that the structure has a high loss factor covering a broad range of frequencies and temperatures. Kim and White [103] designed a model describing the polymer transformation from liquid to solid during the

curing process. Mathematically, they proposed an analytical model describing the relaxation modulus. The results show that the cure state improved the epoxy stress relaxation and increased the sensitivity of the relaxation behaviour. Rao et al [104] developed a polymer using shape memory by curing the epoxy resin. A time-temperature superposition diagram was generated to introduce the loss modulus behaviour due to temperature. They determined the two constants C_1 and C_2 of the Williams Landel Ferry (WLF) formula 2.24. They compared it with the universal constant of an amorphous polymer. The results show that the shape memory behaviour provides useful inputs for a broad frequency range.

$$\log a_T = \frac{-C_1(T - T_g)}{C_2 + (T - T_g)} \quad 2.24$$

Where C_1 and C_2 are relevant to fractional free volumes as

$$C_1 = \frac{B}{2.303f_g} \quad 2.25$$

$$C_2 = \frac{f_g}{\alpha_f} \quad 2.26$$

Originally, the constants $C_1=17.44$ and $C_2=51.6$ were taken as a universal value for amorphous polymers, but these values vary with respect to the polymer material.

Kishi et al [105] characterised the damping properties of carbon fibre-reinforced interleaved epoxy composites. They evaluated the damping properties of the composite with/without the interleaf films using the mechanical impedance method. The loss tangent of the interleaf films at the test temperature was described in the loss factor of the interleaved laminates. The loss factor was affected by the stiffness of the films at the resonant frequency of the laminates. Katunin et al [106] investigated the self-heating of viscoelastic energy dissipation in polymer-based composite structures. A harmonic load was applied under different excitation frequencies and temperatures. This work revealed the effect of temperature and frequency on the loss of rigidity.

Filho et al [107] investigated the thermorheologically simple viscoelastic materials by employing the hyperplastic theory. They integrated an approach to characterise the damping of viscoelastic including the preload effect along with the influence of temperature and frequency. Experimentally, they plotted a reduced-frequency nomogram as shown in Figure 2.24 for viscoelastic Butyl Rubber under a preloaded condition.

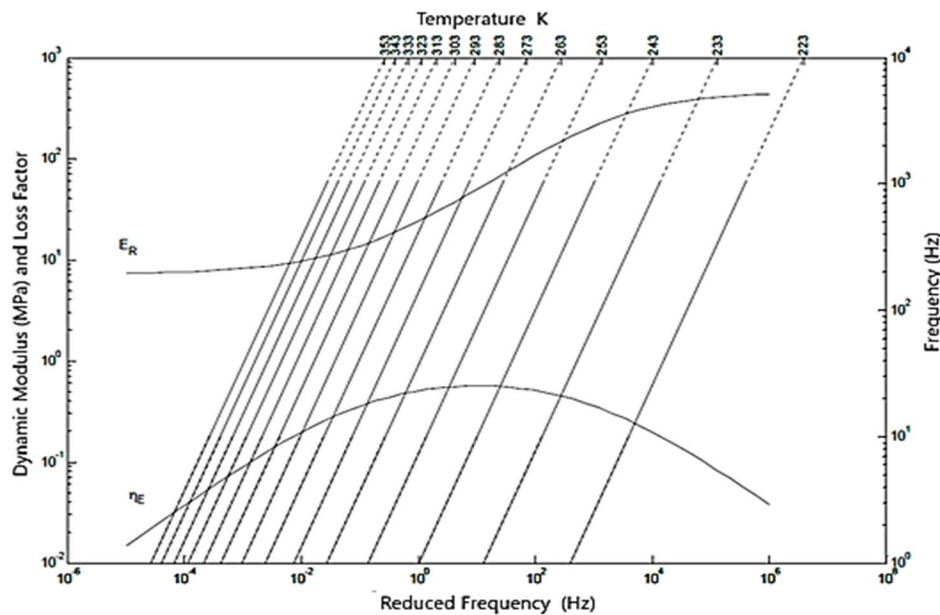


Figure 2.24: Reduced frequency nomogram for Butyl Rubber [107]

In the prior analyses of polymer materials, temperature and frequency dependence provide an understanding in order to identify the dynamic mechanical analysis to make a comparison between the epoxy resin damping characteristics and the platelet-reinforced epoxy.

2.3.4 Poisson's ratio for polymeric materials

The ratio of the lateral strain to the axial strain in a linear solid body is defined as Poisson's ratio. To use polymeric materials efficiently for damping vibration or improving the composite material, knowledge of Poisson's ratio behaviour is essential if the materials are subjected to loading or restraint in more than one direction. In a polymer,

Poisson's ratio depends on temperature and frequency (or time) because the shear modulus is very sensitive to these factors while the bulk modulus is only mildly sensitive. Lakes [108] mentioned that Poisson's ratio is not a constant property for the polymeric materials but can depend on time.

Chen and Worden [109] employed Poisson's ratio in a decomposition method for dynamic viscoelastic composite materials. They analysed and described the behaviour of Poisson's ratio due to the logarithm time as shown in Figure 2.25 based on Equation 2.28, which was derived from Equation 2.27.

$$v_v(t) = v_0 + ae^{-bt} \quad 2.27$$

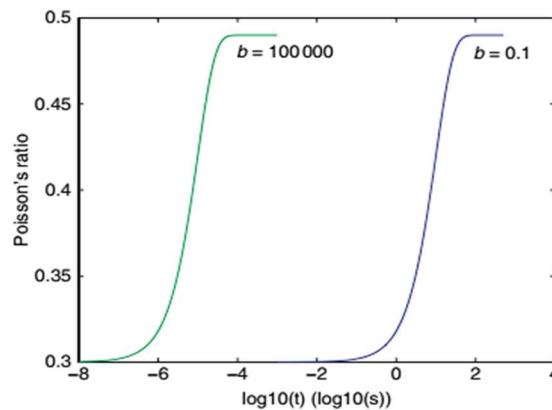


Figure 2.25: Poisson's ratio time scales [109]

Although Poisson's ratio changed over time, they found that the effect of the errors of time-dependency in Poisson's ratio can be ignored in the sandwich beam with a viscoelastic core, as shown in Figure 2.26. This was because the properties of sandwich beams are dominated by the shear modulus of the polymer rather than its bulk behaviour.

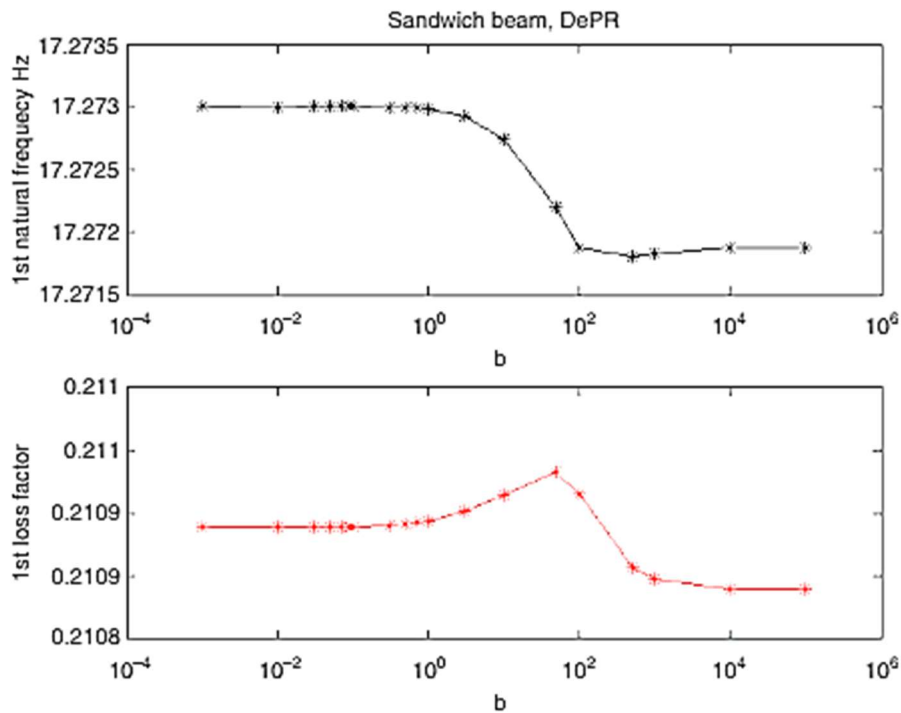


Figure 2.26: First natural frequencies and loss factors with Poisson's ratio
 $v_v(t) = v_0 + ae^{-bt}$ [109]

Sim and Kim [110] introduced a method to estimate the properties of viscoelastic materials using a finite element method. The finite element was designed to determine the relation between the apparent modulus and true modulus, Poisson's ratio and the shape factor. Experimentally, they used a cylindrical specimen with a small shape factor, ignoring the errors due to the diminished lateral deformation at the ends of the specimen, as shown in Figure 2.27.

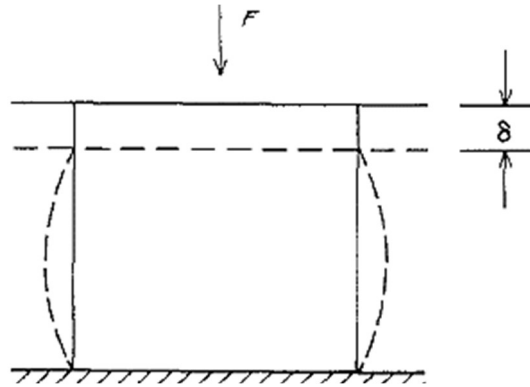


Figure 2.27: Longitudinal deformation to the normal load [110]

Similarly, they applied the finite element model to the larger shape factor specimen. Poisson's ratio domain was found to be between 0.45 and 0.5 for the viscoelastic material, as shown in Figure 2.28.

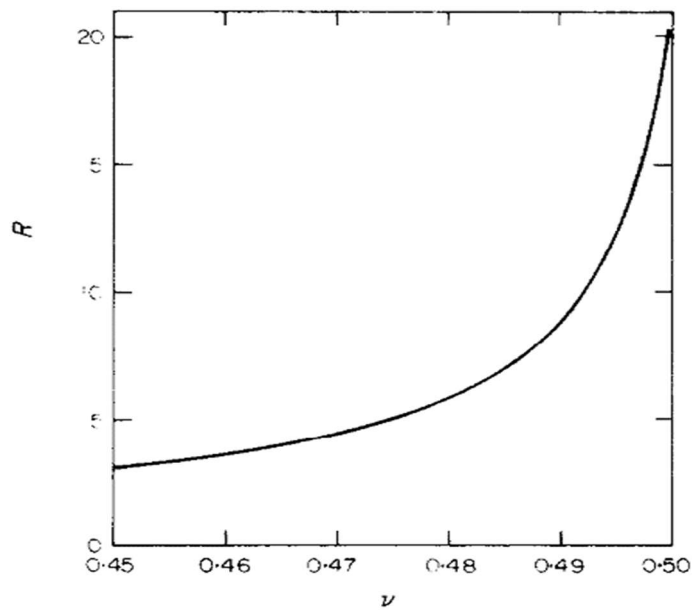


Figure 2.28: Poisson's ratio from FEA for a large shape factor specimen [110] where $R = E^*/E$

Meaud and Hulbert [111] combined a low damping stiff material with a high damping soft material to produce both a high loss factor and high dynamic modulus. They investigated the details for two composite types, Voigt and Reuss, under uniaxial harmonic excitation. Poisson's ratio effect was taken into account when formulating the finite element analysis. They considered the properties of the modulus as 200 and 0.02 GPa and Poisson's ratio was 0.3 and 0.45 for stiff and soft materials, respectively. This was the same as the materials that Chen and Lakes [8] used. They optimised a composite with high stiffness and high damping.

Pritz [112] transformed the typical complex moduli and complex Poisson's ratios of the real solid materials from the time through to the frequency domain. It was shown that the dynamic Poisson's ratio decreased monotonically while the dynamic moduli increased monotonically as the frequency increased. Regarding Poisson's ratio, the decrease was obtained according to Equation 2.29:

$$\bar{\nu}(j\omega) = \frac{\bar{\varepsilon}_y(j\omega)}{\bar{\varepsilon}_x(j\omega)} = \nu_d(\omega) - j\nu_l(\omega) = \nu_d(\omega)[1 - j\eta_v(\omega)] \quad 2.28$$

Pritz [113] investigated the relationship between the bulk and shear loss factors for isotropic materials regarding the complex modulus concept. The bulk and shear loss factors can be related to the dynamic Poisson's ratio. The ratio of the bulk to the shear loss factor was estimated to decrease due to the increase in the dynamic Poisson's ratio. The experimental results for the polymeric materials support the theoretical findings. Pritz [114] studied the role of the complex Poisson's ratio in characterizing the linear dynamic behaviour of solid materials. The ratio of the imaginary number to the real number of complex Poisson's ratio was referred to as a Poisson's loss factor. Pritz also sought to determine the relationship between Poisson's loss factor and the material damping. The analysis shows that the value of Poisson's loss factor is approximately proportional to the difference between the bulk and shear loss factors. He developed relationships to enable the prediction of the value of Poisson's loss factor using Poisson's ratio and the shear loss

factor. The results showed that Poisson's loss factor was smaller than the shear loss factor. The experimental data verified the theoretical findings.

Allou et al [115] developed a 3D linear viscoelastic formulation in order to characterise the complex Poisson's ratio and dynamic modulus for the asphalt mixtures. They assumed conditions of isotropy for the shear and bulk moduli in order to determine Poisson's ratio and dynamic Young's modulus. The FEA model was implemented to predict the 3D linear behaviour. The model was validated by comparing the model results with the experimental data of the asphalt mixture. The comparison showed that the FE model results are close to the 3D linear behaviour. They clarified the complex Poisson's ratio in the frequency domain, as shown in Figure 2.29.

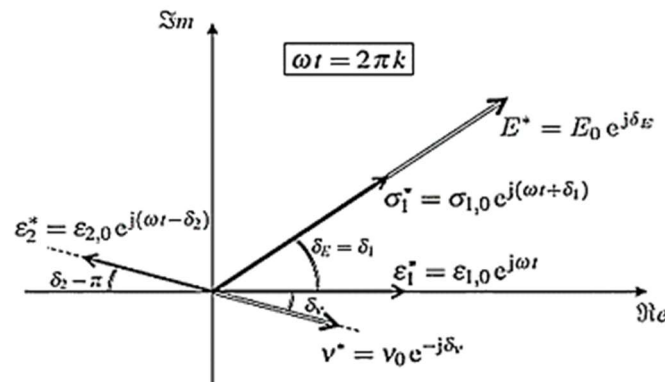


Figure 2.29: The complex plane [115]

Pandini and Pegoretti [116], [117] investigated the Poisson's ratio of viscoelastic materials butylene terephthalate depending on time, temperature and strain rate. Two conditions of loading were applied. First, there was the constant tensile strain rate at various temperatures and second, the constant strain value at a different strain rate and isothermal temperatures. In both conditions, the deformations were measured using an extensometer, as shown in Figure 2.30. They also adopted a correction procedure to reduce the lateral movement error of the extensometer knife edges. The results showed that Poisson's ratio increased with time and temperature and decreased with strain rate.

The stress relaxation was accompanied by a continuous lateral contraction process – indicating a monotonous increase in the Poisson's ratio with respect to the time.

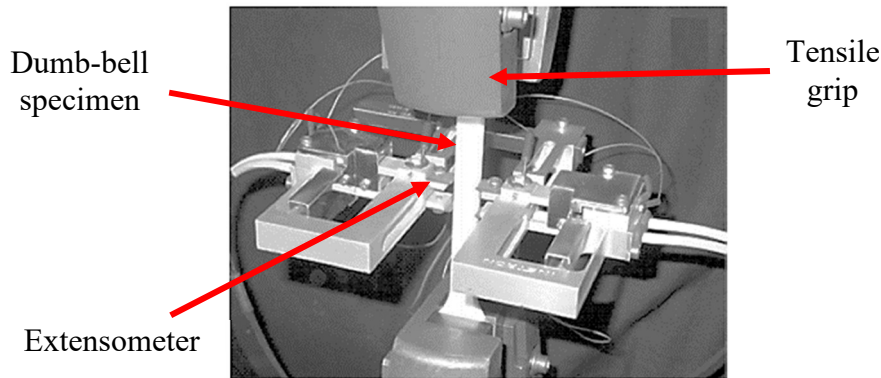


Figure 2.30: Extensometer setup for Poisson's ratio measurement [116]

The significance of the time dependence of Poisson's ratio is that time is related to frequency and temperature in polymers. In the transition zone, Poisson's ratio increases with temperature making the shear modulus much more sensitive to temperature than the bulk modulus. In composite structures with configurations that generate volumetric strains in the matrix, this must be accounted for.

2.4 Summary

The review of the literature shows that the concept of equivalent rigidity for both the staggered and the laminated composite beams has been studied. However, this has not been extended appropriately to bending, particularly in configurations that need to accommodate the Timoshenko shear effect.

This thesis sets out to formulate an analytical model for a staggered sub-structured composite for the purpose of suppressing bending vibrations. Here, a staggered platelet embedded viscoelastic matrix is adopted to compromise between reinforcement and damping.

Section 2.2 dealt with the methods used to obtain an equivalent flexural modulus. The analysis of the strain behaviour through the layers was the most common approach used

to evaluate the equivalent flexural modulus. The straight strain behaviour, zigzag and shear were discussed. Most of the research in this area has studied the equivalent properties by depending on the unit element along the thickness. However, a lack of analysis on the thickness and length of the unit cell can be an obstacle to evaluating the equivalent properties of the staggered configuration unit cell. Moreover, there is a limited amount of literature studying the reinforcement of very soft material using highly stiff material to enhance the damping and the modulus. Section 2.2.4 deals with the zigzag strain behaviour to address the zigzag problem in the finite element models with a three way unified layer, layer wise and RZT features, respectively. In this thesis, it is planned to explore the physical phenomena of the zigzag strain in order to formulate an analytical model purely based on the zigzag mechanism phenomena. It does not depend on any experimental or numerical data to describe the zigzag behaviour. In particular, the strain zigzag results from the staggered heterogenous structure under static and dynamic bending conditions. Finally, this analytical model enables the estimation of its mechanical properties and describes the bending angle mechanism for the zigzag strain behaviour.

To justify the viscoelastic characteristics, Section 2.3 showed that the literature has dealt with the working aspects of the viscoelastic materials. The effect of temperature, frequency and Poisson's ratio on the damping characteristics has been discussed. The analysis regarding the effect of temperature and frequency on the effective flexural and loss factors has been demonstrated in other research in Section 2.3.3. The temperature has the greatest effect on the epoxy properties of the damping characteristics. Like temperature, frequency also affects the complex modulus and loss factors. The modulus of the epoxy always increases with respect to the increasing frequency.

It was mentioned that the Poisson's ratio of the viscoelastic materials varies due to temperature and frequency. Section 2.2.4 the studies showed that the Poisson's ratio value affects the mechanical properties under different conditions. In addition, Poisson's ratio value was evaluated by extensometer. However, in this thesis, the Digital Image Correlation (DIC) was used to measure the Poisson's ratio. The DIC approach provides greater accuracy than an extensometer, particularly when evaluating locally varying strains.

These sections reviewed the estimated equivalent rigidity and the frequency temperature dependency. Although the equivalent rigidity of the staggered structure has been estimated under tension deformation, it cannot estimate the equivalent rigidity under bending deformation. Although the damping level evaluation has been discussed, validation for the selected staggered composite still needs to be conducted

In this study, finite element models of the staggered unit cell were used to simulate the bending strain behaviour concerning the materials modulus ratio involving a soft-stiff structure. The FE models were used to verify the analytical model and reveal the effective bending parts that guided the bending angle. The results from the analytical and simulation models are validated using the experiments. The comparison revealed agreeable results when they compared together.

The findings of the literature review revealed that there is need for further research in the area of staggered reinforcement when considering flexural vibrations. As a result, the objectives for this study (also stated in Section 1.2) are as defined below:

- Introduce an analytical model to estimate the flexural rigidity in a staggered unit cell system constructed from stiffer platelets embedded into a soft viscoelastic matrix purely based on the zigzag mechanism phenomena.
- Determine the effective bending moment parts guiding the local bending angle mechanism.
- Validate the analytical and numerical models using experimental tests at different temperatures.
- Investigate the effect of vibration on the damping value in staggered structure systems.

Chapter 3

Effective flexural rigidity for a staggered unit cell

3.1 Introduction

This chapter presents the development of an analytical model of a composite material designed to provide a compromise between the need for high stiffness and high damping through its construction comprising stiff platelets encompassed by a soft matrix. Under flexure, concentrated bending strains occur in the soft material while the stiff platelets decrease the overall strain of the composite. Thus, the strain distribution through the thickness takes a zigzag form. While such analyses can be carried out using finite element methods, a simpler analytical approach is sought in order to reduce computational cost.

A new method is developed to estimate the flexural rigidity. This method is called the “Effective Bending Moment Method” and combines the bending deflection results from several parts through the cross-section thickness of the unit cell. The method considers that the bending angle is guided by the stiffer material and concentrated at the external soft gaps between the platelet and the unit cell boundaries.

In the work reported, an analytical model was formulated to estimate the flexural rigidity for the staggered unit cell composite made of high stiffness platelets into very small stiffness matrix. Then, a one-element length unit cell was modelled using finite element (FE) analysis to find the rigidity and natural frequencies. These models were followed by experimental work conducted on the designed unit cell to validate the analytical and numerical models.

3.2 Dynamic analysis of unit cell

To calculate the natural frequency of a bending beam, flexural rigidity is a fundamental value to investigate the dynamic response. In this section, the dynamic analysis is presented using analytic and finite element models for estimating the effective flexural rigidity of the staggered unit cell structure, as shown in Figure 3.1. To verify the accuracy of the analytical formulation, a finite element model simulated the unit cell.

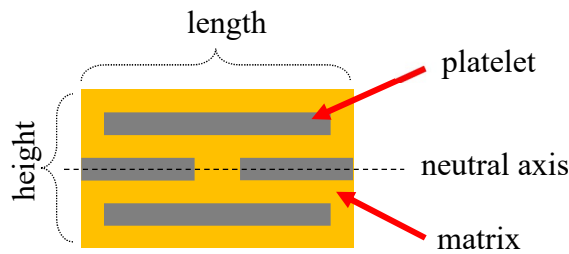


Figure 3.1: Staggered unit cell composite

3.2.1 Analytical effective rigidity

The staggered structure is constructed from multiple layers through the height and different segments through the length. The flexural rigidity can be estimated using an equivalent spring for the unit cell structure. The theorems of effective stiffness for springs system are given for parallel and series respectively as,

$$k_e = \sum_{i=1}^{i=n} k_i \quad 3.1$$

$$k_e = \frac{1}{\sum_{i=1}^{i=n} 1/k_i} \quad 3.2$$

This section presents an analytical method to determine the effectiveness rigidity of the staggered composite. In this method, the unit cell is assumed to be divided into 5

vertical layered slices, as shown in Figure 3.2a. Each slice contained layers of the two materials, as shown in Figure 3.2b. Under flexural load, each layer of slice takes the same bending angle value of the slice. Thus, the layers at each slice can be modelled as parallel springs to estimate the effective rigidity of each slice. Then, the slices take a different bending angle value along the unit cell. Thus, the slices can be modelled as series springs to estimate the effective rigidity of the unit cell.

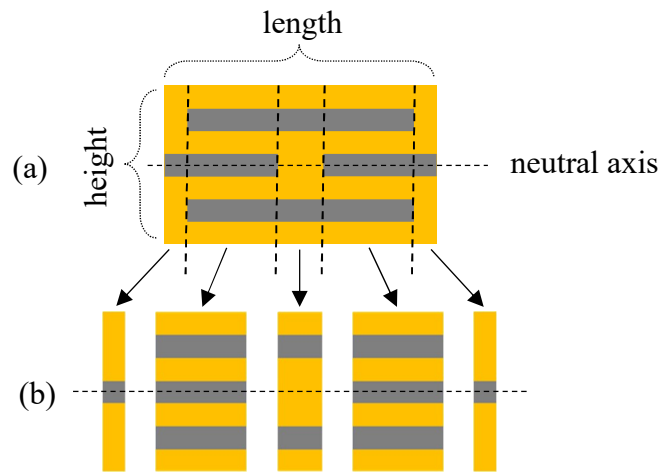


Figure 3.2: Staggered composite (a) unit cell (b) assumed slices

In this case, the rigidity of each slice can be calculated according to Equation 3.3 based on effective parallel springs,

$$EI_i = EI_{pi} + EI_{vi} \quad 3.3$$

where EI_p and EI_s are the equivalent rigidity of parallel and series layers, respectively. by assuming it is subjected to constant bending moment, the bending angle equation is,

$$\theta = \frac{ML}{EI} \quad 3.4$$

since the bending angular stiffness k for each slice is,

$$k_i = \frac{EI_i}{L_i} \quad 3.5$$

as a series springs, the effective k will be,

$$k_e = \frac{1}{\sum_{i=1}^{i=n} 1/k_i} \quad 3.6$$

since the effective rigidity is formulated as,

$$EI_e = k_e * L \quad 3.7$$

For a given modulus of the two materials, the effective rigidity EI_e can be obtained by using the ratio of the matrix modulus to the platelet modulus E_r . The effective rigidity behaviour is estimated with respect to the ratio E_r , as shown in Figure 3.3a.

As a dynamic characteristic, to obtain the natural frequency, a composite cantilever was assumed to be made of 16 unit cells. The natural frequency behaviour was estimated, as shown in Figure 3.3b, using the effective rigidity in the cantilever natural frequencies equation as,

$$f = \frac{\lambda^2}{2\pi L^2} \sqrt{\frac{EI_e}{\rho A}} \quad 3.8$$

where λ are 1.875 for first natural frequencies f_1 of the cantilever condition.

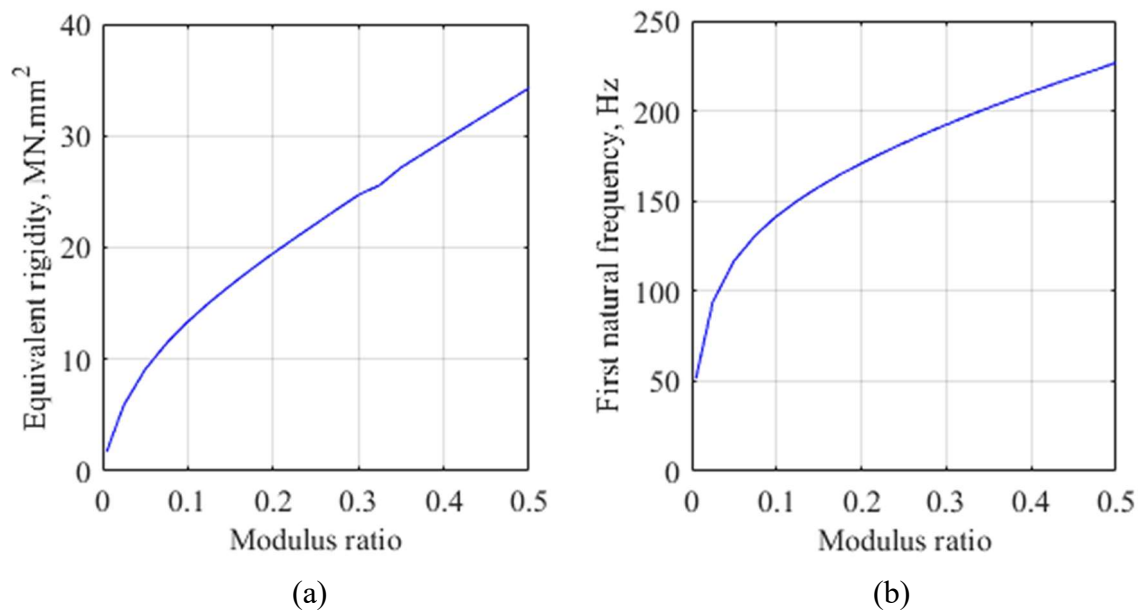


Figure 3.3: Cantilever boundary conditions (a) first natural frequency versus modulus ratio (b) effective rigidity versus modulus ratio

3.2.2 Numerical model of the unit cell

The unit cell was designed by using one element thickness composite materials to compute the effective rigidity and natural frequency. A composite cantilever was designed from 14 units. In this simulation, the system dimensions and material properties are given in Table 3.1.

Table 3.1: Materials properties

Material	Dimensions, mm			Material properties	
	Length	Height	Width	ρ , kg/m ³	ν
Matrix	154	7	1	950	0.42
Patelet	10	1	1	7850	0.3

The modelled cantilever has a number of nodes and elements 8354 and 1078 respectively, the number of platelets was 43 arranged as shown in Figure 3.4. 20 node brick elements were used for the mesh with each element having a typical size of 1 mm.

The behaviour of first natural frequency and effective rigidity were estimated and compared with the analytical results.



Figure 3.4: Cantilever of staggered composite

Figure 3.5 showed that the analytical results give a good agreement with the finite element results when the modulus ratio is greater than 0.125. However, comparison of analytic and numerical results for the analytical and numerical behaviours are separated for effective rigidity and first natural frequency. The ratio between values obtained using the analytic model and the numerical are presented in Figure 3.6. It can be seen that significant separation between the two methods only occurs for modulus ratio values below 0.125.

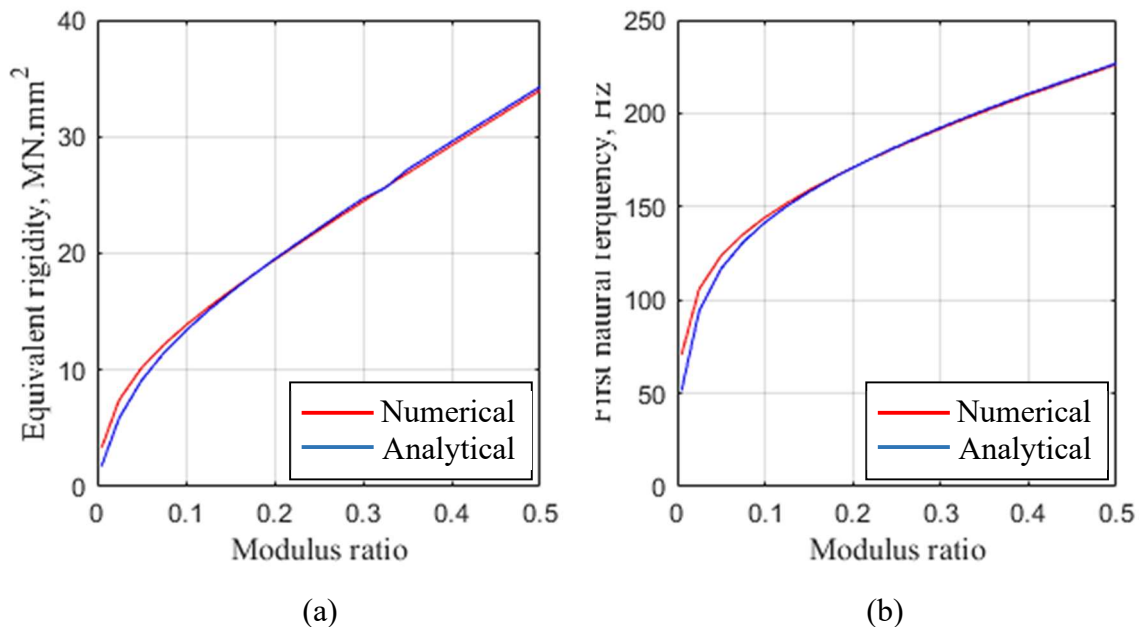


Figure 3.5: Comparison of analytic and numerical result for (a) first natural frequency versus modulus ratio (b) effective rigidity versus modulus ratio

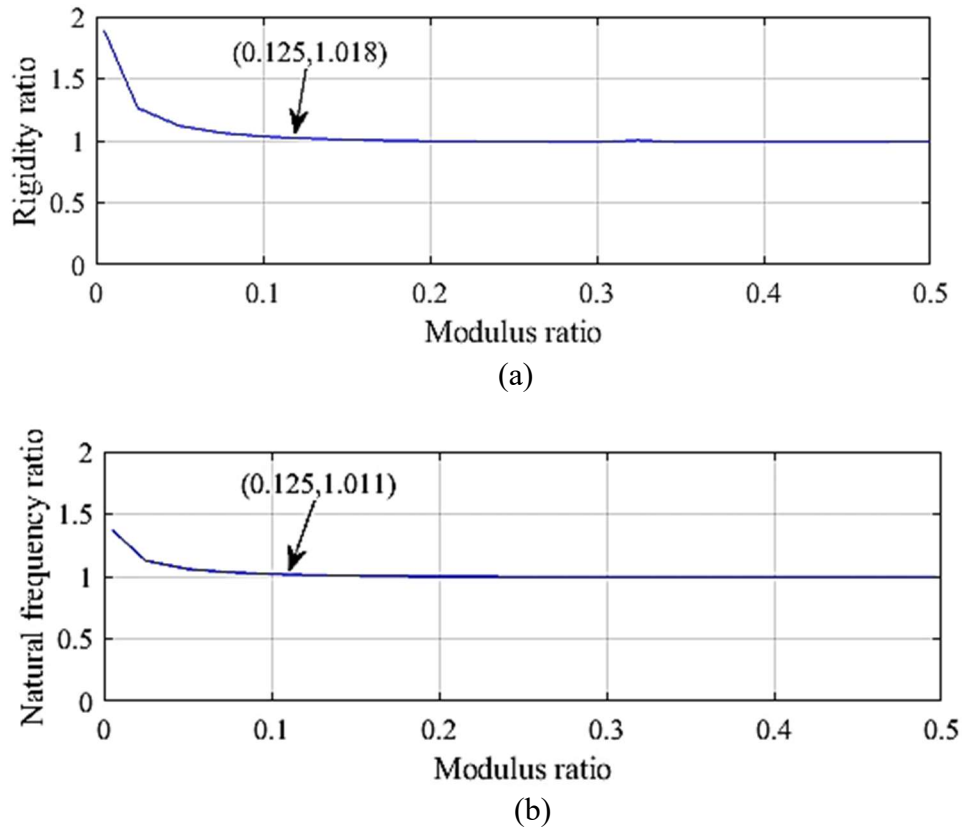


Figure 3.6: Analytical and numerical comparison (a) first natural frequency versus modulus ratio (b) effective rigidity versus modulus ratio

3.3 Strain behaviour analysis

The previous section examined the analytical model using the equivalent spring system method. The comparison with the finite element model showed that the limitation of the method occurred when the modulus ratio was greater than 0.125. To estimate the effective rigidity at a modulus ratio value less than 0.125, this section studies the strain behaviour of bending deformation with respect to the modulus ratio. This can be extended into a combination of soft-stiff staggered composite materials to achieve a structure made of soft damping material and high stiffness material.

3.3.1 Normal strain analysis

A constant bending moment of 100 N.mm was applied to the cantilever model. Four cross-sections were selected in the unit cell, as shown in Figure 3.7a, to obtain the strain behaviour at each section and modulus ratio 1, 0.7, 0.4, 0.1 and 0.01.

The platelet modulus was set as 200 GPa while the matrix modulus was assumed at four values 200, 140, 80, 20 and 2 GPa. When the modulus ratio was 1, the unit cell structure became as one material. Therefore the strain behaviour was linear through the thickness, as shown in Figure 3.7b, at all sections. At modulus ratio 0.7, the strain was more-or-less linear, as shown in Figure 3.7c, which is why there was good agreement between finite element and analytical results, as shown in section 3.2.2 Figure 3.5. At modulus ratio 0.4, it can be seen that the strain was linear at sections b-b, c-c and d-d but starts to become zigzag at the matrix space between the platelets as shown in Figure 3.7d section a-a. At modulus ratio 0.1 as shown in Figure 3.7e, the strain was zigzag between the upper and lower platelets ends at sections a-a, where at the sections b-b, c-c and d-d were linear between the upper and lower platelets but began to be zigzag between the outer platelets and the free surface. For further modulus ratio reduction to the smallest value 0.01 as shown in Figure 3.7f, the strain was clearly zigzag and concentrated at section a-a while it was minimal value and nearly linear at sections b-b, c-c and d-d.

This thesis targets the staggered structure with the smallest modulus ratio to reinforce the soft damping matrix by high modulus platelets. Thus, the working modulus ratio range in this work was adopted to be less than 0.1.

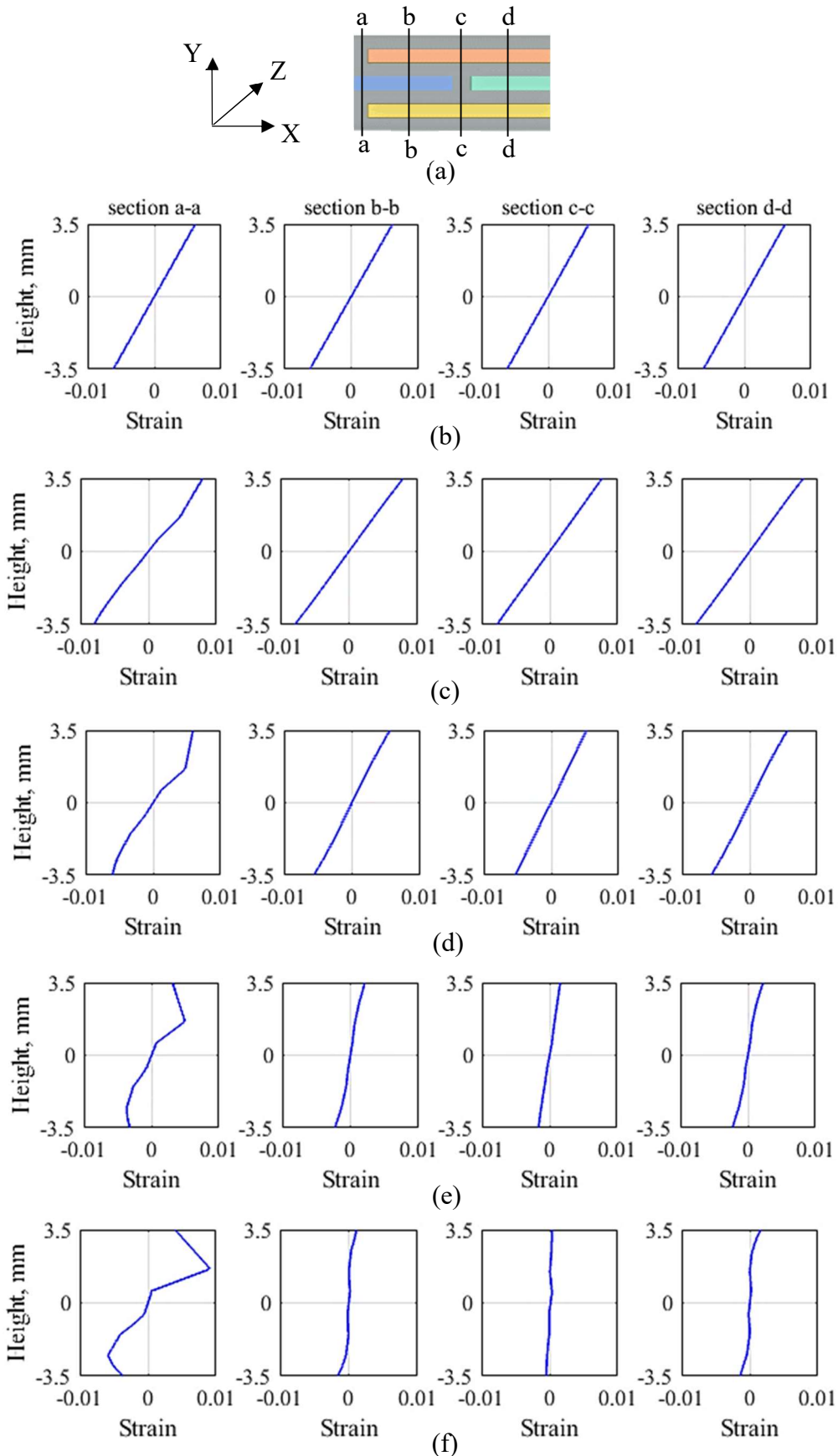


Figure 3.7: Strain behaviour (a) selected sections (b) modulus ratio 1 (c) modulus ratio 0.7 (d) modulus ratio 0.4 (e) modulus ratio 0.1 (f) modulus ratio 0.01

3.3.2 Shear strain analysis

The load, dimensions and properties in Section 3.3.1 were used herein to indicate the shear strain behaviour in the x-y plane.

When the modulus ratio is 0.4, the unit cell structure becomes as one material. Therefore, the XY plane shear strain behaviour is linear with a minimal value that can be ignored, as shown in Figure 3.8a, at all cross sections. Also, it can be ignored at modulus ratio 0.1, where the shear strain was minimal value through the composite thickness.

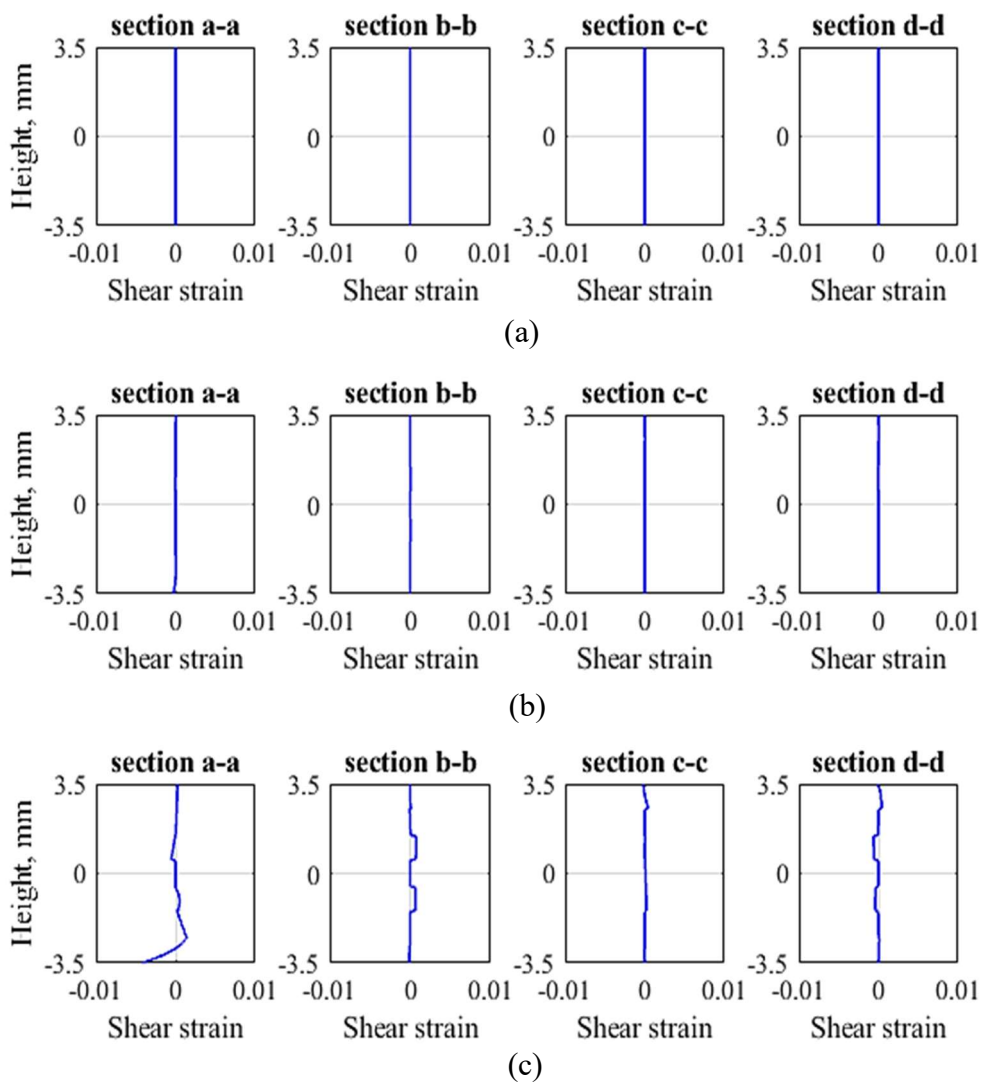


Figure 3.8: Shear strain behaviour (a) modulus ratio 0.4 (b) modulus ratio 0.1 (c) modulus ratio 0.01

At the modulus ratio 0.01, as shown in Figure 3.8c, the shear strain behaviour was linear at cross section a-a above the neutral axis with the minimal value that can be ignored. In contrast, the shear strain at the matrix between the lower platelets ends was considerable. At cross sections b-b and d-d, the shear strain was considerable between the central and external platelets and symmetric around the external matrix gap. Finally, the shear strain at cross section c-c can be ignored.

Regarding the Timoshenko shear effect, when the modulus ratio is 0.4, the unit cell structure becomes as one material as well. The shear strain behaviour was linear with the minimal value that can be ignored, as shown in Figure 3.9a, at all cross sections.

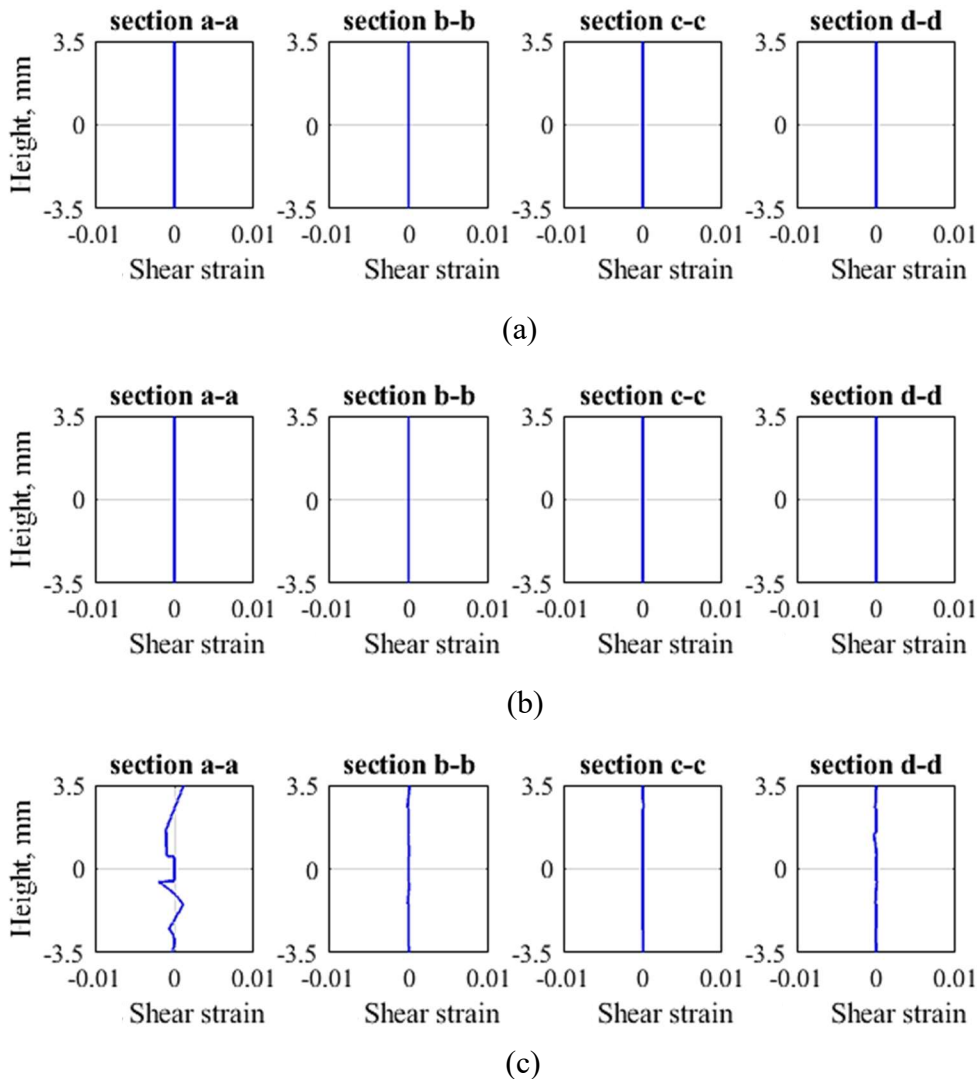


Figure 3.9: Timoshenko shear strain behaviour (a) modulus ratio 0.4 (b) modulus ratio 0.1 (c) modulus ratio 0.01

Also, it can be ignored at modulus ratio 0.1. At modulus ratio 0.01, as shown in Figure 3.9c, the shear strain behaviour was considerable value at cross section a-a upper and lower the central platelets. At cross sections b-b, d-d and c-c, the Timoshenko shear strain was linear behaviour and minimal value that can be ignored. Therefore, the effective viscoelastic part at section a-a will be solved by the Timoshenko beam theory.

3.3.3 The forces flow mechanism

In Figure 3.7f and Figure 3.8c were shown, under flexure, the concentrated bending strains were induced in the soft material, while the stiff platelets decreased the overall strain of the composite. The normal strain is concentrated in the matrix gaps between both the upper and lower platelet ends, while the shear strain is concentrated between the central platelets and upper and lower platelets. Thus, the influential forces flow against the concentrated flexure deformation, as shown in Figure 3.10.

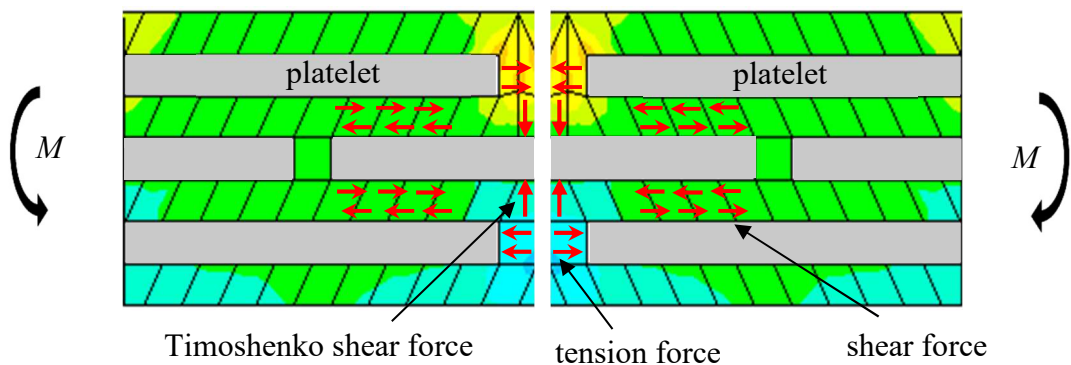


Figure 3.10: Effective forces flow

These shear forces flow deform the polymer matrix through the thickness during bending when the modulus ratio is less than 0.125. The shear strain transfers the load through the thickness at cross section b-b, while the tension force acts along the cross-section a-a.

3.4 The Effective Bending Moment Method (EBMM)

To study the dynamic mechanical analysis, the equivalent rigidity of heterogeneous staggered composite needed to be formulated for estimating the natural frequencies. As shown in the previous section, the bending deformation resulted from the concentrated strains at the polymer material between the upper and lower platelets ends and from the shear strain concentration between the central and the upper and lower platelets. Thus, the equivalent rigidity was formulated depending on effective concentrated strain regions that dominated the bending deformation. The hatched sections in Figure 3.1 show the key regions that contribute to bending. The angle is guided by the upper and lower platelets and the matrix gaps between them. The hatched matrix region (yellow background) gives the bending angle caused by the tension stress, while the hatched platelets rotate in a rigid manner resulting in the lower shear deformation of the matrix layer.

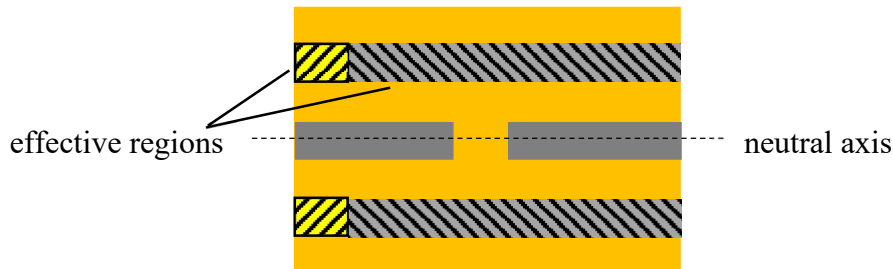


Figure 3.11: Effective bending guide regions

3.4.1 Bending angle mechanism

The flexural rigidity of a staggered unit cell beam can be obtained using the resultant bending angle or the total resultant deflection. In this work, assuming a perfect bond between the matrix and platelets, the resultant bending angle comes from the shear strain and tension strain (see Figure 3.10). As a result, the bending angle comes from the effective region between the ends of upper and lower platelets while the platelets themselves guide the unit cell as a rigid, as shown in Figure 3.12.

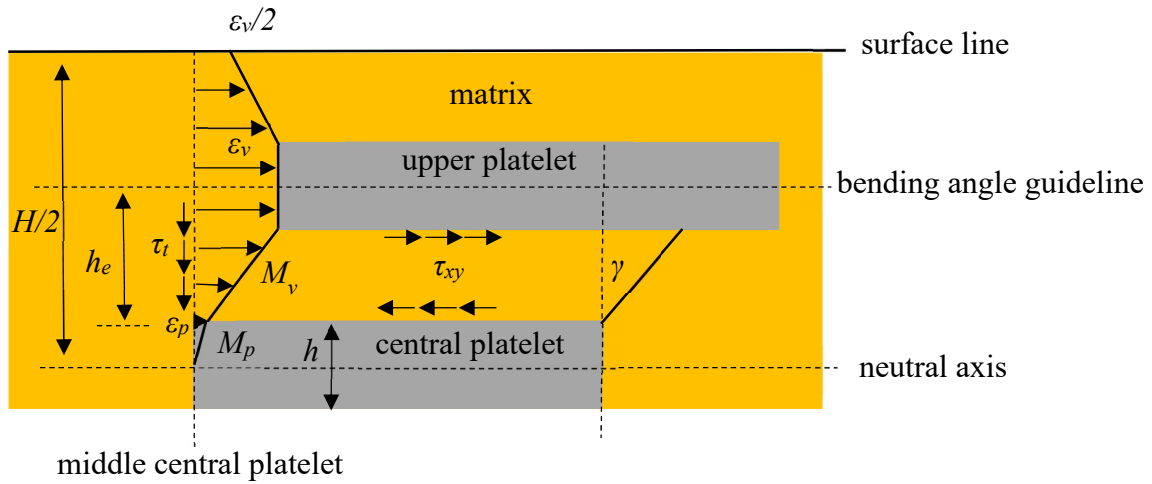


Figure 3.12: Resultant bending angle mechanism (upper half of unit cell) where ε_p , ε_v , τ_{xy} and τ_t are, respectively, platelet strain, matrix strain, XY shear strain and Timoshenko shear strain

Therefore, the EBMM was formulated based on the zigzag strain in middle matrix gaps and Timoshenko shear strain. As a result, the resultant angle can be estimated from a guided angle of these effective strain regions.

3.4.2 The analytical model

The developed analytical model in this section addressed the non-uniform strain behaviour through the thickness and various strains over the length of the unit cell. Under flexure, concentrated bending strain was induced in the soft material, while the stiff platelets decreased the overall strain of the composite. The platelets resulted in an increase in the equivalent rigidity.

A multi-layered staggered beam contains many shear deformations along the matrix material and through the thickness. The adopted assumption in this analytical model formulation is that the upper and lower matrix layer move with platelet when the magnitude of the modulus ratio is less than 0.125. Therefore, the upper and lower platelet layer movement was induced by the applied moment but guided the angle as a rigid unit based on the resultant bending angle.

Therefore, based on the above guide angle and Section 3.4.1, the analysis of stiff-soft staggered composite materials in bending was based on the five primary assumptions:

1. The bending moment reaction in the central platelets is constant in the middle of the platelet and equal to the bending moment reaction in the matrix when the modulus ratio is less than 0.125 (see Figure 3.7f).
2. The composite unit is under Timoshenko beam theory at the effective matrix region between the external platelets ends.
3. As a small matrix space gap s between the ends of platelets, the bending moment and shear load are constant along it.
4. Also, The Timoshenko shear strain is concentrated between the ends of external platelets (see Figure 3.9).
5. The tension strain at the free surface of the matrix gap is half of the strain at the matrix gap between the platelets ends (see Figure 3.7).

When the contact between matrix platelets is bonded, the diagram of unit cell deformation can describe the equivalent rigidity, as shown in Figure 3.13.

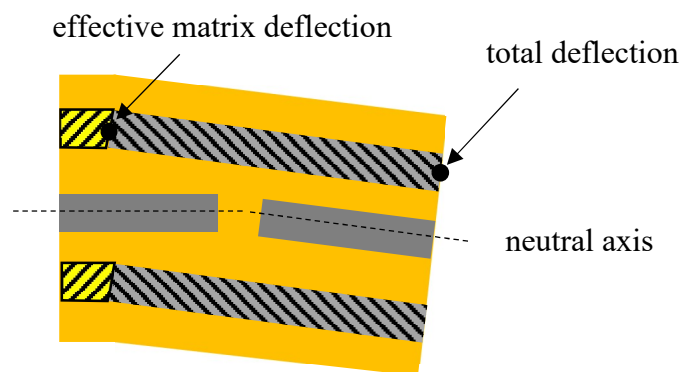


Figure 3.13: Diagram of unit cell deformation

As the Timoshenko beam theory that deals with beam bending angle θ and shear deflection w , the two governing equations of deflection are,

$$EI \frac{d\theta}{dx} = M \quad 3.9$$

Timoshenko formula as,

$$\frac{dw}{dx} = \theta - \frac{Q_x}{k_t A_t G} \quad 3.10$$

where,

$$G = \frac{E}{2(1 + \nu)} \quad 3.11$$

where M , Q_x , G , ν and k_t are the bending moment, local shear load, shear modulus, Poisson's ratio, and Timoshenko shear coefficient, respectively.

The moment in Equation 3.9 can be described by considering the equilibrium of the moment of effective regions at cross section a-a giving (see Figure 3.12),

$$2M_p + 2M_v = M \quad 3.12$$

where M_p and M_v are the moment reaction in platelet and moment in viscoelastic matrix, respectively. Each reaction moment for one-unit width (see Figure 3.12) can be calculated as,

$$M_p = \int_0^{h/2} \sigma_p y dy \quad 3.13$$

$$M_v = \int_{h/2}^{H/2} \sigma_v y dy \quad 3.14$$

where σ_p at $0 \leq y \leq h/2$ as,

$$\sigma_p(y) = E_p \varepsilon(y) \quad 3.15$$

at $h/2 \leq y \leq H/2$ as,

$$\sigma_v(y) = E_v \varepsilon(y) \quad 3.16$$

where E_p , E_v , G_v , σ_p and σ_v are the platelet modulus, viscoelastic modulus, viscoelastic shear modulus, normal platelet stress and viscoelastic normal stress, respectively.

By substituting Equations 3.16 and 3.17 into Equations 3.14 and 3.15, and substituting them into the preceding equations, the total bending moment formula is,

$$M = 2E_p \int_0^{h/2} \varepsilon(y) y dy + 2 E_v \int_{h/2}^{H/2} \varepsilon(y) y dy \quad 3.17$$

Substitute Equation and

$$M = \varepsilon_v h^2 E_v \left(1.2 + \frac{6E_v}{E_p - 5E_v} \right) \quad 3.18$$

Setting variable D as,

$$D = h^2 E_v \left(1.2 + \frac{6E_v}{E_p - 5E_v} \right) \quad 3.19$$

Then,

$$M = \varepsilon_v D \quad 3.20$$

Cantilever bending moment is,

$$M = PL \quad 3.21$$

Substituting Equation 3.21 into 3.22 gives,

$$\varepsilon_v = \frac{PL}{D} \quad 3.22$$

and noting that,

$$P = Q_x \quad 3.23$$

it is possible to write,

$$\varepsilon_v = \frac{Q_x L}{D} \quad 3.24$$

Effective bending angle (see Section 3.4.1) gives,

$$\theta = \frac{\Delta s}{h_e} \quad 3.25$$

where Δs is defined as,

$$\Delta s = \int_0^s \varepsilon_v dx \quad 3.26$$

Substituting Equation 2.26 into Equation 3.25,

$$\theta = \frac{s \varepsilon_v}{h_e} \quad 3.27$$

and therefore,

$$\theta = \frac{s}{h_{ef}} \frac{Q_x L}{D} \quad 3.28$$

The total deflection (see Figure 3.13) is,

$$\delta = w + \theta L_p \quad 3.29$$

where L_p is the platelet length

substitute Equation 3.21 into Equation 3.23,

$$\delta = \theta(s + L_p) - \frac{s Q_x}{k_t A_t G_v} \quad 3.30$$

the unit cell length L as,

$$L = L_p + s \quad 3.31$$

Then it can reformulate Equation 3.30 as,

$$\delta = \theta L - \frac{s Q_x}{k_t A_t G_v} \quad 3.32$$

Substitute Equation 3.28 into Equation 3.32,

$$\delta = \frac{s}{h_{ef}} \frac{Q_x L}{D} L - \frac{s Q_x}{k_t A_t G_v} \quad 3.33$$

The cantilever rigidity as,

$$EI_e = \frac{PL^3}{3\delta} \quad 3.34$$

Substitute Equation 3.33 into Equation 3.34,

$$EI_e = \frac{PL^3}{3 \left[\frac{s}{h_e} \frac{Q_x L}{D} L - \frac{s Q_x}{k_t A_t G_v} \right]} \quad 3.35$$

It can be simplified as,

$$EI_e = \frac{L^3}{3s \left[\frac{L^2}{h_e D} - \frac{1}{k_t A_t G_v} \right]} \quad 3.36$$

where the Timoshenko shear k_t constant is,

$$k_t = \frac{5}{6} \quad 3.37$$

3.4.3 Numerical model

This section presents the comparison between the equivalent rigidity obtained using a numerical model using the Finite Element (FE method) and the equivalent rigidity of the analytical model developed in Section 3.4.2. The purpose of this comparison was to evaluate the suitability of the assumptions and simplifications incorporated in the analytical model.

The comparison was carried out at modulus ratios of 0.01, 0.005 and 0.0005. Three specimens were designed with lengths 44, 88 and 176 mm each having 2414, 4790 and 9542 nodes and 308, 616 and 1232 elements, respectively. 20 node, three-dimensional brick elements were used to ensure that the strain distribution was represented as accurately as possible. The sensitivity of the equivalent rigidity to the Poisson's ratio of the matrix material was examined at the values 0.4, 0.44 and 0.48. The platelets were arranged as a staggered configuration within the matrix. The behaviour of equivalent rigidity was estimated numerically and compared with the analytical results. The FE run under static and dynamic conditions. The FE static equivalent modulus values were calculated by Equation 3.27, where the deflection was estimated from the FE model under cantilever conditions. Also, the equivalent modulus was calculated under the dynamic condition at the first three natural frequencies by Equation 3.8 as a cantilever model. A Matlab script was formulated to compute the equivalent rigidity according to the analytic EBMM model, as shown in Section 3.4.2.

Results for each different modulus ratio are presented in Tables 3.2, 3.3 and 3.4.

Table 3.2: Equivalent modulus of composite at $E_p=200$,
 $E_v=2$ GPa, $\rho_p=7850$ $\rho_v=950$ kg/m³, $\nu_p=0.3$

units	L mm	ν_v	E_e GPa		
			analytic	FE static	FE at f_l
4	44			12.2	10.3
8	88	0.4	13.52	13.73	12.26
16	176			14.3	11.34
4	44			12.4	11.54
8	88	0.44	13.8	13.9	12.6
16	176			15.3	14.7
4	44			12.5	11.9
8	88	0.48	14.19	14.7	13.2
16	176			16.6	16.7

Table 3.3: Equivalent modulus of composite at
 $E_p=200$, $E_v=1$, GPa, $\rho_p=7850$ $\rho_v=950$ kg/m³, $\nu_p=0.3$

units	L mm	ν_v	E_e GPa		
			analytic	FE static	FE at f_l
4	44			7.3	6.4
8	88	0.4	7.16	8	7.1
16	176			8.5	8.23
4	44			6.6	6.5
8	88	0.44	7.31	8.1	7.38
16	176			9.1	8.56
4	44			6.8	6.7
8	88	0.48	7.47	8.6	7.8
16	176			8.9	10.2

Table 3.4: Equivalent modulus of composite at $E_p=200, E_v=0.1$ GPa, $\rho_p=7850, \rho_v=950$ kg/m³, $\nu_p=0.3$

units	L mm	ν_v	E_e GPa		
			analytic	FE static	FE at fI
4	44			1.01	0.94
8	88	0.4	0.955	1.2	1.12
16	176			1.3	1.23
4	44			1.04	0.97
8	88	0.44	0.973	1.25	1.17
16	176			1.41	1.44
4	44			1.11	1.02
8	88	0.48	0.991	1.35	1.26
16	176			1.51	1.7

From the results presented, a number of important observations can be made. These relate to the effect of beam length, Poisson's ratio and type of analysis.

It is clear the beam length has an effect on the equivalent modulus obtained using the FE results. This is because shear deformation becomes a significant component in the flexural deformation of short beams, but this is not captured by Equation 3.34, which attributes all the deflection to bending. As a result, the equivalent modulus of the shorter beams can be as much as 25% lower than that for the longer beams.

The FE results are sensitive to Poisson's ratio. Equivalent modulus values can be up to 15% higher when the Poisson's ratio is 0.48 than when it is 0.4. This trend in sensitivity is also matched by the analytical model and shows the importance of the matrix zone around the plate ends (illustrated in Figures 3.11 to 3.13).

The FE dynamic analyses generally provide lower values of equivalent modulus than the equivalent static cases. The likely reason for this is that the platelets gain additional rotation inertia in the dynamic analyses, thereby reducing the natural frequency in a way that is not captured by Equation 3.8.

Overall, the analytical results match the FE results in a reasonably close manner, being within 10% for most cases. Clearly, the analytical results are not affected by the length of the specific loading type because of the nature of the formulation. The differences arise where the local deformations depart from the assumptions inherent in the model - this is particularly the case for the results in Table 3.4 where the extremely low modulus ratio allows platelets to rotate such that they are no longer parallel with each other.

3.5 Conclusions

Several conclusions can be drawn from the work done in this chapter:

- The analytic model using EBMM is able to estimate the effective flexural modulus, accounting for a modulus ratio less than 0.125 of the two materials used in the composite.
- The parallel/series approach can be used instead for staggered structure when the modulus ratio greater than 0.125 to estimate the effective modulus.
- The dominant strain concentration is between the ends of the upper and lower platelets.
- The strain distribution is zigzag at the polymer between the platelets ends.
- The bending angle comes from the effective region where the zigzag strain occurs.
- The effective region can be used to formulate the effective flexural modulus.
- The Timoshenko shear load appeared around the middle of the central platelets as a thick unit cell.
- The effective flexural modulus is sensitive to the Poisson's ratio of the polymer.

Chapter 4

Experimental studies of the staggered composite

4.1 Introduction

Composites comprising viscoelastic matrix can provide considerable levels of damping, allowing vibrations to be suppressed. However, properties can vary with temperature. In particular, stiffness usually drops considerably as damping increases and can result in reduced vibration suppression. The ability to predict the sensitivity of the stiffness to temperature is therefore very important.

In Chapter 3, the equivalent modulus of the staggered composite under bending deformation was investigated through a formulated analytical model and compared with results from finite element analysis. The comparison showed that the analytical model was able to match finite element results with reasonable accuracy. This chapter focuses on the ability to predict theoretically the equivalent modulus of systems experiencing massive modulus difference between the viscoelastic matrix and platelet reinforcement as the properties change with temperature. Validation is carried out by comparing predicted behaviour with that observed during physical experiments.

4.2 Methodology

This chapter reports experiments that examine the performance of the staggered composite under flexural loading and compares experimentally observed behaviour with theoretical predictions. These studies involved several stages as described below.

The first step was to manufacture test specimens. Dimensions and materials were selected to simplify manufacture and ensure repeatability rather than to optimise performance for a particular set of conditions. This was particularly important when considering the need to allow comparison with theoretical predictions.

Quasi-static three-point bend testing was conducted at room temperature in order to allow investigation of the strain distribution through the beam thickness. Using Digital Image Correlation (DIC) This was an important activity as the analytical model was based on assumptions of the strain distribution in the matrix. These studies also provided load-deflection data.

To cover a large range of modulus ratios, dynamic testing was required at different temperatures and frequencies. This was considered important as it was noted in Chapter 3 that performance was strongly dependent on the modulus ratio. Initial dynamic testing was conducted at room temperature in the form of free vibration tests with cantilever boundary conditions. Equivalent properties of the composite were then obtained from the tests. While the testing was relatively easy to carry out at room temperature, it was considered unsuitable for use at different temperatures. Consequently, the temperature-frequency testing was carried out in a Dynamic Mechanical Analysis (DMA) machine using a three point bend configuration. The disadvantage of this approach was that it required a shorter beam which would be subject to significant shear deformation not captured in the analytical model. However, the ability to control temperature and frequency more precisely was considered to be more important.

The final stage in this activity was to compare the measured flexural rigidity with that predicted theoretically. The main focus was on FE predictions because of the use of the short beam that was used in the experiments.

4.3 Specimen manufacture

For convenience, specimens were produced using epoxy with viscoelastic behaviour near room temperature and steel platelets. These were selected as they had properties known to be stable with time, temperature and humidity and therefore would provide reliable results for validation purposes.

An aluminium mould was designed and manufactured to produce a rectangular epoxy specimen as a viscoelastic material. The mould was made from a base, four bars and two fasteners plates, as shown in Figure 4.1a. Plastic straps were printed by a 3D printer, as shown in Figure 4.1b, for fitting and guiding the steel platelets as a staggered pattern into the epoxy matrix. A steel upper holder was designed and manufactured, as shown in Figure 4.2. This holder was designed to keep the plastic strips locating the platelets firmly in position the polymer matrix cured.

The viscoelastic material was an epoxy-resin with low pre-cure viscosity and glass transition close to room temperature. This was selected to simplify specimen manufacture and subsequent testing. The matrix mixture involved the co-reaction of the base resin EL5, curing agent polyetheramine D400, co-reactant polyetheramine D2000 and accelerator A399 with mass fractions as indicated in Table 4.1.

Table 4.1: Epoxy ingredient mass fraction

Material	base resin	curing agent	co-reactant	accelerator
Mass fraction %	52.19	21.66	23.54	2.61

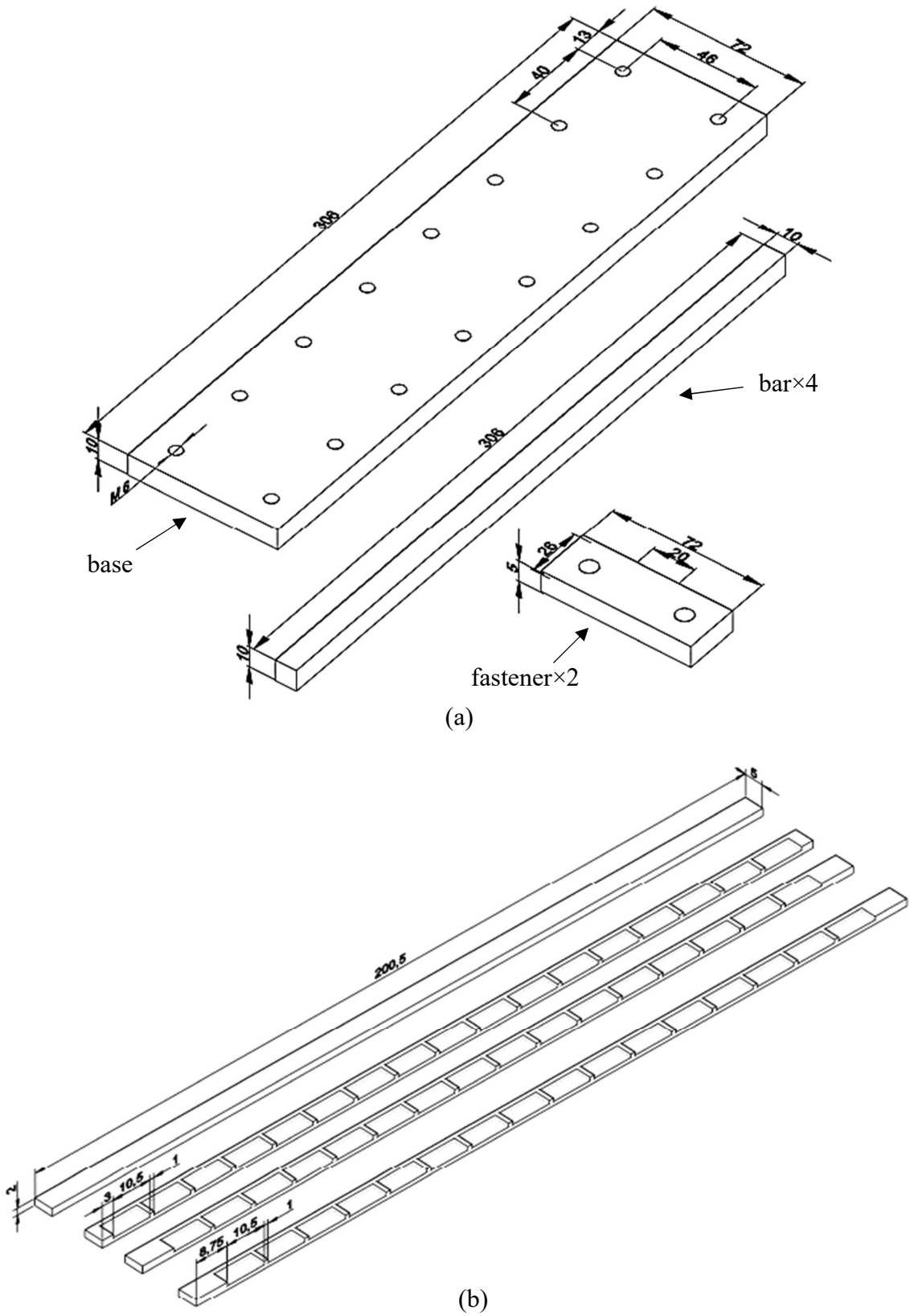


Figure 4.1: Drawing of Specimen mould (a) aluminium elements (b) plastic straps

Mould release spray was applied to release casting materials from the epoxy-resin matrix. Specimens were made by mixing the ingredients thoroughly in an epicyclic mixer and pouring them into the mould. Next, the holder steel clamped the platelets as the designed configuration, as shown in Figure 4.3a. The rectangular mould, as shown in Figure 4.3b, cast the epoxy-resin and the clamped platelets, as shown in Figure 4.3c. Next, the composite was allowed to cure at room temperature for 24 hours. Then, the upper holder can be removed, as shown in Figure 4.4a. The matrix specimen can be prepared by casting the epoxy resin mixture directly into the mould, as shown in Figure 4.4b. The specimen within the mould was cured in an oven for 10 hours at $100\text{ }^{\circ}\text{C}$. Finally, the specimens were obtained, as shown in Figure 4.4c.

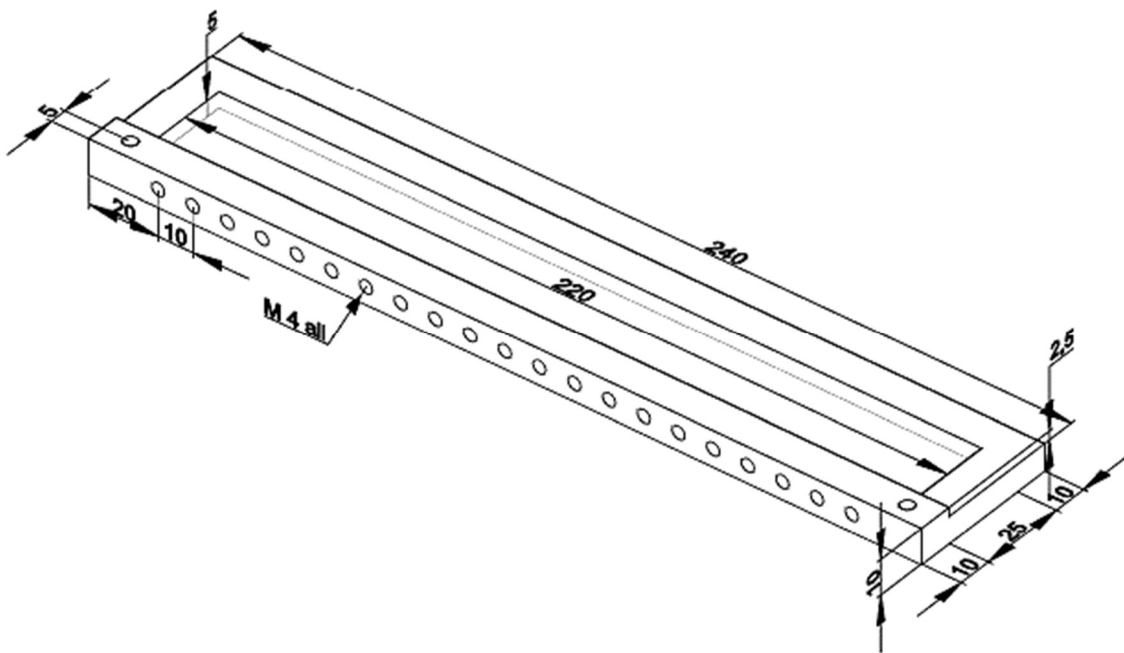
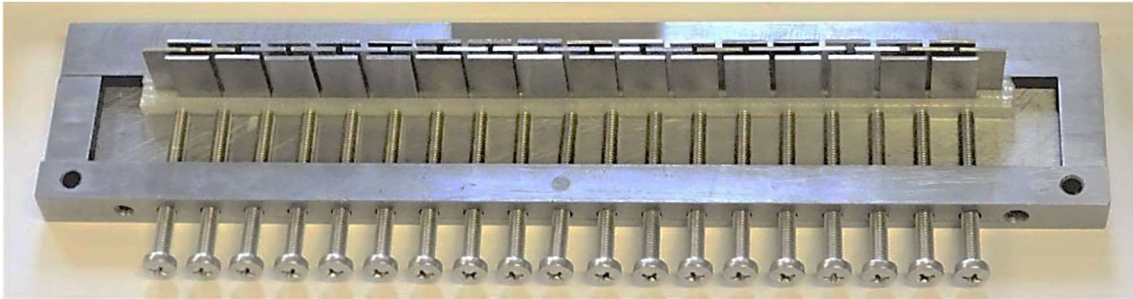


Figure 4.2: Steel upper holder drawing



(a)

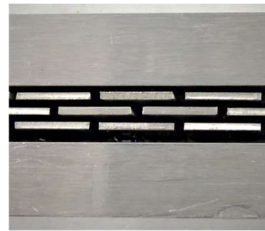
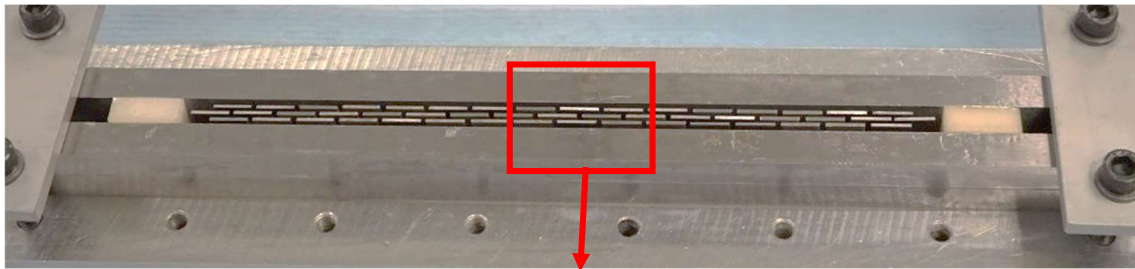


(b)

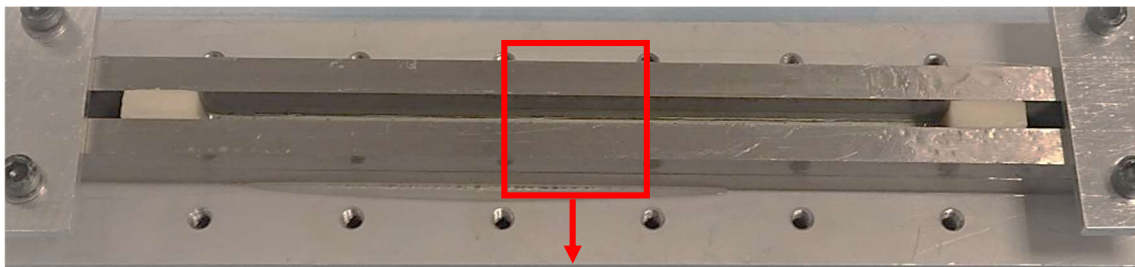


(c)

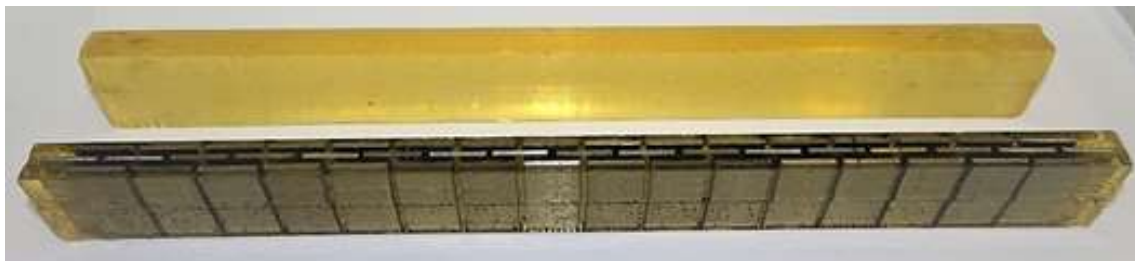
Figure 4.3: The mould elements (a) platelets holder (b) mould (c) platelets into matrix



(a)



(b)



(c)

Figure 4.4: The casting (a) platelets-matrix (b) matrix (c) specimens

4.4 Three point bending test

Bending tests were conducted at a deflection rate of 1 mm/min using a Tinius Olsen H25KS test machine. The specimen setup for each test is shown in Figure 4.5. Each beam was supported on 10 mm diameter rollers. The load was applied as a displacement-controlled motion of the same diameter central roller. The span distance between the two supporting rollers was 80 mm. The three specimens steel, epoxy and platelets-epoxy were tested to find the flexural modulus for each of them.

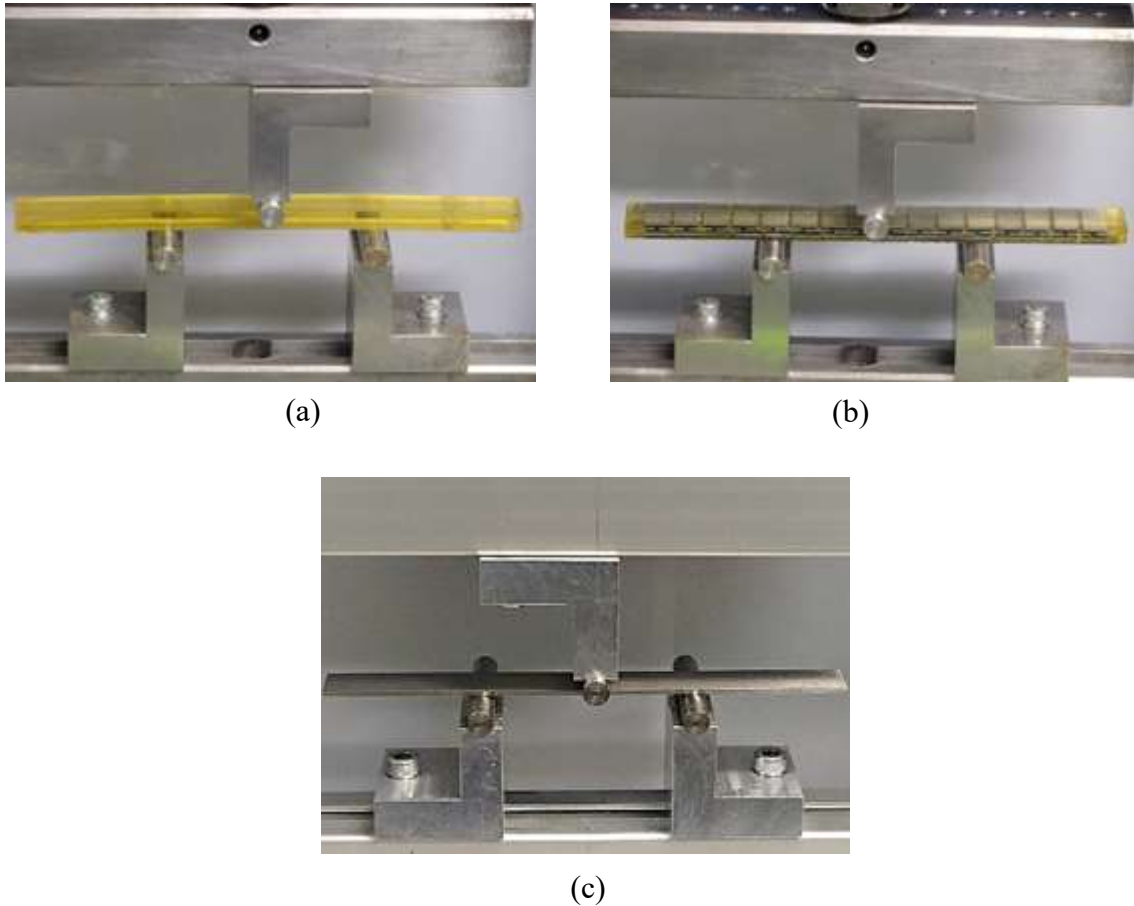


Figure 4.5: Three-point bending beam test (a) epoxy (b) platelets-epoxy (c) steel

The individual and composite specimen properties weight, dimensions and density were measured as shown in Table 4.2.

Table 4.2: Dimensions and density of specimens

Specimen	Length mm	Width mm	Height mm	Mass g	ρ kg/m ³
Epoxy-steel	196	20.24	8.05	104.75	3270
Epoxy	196	20.12	7.85	34.9	1130
Steel	198	20	2	62.44	7889

These properties affected the static and dynamic behaviour of the staggered composite. Also, the mechanical properties were one of the requirements to design the numerical models.

Load–deflection diagrams were obtained for each specimen, as shown in Figure 4.6. The average (tangent) flexural modulus of each diagram has been computed under elastic zone by three-point bending deflection equation as,

$$\delta = \frac{Pl^3}{48EI} \quad 4.1$$

These results showed that the flexural modulus of the epoxy-resin beam was 12.6 MPa while the equivalent modulus of the composite beam was 137.8 MPa, which means the modulus was increased by nearly 11 times. Note that the behaviour in the platelet-epoxy curve (4.6c) is thought to be caused by local yielding in the specimen. The modulus estimate was made from data below this kink only. Then, the analytic and numerical results agree with the experimental modulus result, as shown in Table 4.3.

Table 4.3: Modulus results for the epoxy-steel specimen from three point bend test

Modulus	FE	Experimental	Analytic
E MPa	128.9	137.8	133.5

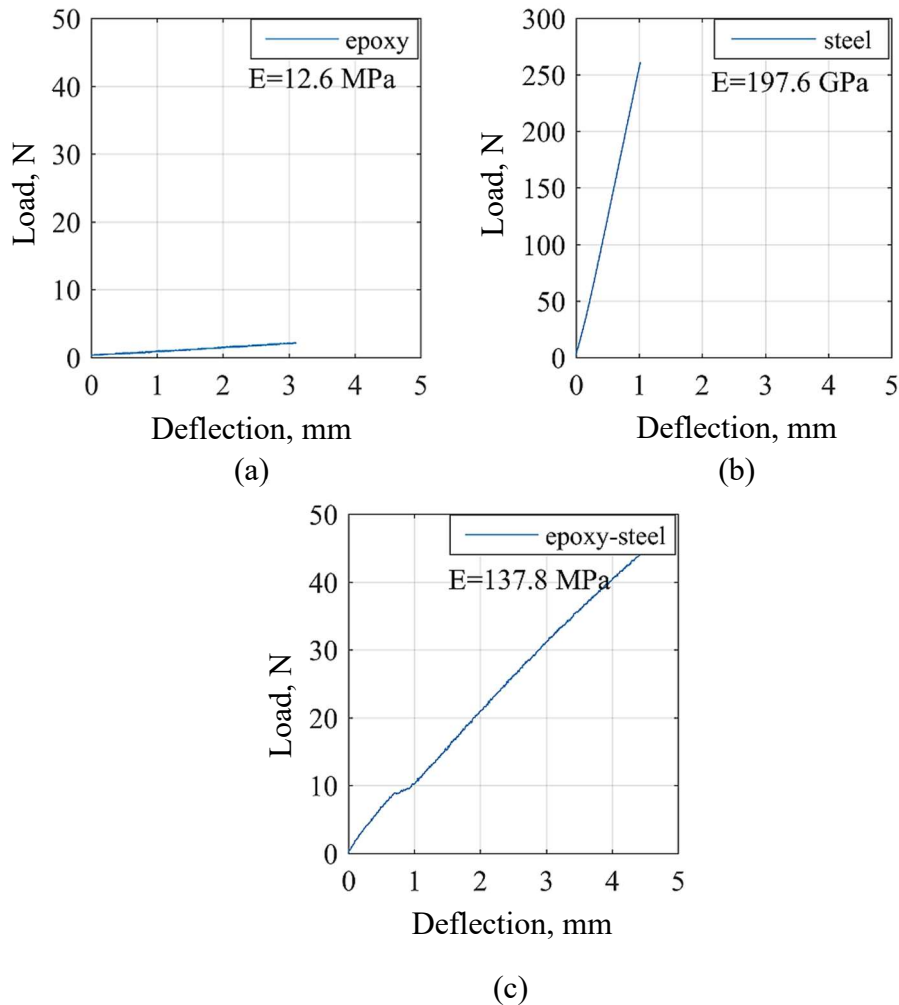


Figure 4.6: Three point bending test (a) epoxy beam (b) steel beam specimens (c) platelets-epoxy beam

4.5 Digital Image Correlation experiment (DIC)

DIC was conducted to measure the surface strain distribution across the thickness of the staggered specimen during three-point bending deformation. The specimen side was painted white and sprayed black colour for optical detecting the displacements during bending deformation, as shown in Figure 4.7. This correlation technique is designed to detect the points of the highest grayscale colour. The displacement vector was measured between the highest grayscale point during the detecting.

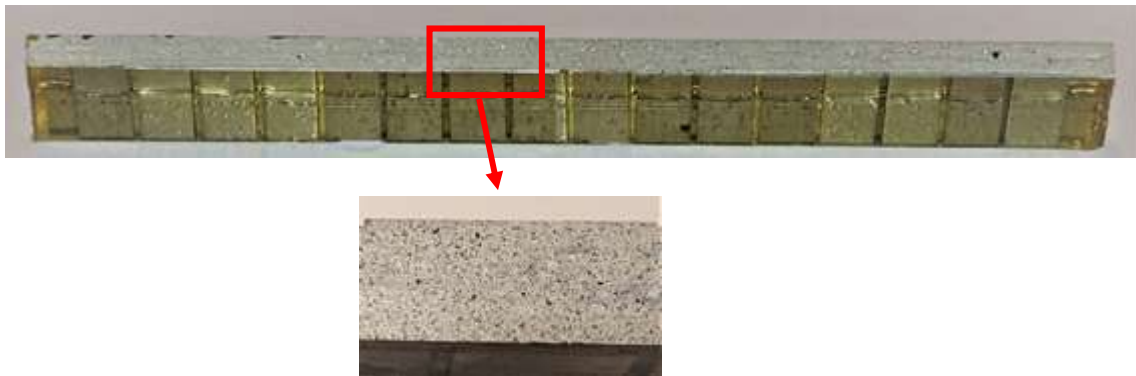


Figure 4.7: The painted and sprayed composite specimen

The DIC optical system was controlled by software calibrating the parameters of displacement measurement. In this test, the DIC was organised for recording 10 images rate, and the total images number were 5000. The resolution was calibrated to be 250 pixel/mm, which gave highly accurate data of strain through the surface. The camera amounted perpendicular to the targeted surface of the specimen to be recorded, as shown in Figure 4.8.

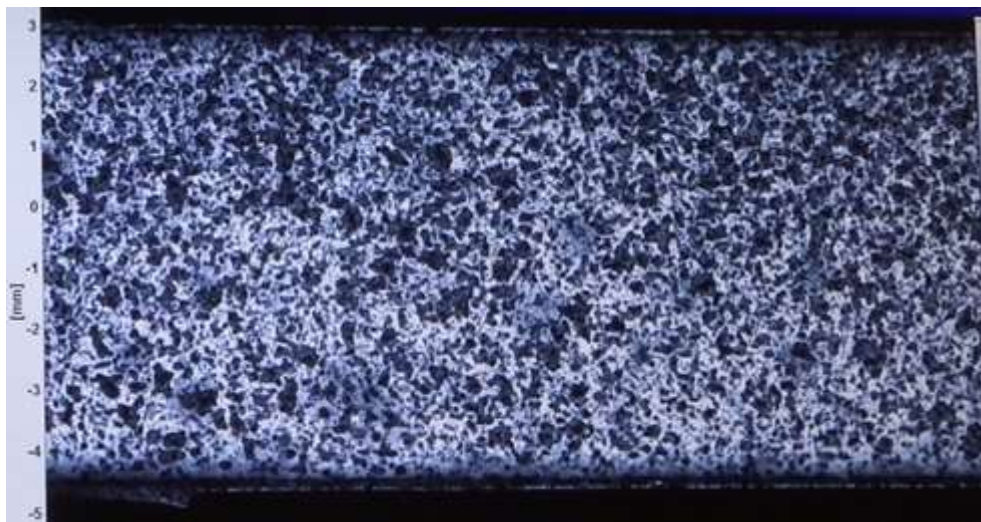


Figure 4.8: The monitored painted surface of specimen

The Poisson's ratio can be obtained from the results of the DIC experiment to justify the estimation of effective deflection, as shown in Equation 3.26. The measured Poisson's ratio was at the effective region between the ends of lower platelets, as shown in Figure 4.9a at the red line. The results were obtained in the diagram, as shown in Figure 4.9b. The average Poisson's ratio value was 0.488, which is reasonable for a polymer in the transition zone.

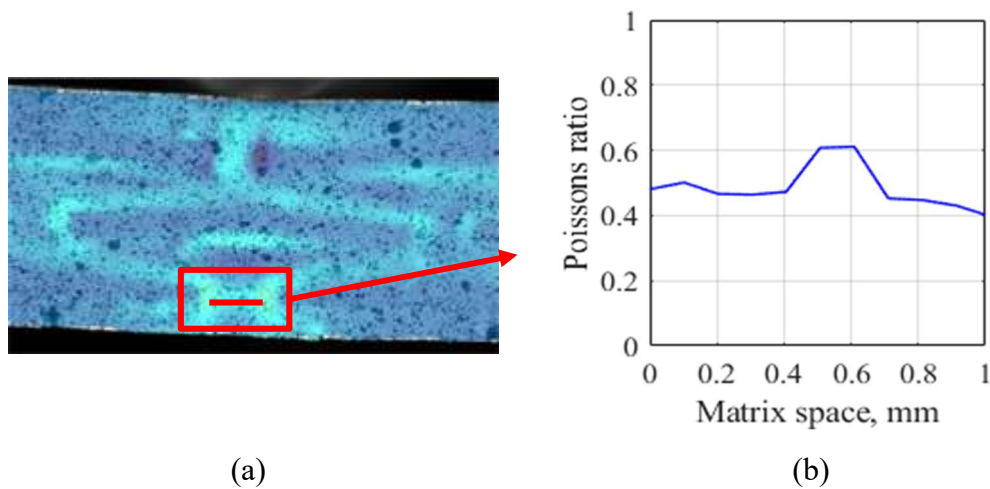


Figure 4.9: Three point bending test (a) monitored composite region (b) Poisson;s ratio results

However, the two results, as shown in Figure 4.9b above 0.5 because the uncertainty movement at few points, may occur due to noncorresponding paint deformation with the specimen surface. Standard deviation calculated for Poisson's ratio results according to the formula as,

$$dev = \sqrt{\frac{\sum_{i=1}^{i=n} (v_i - v_{av})^2}{n}} \quad 4.2$$

where dev and n are the standard deviation and the number of results, respectively.

The standard deviation calculated was 0.04, which means the most considerable results between the average value plus/minus the deviation standard. As a result, the two results of Poisson's ratio where outside the deviation limit can be considered as uncertain results.

In this experiment, the strain distribution through the composite at sections a-a and b-b (see Figure 3.7a) were obtained during the monitoring three-point bending test by the DIC system. The data was selected at deflection 2 and 4 mm to compare the equivalent modulus results at each of them with the value obtained from the load-deflection diagram (see Figure 4.6c). The DIC experimental strain distribution had a zigzag form, as shown in Figure 4.10, at section a-a like the zigzag strain behaviour of the numerical model in Section 3.3. The strain is concentrated at the matrix material between the platelets ends in zigzag behaviour. Also, the strain behaviour at section b-b is like the strain behaviour at section b-b in the numerical model in Section 3.3. As a result, the DIC experimental strain behaviour agrees well with the numerical results.

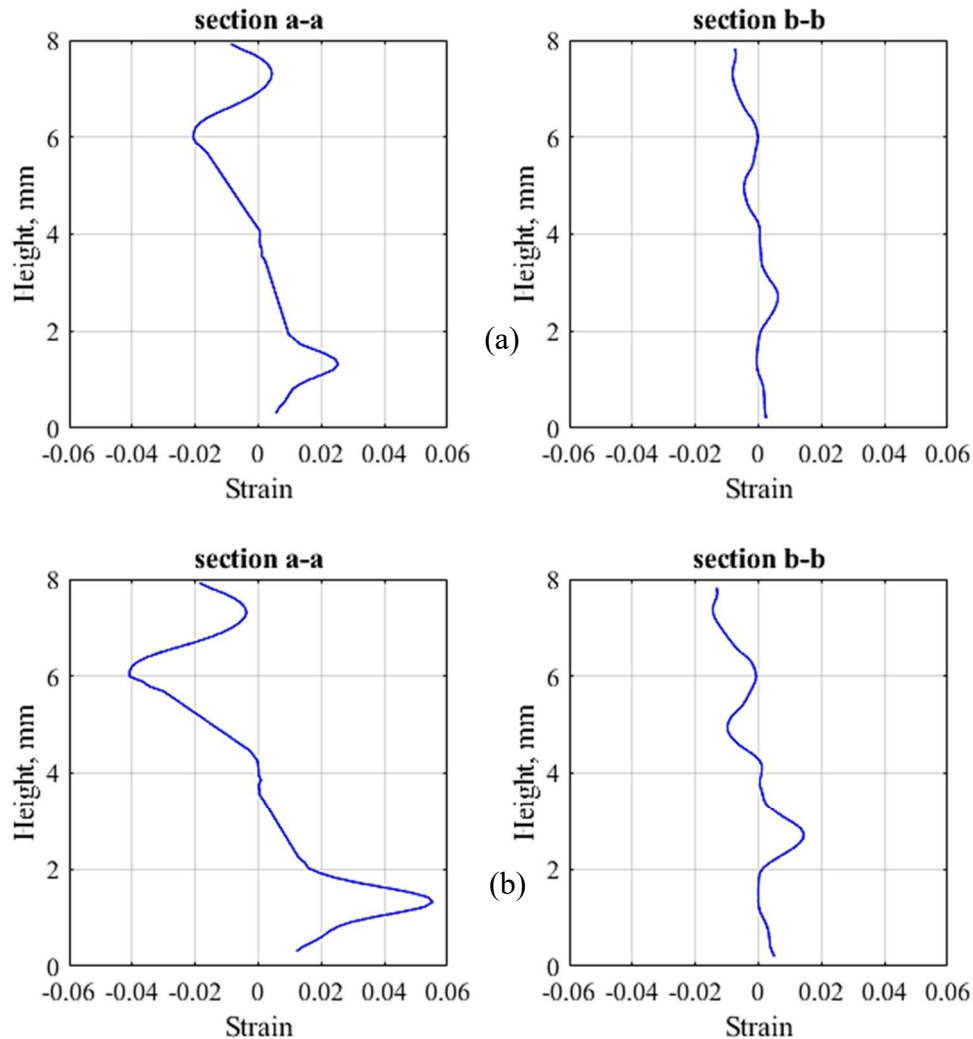


Figure 4.10: DIC normal strain result of three point bending test (a) at 2 mm deflection (b) at 4 mm deflection

4.6 Free vibration test

Free vibration tests were conducted to obtain the natural frequencies for epoxy and staggered composite specimens. Rectangular cross-sectioned beams with dimensions (see shown in Table 3.6) were used. As part of the specimen had to be clamped, a free length of 166 mm was used for both beams. The equivalent modulus of elasticity was computed using the natural frequency formula (see Equation 3.8). This experiment followed the validate the analytical model in dynamic load.

The vibration response of each specimen was obtained in the cantilever condition by impacting the free end using an instrumented hammer. The test setup is shown in Figure 4.11. An accelerometer of mass 1.36 grams and sensitivity 100.7 mV/ms^{-2} was fixed at the free end of the cantilever. The force transducer of sensitivity of 43.1 mV/N was connected at the end of the hammer.

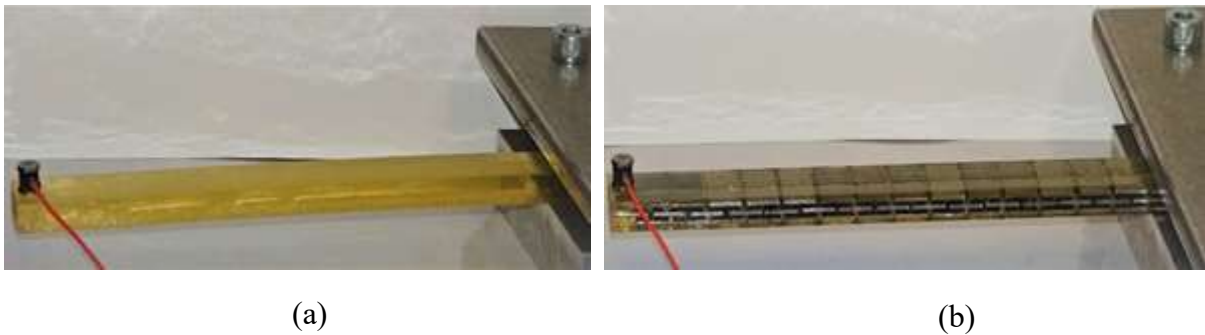


Figure 4.11: Free vibration test (a) epoxy specimen (b) staggered epoxy-steel specimen

The purpose of the free vibration tests was to obtain the frequency response function (FRF) in order to estimate the fundamental natural frequency and compute the flexural modulus under dynamic conditions. Matlab code was used to translate vibration signal from the time domain to the frequency domain. The results of frequency domain signals of both epoxy and the epoxy-steel beams are shown in Figure 4.12. The staggered platelets effect can be seen in the behaviour of the frequency response. The natural

frequencies of the cantilever beams obtained from the free signal for each specimen vibration were shown in Table 4.4, and then the modulus was calculated by Equation 3.8.

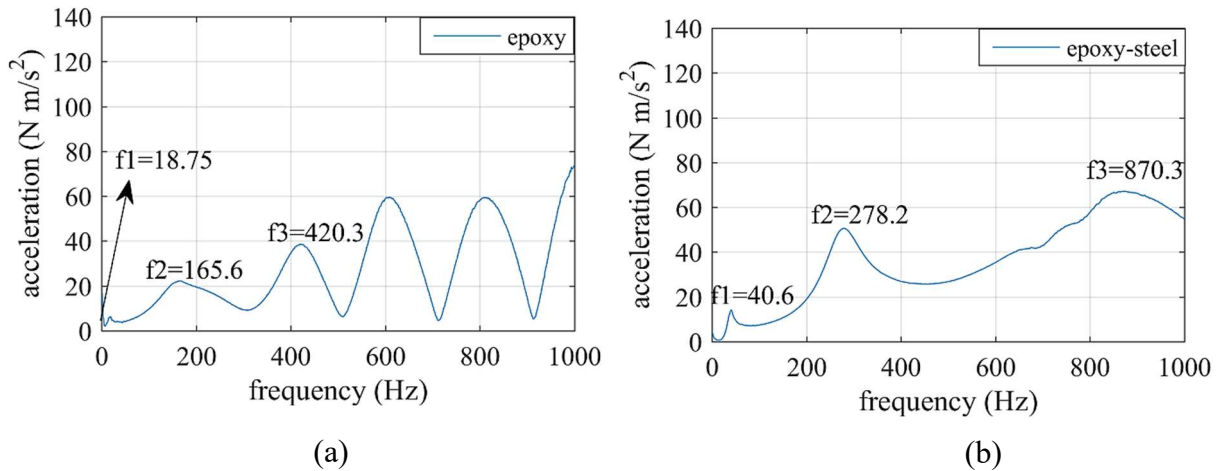


Figure 4.12: Frequency response function test (a) epoxy specimen (b) staggered epoxy-steel specimen

To allow comparison, the epoxy-steel composite specimen was modelled and simulated by finite element method with FE software. A modal analysis feature was employed to work out the natural frequency. Element size was determined to be 1 mm of 20 node-brick element to generate a fine three-dimensional mesh of the cantilever model. The dimensions of the steel platelets are 10 mm in length, 1 mm in width and 1 mm in height. The dimensions of the specimen were 166 mm in length, 1 width and 8 height. One element of 1 mm results in faster computation than the real width 20 mm without influencing the output results according to Equation 3.8.

The equivalent modulus values of the composite obtained from prediction and experiment are shown in Table 4.4. Here, the FE and experimental predictions used results for the first natural frequency.

Table 4.4: Flexural modulus results for epoxy-steel specimen

Modulus	FE	Experimental	Analytic
E MPa	2220	2458	2381

It can be seen from the results of the free vibration test (Table 4.4) that the differences in equivalent modulus between experiment, FE and analytic models are less than 10%. An equivalent level of similarity can be seen for the earlier static bend test results in Table 4.3. This gives an indication of the accuracy of the models. Note that the actual stiffness values in the dynamic test are much higher than those seen in the static test because of the viscoelasticity of the polymer.

4.7 Temperature and frequency dependency test

The Metravib Viscoanalyser VA2000 machine was used to conduct low-frequency dynamic mechanical analysis (DMA) tests on the viscoelastic and staggered composite beams. For this testing, shorter beams were manufactured – as shown in Figure 4.13 – where both configurations have 8 mm height, 20 mm width and a total length of 70 mm. The specimen length dimensions were chosen according to the chamber size of the DMA machine. Both support ends were clamped to maintain the specimens during the test. The span distance was 50 mm according to the available space for the roller support ends.

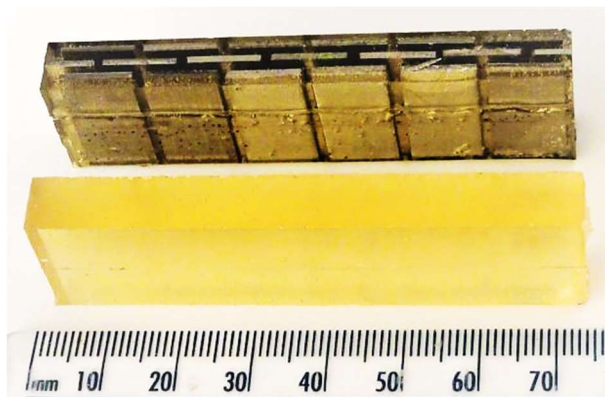


Figure 4.13: DMA specimens

Cyclic sinusoidal displacement was applied at the middle of the specimens. The experiment was conducted at a range of frequencies and temperatures values.

4.7.1 Methodology

Three-point flexure experiments were performed on viscoelastic beam and staggered composite beam using the DMA machine. The loss factor values were obtained from the phase angle between applied force and resulting displacement. The equivalent modulus was provided by the software of the DMA machine. The clamped force was applied on the middle of the clamped-clamped beam as a three point bending setup, as shown in Figure 4.14. and was obtained from the specimen stiffness and an assumption of homogeneous properties for the dimensions and loading regime considered.

The temperature domain and frequency domain for viscoelastic beam and staggered beam were depicted to show the compromising between the modulus and damping. The effect of reinforced platelets appeared in the plot behaviour of the two beams. These two domains can be used to balance between the damping and modulus of viscoelastic material and the damping and equivalent modulus of staggered platelets composite material.

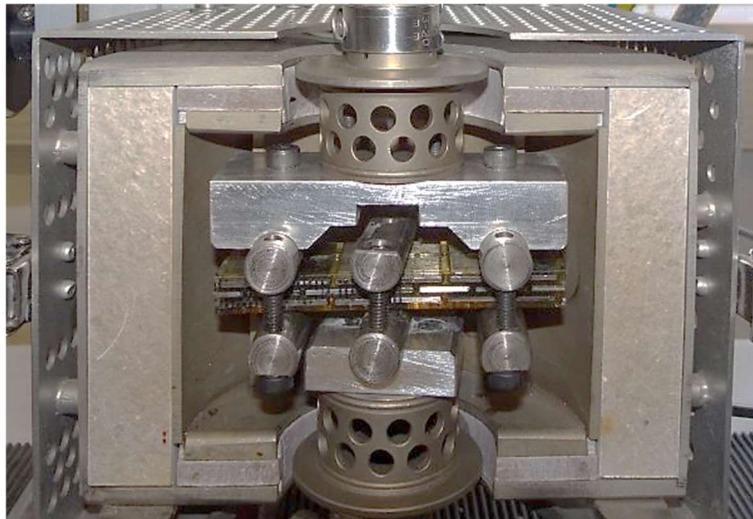


Figure 4.14: Specimen test setup

4.7.2 The temperature domain

During the DMA test, experimental loss factor, loss modulus and elastic modulus of the epoxy and epoxy-platelets beam were plotted with respect to the temperature. The domain of temperature was between 25 °C and 100 °C with interval step 5 °C. The temperature effects between the specimens can be seen in the elastic modulus and loss factor behaviour.

In a thermoset epoxy, the mechanical properties vary depending on the region in which they are operating. The glassy region is at the lowest temperature. In this region, the loss factor is at a minimum value while the material's elastic modulus is at its maximum value. In the glassy region, the loss factor increases rapidly with respect to the temperature increase while the modulus decreases gradually. The second region is the transition where a peak occurs for the loss factor. In this region, the modulus decreases rapidly with temperature increase. The third region is rubbery where both the loss factor and the modulus are low.

4.7.3 The frequency domain

The domain of frequency was applied at 0.02 mm displacement, between 5 Hz and 100 Hz with interval step 5 Hz.

For viscoelastic materials such as polymers, the mechanical properties vary with the rate of loading. Increasing strain rate results in increasing the elastic modulus. Consequently, the value of frequency affects the flexural modulus in this experiment. The modulus of the epoxy increases with respect to the increase of frequency. The loss factor initially increases with respect to the frequency increase to the peak value and subsequently decrease with respect to the frequency increase.

4.7.4 The results of the experiment

The section is devoted to the discussion of the results of the epoxy and composite beams that were obtained under flexural loading at different frequencies and temperatures. The loss factor, loss modulus and flexural modulus were plotted with respect to the temperature and frequency. The loss factor was considered to evaluate the

damping levels in both beams. The results then for the properties comparison between the epoxy and epoxy-platelets beams.

For the loss factor with respect to the temperature, as shown in Figure 4.15, the loss factor initially increases with respect to the temperature increase. Then, it reaches the peak values at T between $40\text{ }^{\circ}\text{C}$ and $45\text{ }^{\circ}\text{C}$ for both the epoxy and staggered specimens. Subsequently, it decreases with respect to the temperature. This behaviour occurs in transition region that the viscoelastic materials have practical damping. These behaviours for both specimens occur at frequency levels between 25 Hz and 100 Hz .

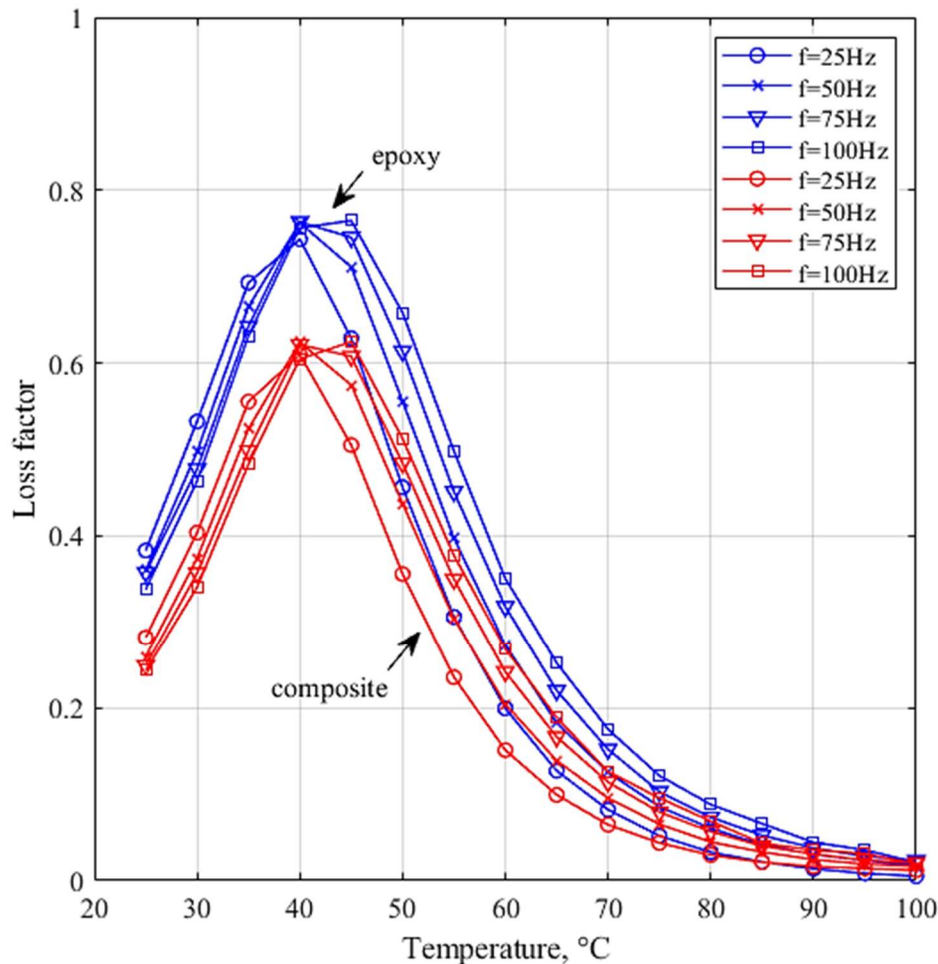


Figure 4.15: Loss factor behaviour with respect to the temperature

The loss factor values are plotted against frequency rather than the temperature in Figure 4.16. It can be seen that the values change only slightly over the frequency range 20-100

Hz. This is because the temperature-frequency equivalence for polymers links temperature change to the logarithm of frequency change - so in this case, the range considered (from 20-100 Hz) is relatively narrow.

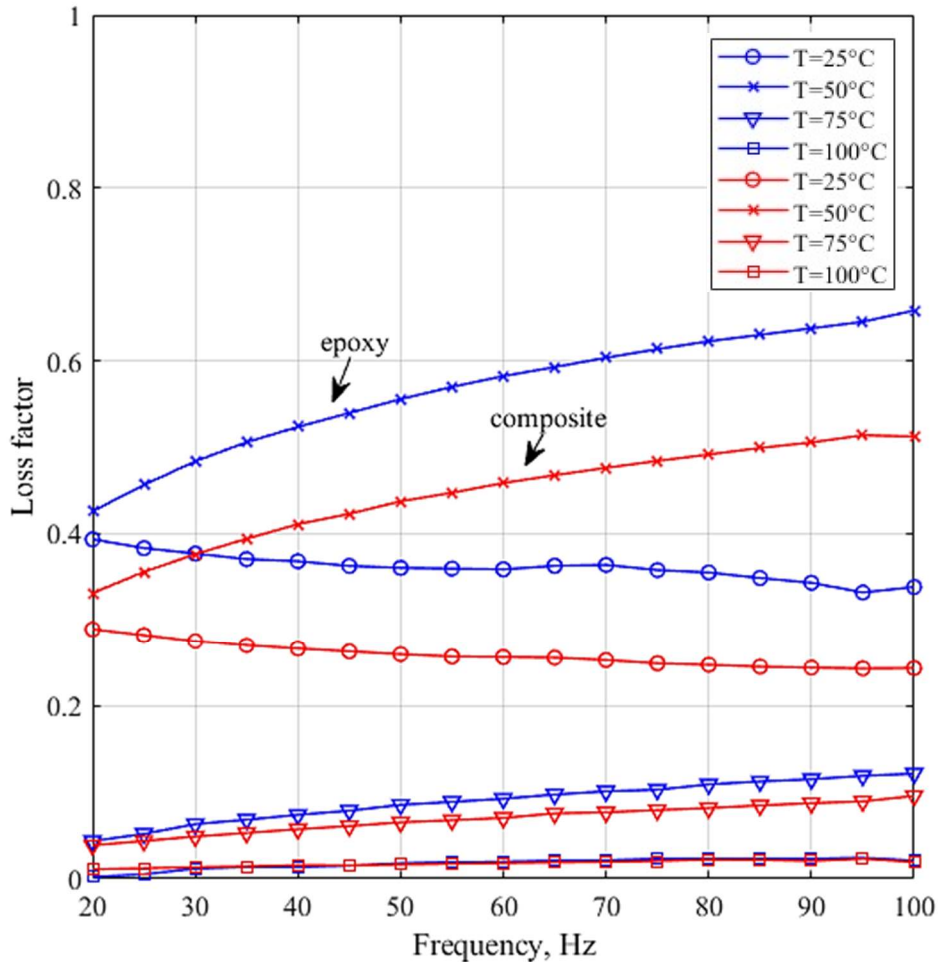


Figure 4.16: Loss factor behaviour with respect to the frequency

The loss modulus has an inverse correlation with respect to the temperature in the transition region, as shown in Figure 4.17. Physically, vibration attenuation is directly correlated to loss modulus. While the reduction in modulus over the temperature range is dramatic, it can be seen that the composite is consistently much higher than the epoxy alone, demonstrating its effectiveness.

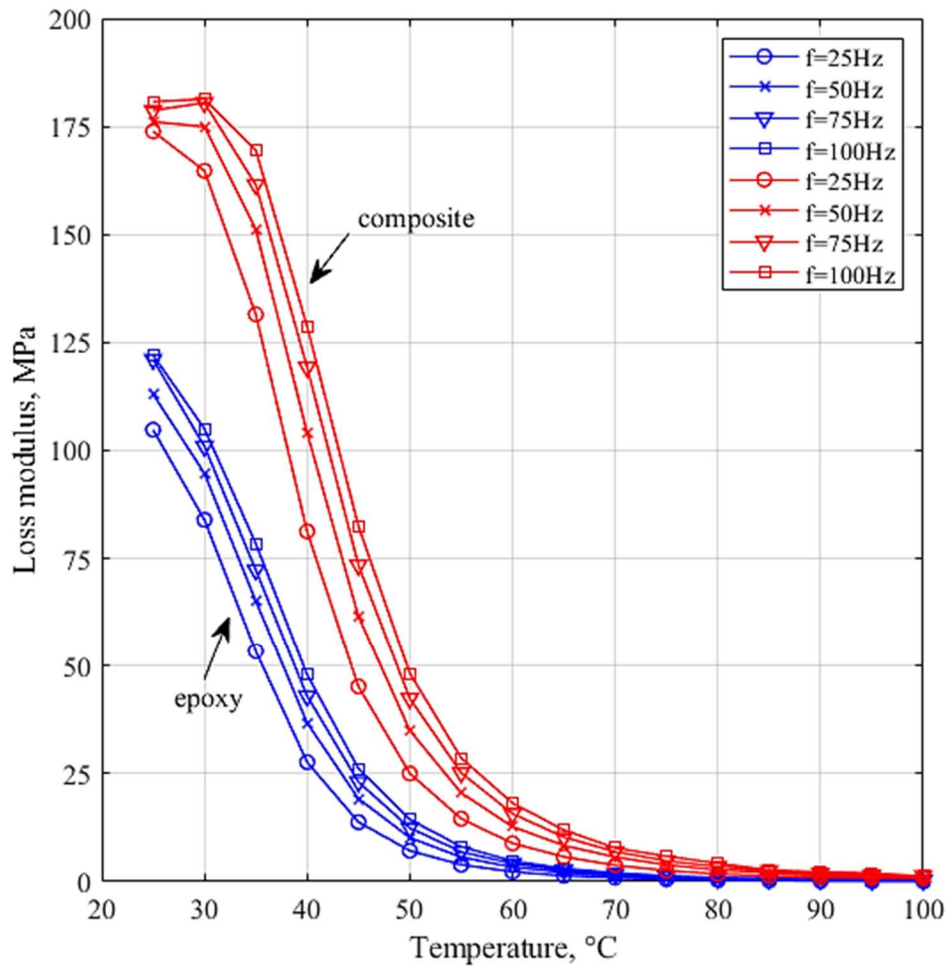


Figure 4.17: Loss modulus behaviour with respect to the temperature

The loss modulus increases with respect to the frequency increase for both specimens with respect to the frequency range, as shown in Figure 4.18. The largest values of loss modulus were described in behaviours at temperature 25 °C, while the largest loss factor behaviours were at temperature 50 °C (see Figure 4.16) because of the behaviour of elastic modulus, as shown in the next figures.

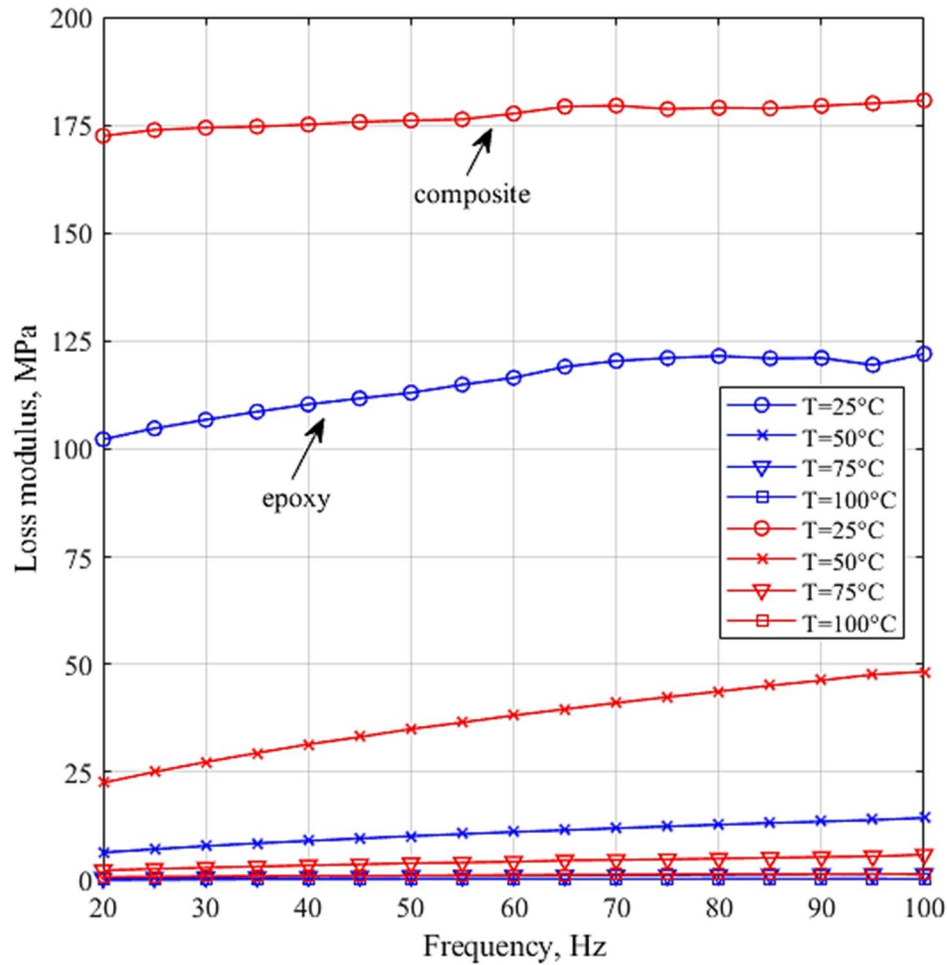


Figure 4.18: Loss modulus behaviour with respect to the frequency

Like the loss modulus, the elastic modulus value has an inverse correlation with respect to the temperature in the transition region, as shown in Figure 4.19. The elastic modulus of the epoxy and composite specimens are at the lowest value with the highest temperature. Sensitivity to temperature tends to vanish above 60 °C indicating that above this, the material is in the rubbery zone. It can be seen that the reinforcing effect of the platelets is highest when the modulus of the viscoelastic is in the rubbery zone but remains significant right down to room temperature.

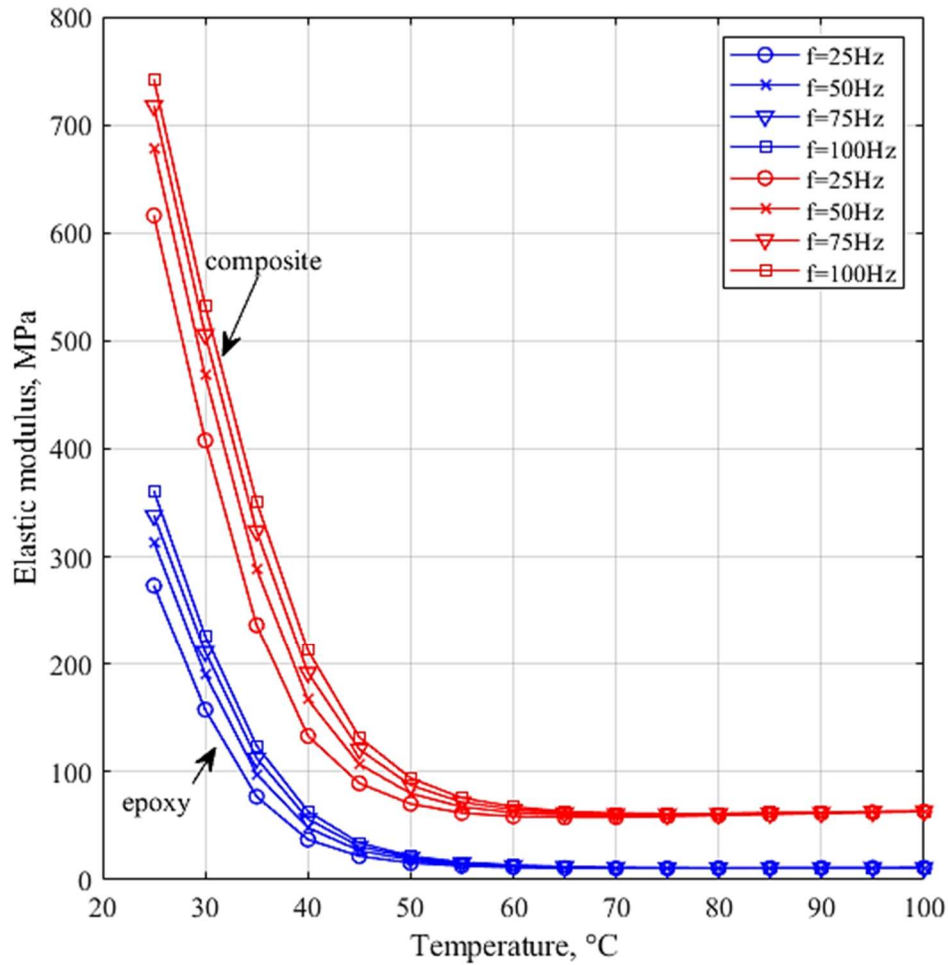


Figure 4.19: Elastic modulus behaviour with respect to the temperature

As the strain rate increases, the elastic modulus has a direct proportion to the frequency values for both specimens, as shown in Figure 4.20. However, the slope of the increase behaviour has an inverse proportion to the temperature. Also, the rapid decrease of the elastic modulus with respect to the temperature result in the massive difference between the behaviour at temperature 25 °C and the behaviours at temperatures 50, 75 and 100 °C.

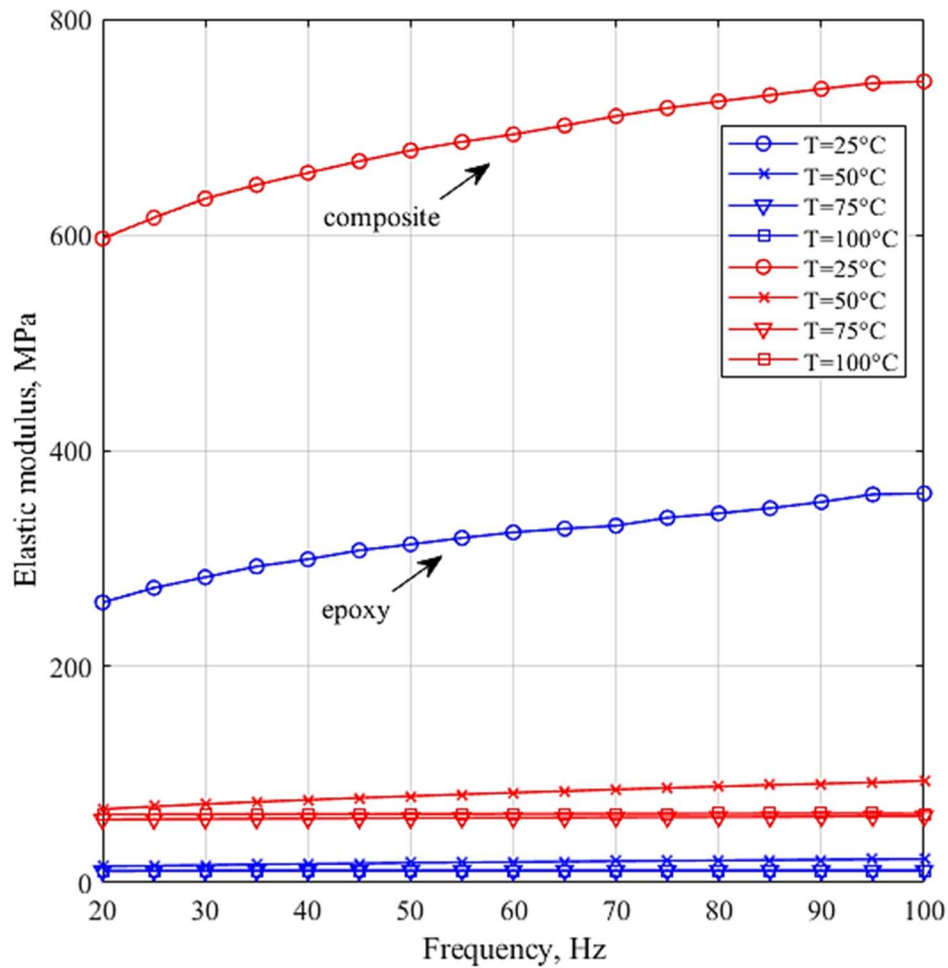


Figure 4.20: Elastic modulus behaviour with respect to the temperature

4.8 DMA numerical simulation

Finite element models were constructed to simulate the dynamic reaction behaviour during the DMA test. The epoxy properties were determined for the staggered composite based on the experimental results for the epoxy specimen at each frequency.

4.8.1 Boundary conditions and loading

A finite element model was constructed of the short beam reinforced with platelets to replicate the physical specimen shown in Figure 4.13. The boundary conditions were built to simulate the experiment, as shown in Figure 4.14. The clamped ends were simulated using fixed edges, as shown in Figure 4.21. Finite element commercial package ANSYS was employed to construct the staggered specimen. The mesh and contact details were as same as in Section 3.2.2.

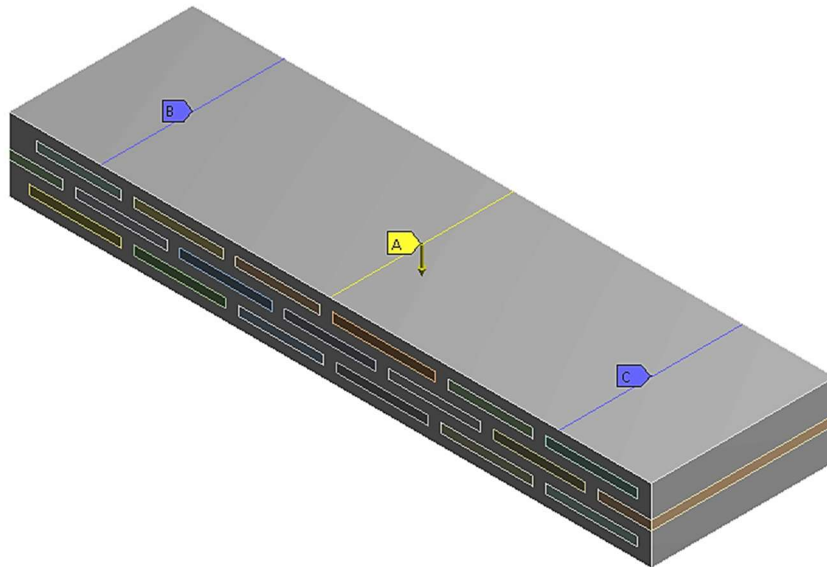
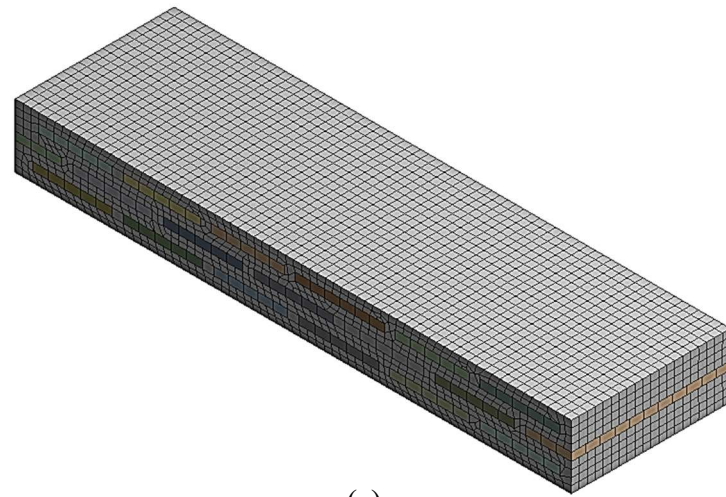
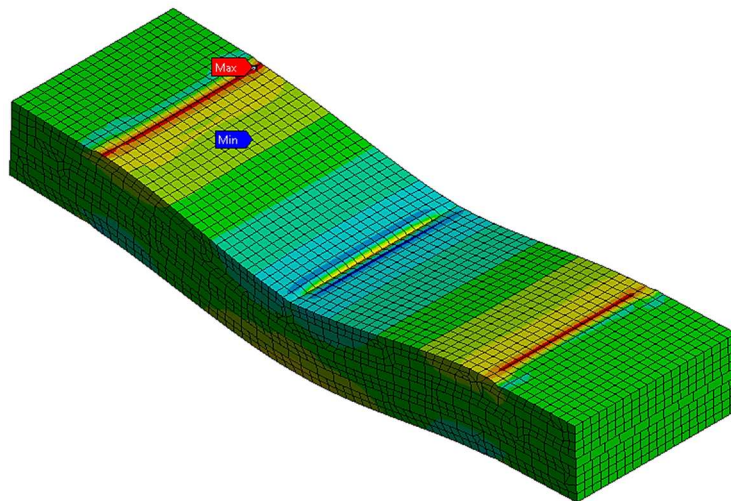


Figure 4.21: FE design, (B and C) sinusoidal displacement edges (A) face fixed support

The simulated three point bending test applied sinusoidal displacement of a maximum value of 0.02 mm at the middle of the specimen model. The beam experienced flexural displacement, as shown in Figure 4.22.



(a)



(b)

Figure 4.22: FE model (a) staggered model (b) dynamic three point bending deformation

4.8.2 Simulation results

The simulated DMA data were obtained from the numerical models for both the epoxy and the staggered configurations. The sinusoidal displacement of 0.02 mm was applied to the FE models of dynamic force response obtained during the simulation. The selected experimental and simulation load are shown in Table 4.5. The epoxy elastic modulus beam was provided to composite properties of simulation at each frequency. Then, the properties of the FE model correspond to the specimens in the test. As a result, the dynamic force response obtained from the FE simulation can be compared with the dynamic force obtained from the test.

Table 4.5: Comparison of the dynamic reaction

T °C	f Hz	E_v MPa	Dynamic reaction N	
			Experimental	FE
25	25	273.5	16.45	17.2
	50	313.8	17.97	18.6
	100	360.8	19.97	20.6
35	25	77	7.02	6.03
	50	98	8.49	7.4
	100	124.2	10.40	9.1
40	25	37.2	3.98	3.2
	50	48.2	5.06	4.07
	100	63.3	6.65	5.03
45	25	21.9	2.53	1.95
	50	27	3.23	2.44
	100	34.2	4.08	2.97
50	25	15.6	1.91	1.47
	50	18.3	2.19	1.7
	100	21.8	2.69	1.91
100	25	11.2	1.63	1.04
	50	11.3	1.62	1.03
	100	11.3	1.68	0.98

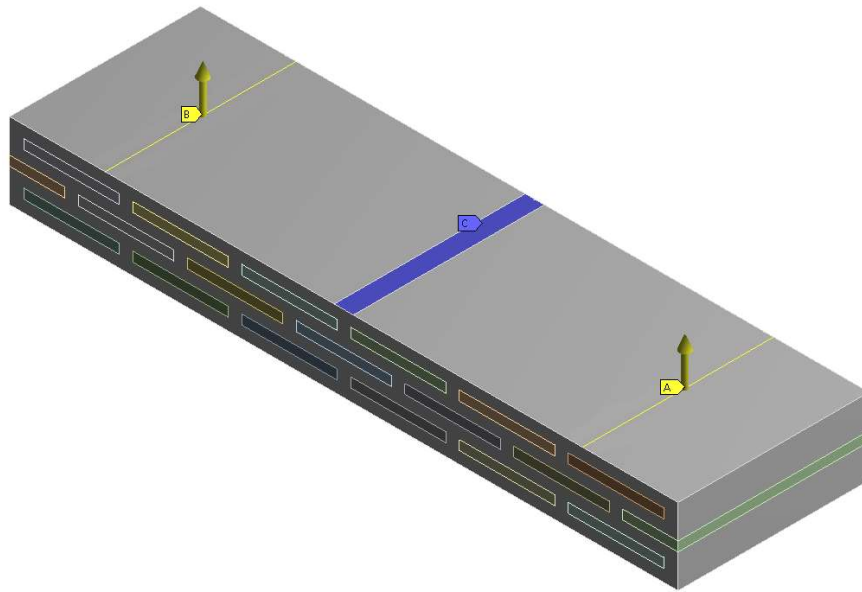
The dynamic force obtained from the FE simulation agrees well with the DMA test dynamic force reaction when the temperature is between 25 °C and 45 °C. At higher temperatures, the results appear to differ, with the model underpredicting the system stiffness. Close observation of the deformed shape, however, reveals that there is significant local deformation along the line restraint - something that would not happen in the physical experiment because the contacts are rollers.

To improve the accuracy of the FE model when the temperature between 45 °C and 100 °C, area support was designed with 2mm width as shown in Figure 4.23a. The reaction force results of the FE and experiment are shown in Table 4.6.

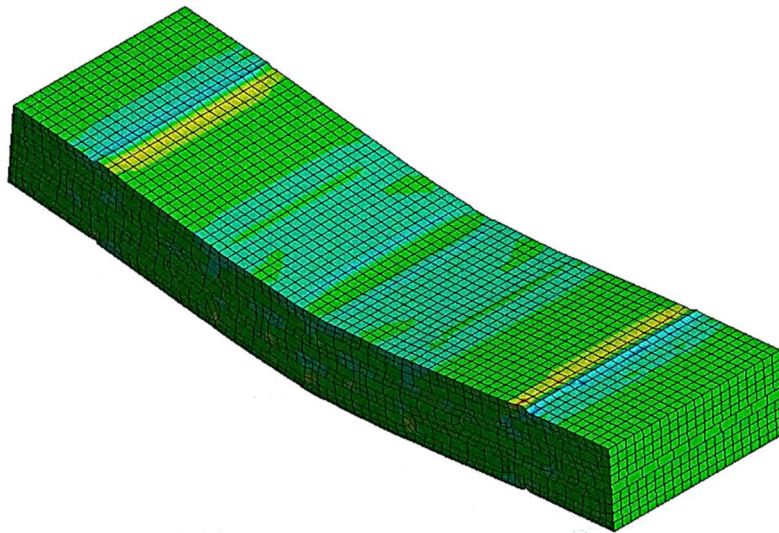
Table 4.6: Comparison of the dynamic reaction

T °C	f Hz	E_v MPa	Dynamic reaction N	
			Experimental	FE
45	25	21.9	2.53	2.4
	50	27	3.23	3
	100	34.2	4.08	3.8
50	25	15.6	1.91	1.8
	50	18.3	2.19	2.1
	100	21.8	2.69	2.5
100	25	11.2	1.63	1.43
	50	11.3	1.62	1.43
	100	11.3	1.68	1.43

As expected, the FE reaction force obtained with the 2 mm width supports is much closer to that seen in experiments. Also, the results agreed with the rubbery matrix material region (see Figure 4.19).



(a)



(b)

Figure 4.23: FE model (a) FE design (b) dynamic deformation for face fixed support

4.9 Comparison of analytical model with experiment

The effectiveness of the analytic model was considered with respect to the FE model in Chapter 3. This showed that the EBMM method produced equivalent stiffness values close to those from FE. The FE method was shown to be accurate through comparison with the experiment in Section 4.8. For completeness, this section compares the results from the analytic model with those from the experiment.

The work in this section compared the equivalent flexural modulus values between the experimental DMA results and the analytic results. A Matlab script was written the formula for clamped-clamped boundary conditions to calculate equivalent flexural modulus for the composite at all the temperatures and frequencies data in the test according to Equation 4.1,

When the temperature between 25 °C and 45 °C, the analytic equivalent flexural modulus agreed well with the experimental results, as shown in Table 4.7. Differences were found between the results when the temperature was between 45 °C and 100 °C

Table 4.7: Comparison of experimental and analytic equivalent modulus

T °C	f Hz	Experimental		Analytic
		E_v MPa	E_e MPa	E_e MPa
25	25	273.5	616.1	605.8
	50	313.8	678.4	691
	100	360.8	742.2	791
35	25	77	236.7	226
	50	98	288.5	287
	100	124.2	351	363.2
40	25	37.2	133.2	110
	50	48.2	166.8	142.44
	100	63.3	212.7	186.825
45	25	21.9	89.4	64.9
	50	27	107.1	80.1
	100	34.2	132	101.26
50	25	15.6	70.4	46.4
	50	18.3	80	54.34
	100	21.8	94.1	64.9
100	25	11.2	63.2	33.38
	50	11.3	63.5	33.5
	100	11.3	63.8	33.6

At higher temperatures, the analytic model underestimates the stiffness. This observation about the EBMM model is consistent with the comparisons with FE at the end of Chapter 3. However, some of this could be because the Poisson's ratio was not known and a value of 0.4 was assumed, although this would probably be higher at higher temperatures.

4.10 Conclusions

Four experiments have been conducted for the staggered composite beam a) three point bending test b) digital image correlation DIC c) free vibration test d) temperature and frequency dependency test. The conclusions obtained from the work in these experiments can be summarised in several conclusions as,

- The stiff platelets increased the flexural modulus of the staggered composite in comparison to the decrease relatively the loss factor values.
- The staggered composite is able to dissipate the energy under bending dynamic loading.
- Epoxy transition region gives an agreement results analytically, numerically, and experimentally where the temperature value less than 45 °C, while in the rubbery region, however, the analytical results underestimated the experimental stiffness the temperature between 45 °C and 100 °C
- The analytical model for the clamped-clamped beam is able to simulate the dynamic reaction behaviour during flexural sinusoidal displacement when the temperature value is between 25 °C and 45 °C.
- Although the changes in the boundary conditions when the temperature between 45 °C and 100 °C, the FE model for the beam is able to simulate the dynamic reaction behaviour during flexural sinusoidal displacement because the FE involved the boundary conditions changes.
- The behaviour of the composite can be predicted accurately using FE provided that boundary conditions and material properties (including Poisson's ratio) are available. The EBBM method also provides accurate predictions but over a limited range for the modulus ratio. The lower limit appears to be around 0.0002.

Chapter 5

Case study: vibration suppression of the swing mode of a fluid-filled tank

5.1 Introduction

This chapter involves a case study in which the staggered composite is employed to suppress vibration in a fluid-filled tank. Such tanks occur in many applications such as vehicles, ships, aircraft and rockets. High levels of vibration are undesirable for several reasons including agitation of the fluid, fatigue of the tank itself and the generation of noise. From a vibration perspective, the design has to consider the connection of the tank to the host structure and the inertia effects of the fluid, which are usually much higher than that of the tank itself.

Godderidge et al [118] noted that the lowest natural frequency of the sloshing modes of a fluid in an open rectangular tank is given by,

$$\omega_n^2 = \frac{\pi g}{a} \tanh\left(\pi \frac{b}{a}\right) \quad 5.1$$

where ω_n , a , b and g are first natural frequency, tank length in the direction of motion, liquid depth and the gravitational constant, respectively. Where sloshing modes coincide with vibration modes of the structure (including the mass loading from the fluid), significant vibrations can result.

The numerical simulation of sloshing for the fluid interaction can be designed using the volume fraction to estimate the fluid mixture properties. The results show that the inhomogeneous fluid is the appropriate model to apply for the simulation of sloshing. In this study, the system that was considered represented, in a simplified manner, the oil pan (or sump) in a large internal combustion engine. Vibrations of this component have been of considerable recent interest as they contribute significantly to powertrain noise generation. This has become particularly important in recent years as the move to lightweight components has increased susceptibility to vibration problems. Accordingly, different approaches have been taken to reduce vibration levels.

Rajendraprasad and Ravi [119] developed a methodology for increasing the oil pan stiffness. They generated an oil pan geometry for applying an optimisation with finite element software. Two conditions of loading were used, first, a static load to minimize the deflection, second, a harmonic response analysis to compute the natural frequencies and determine the mode shapes. Kamalakar and Prakash [120] also optimised a finite element model in order to reduce the noise of the oil pan arising from resonances occurring during various vibration conditions. Ramesh and Prashanth [121] developed a model of an oil sump and used it to evaluate frequency ranges where excitation was considered likely to occur. Liu et al [122] reduced the noise generated by a vehicle oil pan by applying an additional viscoelastic material. Madake and Hujare [123] compared constrained and free layer damping treatments for oil pans. The comparison showed that the constrained layer damping system was more effective.

While the previous work has focused on the modification of metal structures, a move to a polymeric construction could potentially reduce weight (much lower density material) and reduce resonant vibration (much higher inherent loss factor). While polymeric structures themselves vibrate less than equivalent metal ones, in this application, the presence of considerable inertial loading from the fluid may be significant. This chapter, therefore, reports a numerical study involving the evaluation of the effectiveness of the staggered platelet structure as a reinforcement for a fluid-filled tank. Additionally, because modelling each platelet requires a highly dense mesh, the accuracy of using homogenised properties was also considered.

5.2 Selection of the tank structure for the study

Godderidge et al [118] studied a container with length, height and liquid depth of 400, 200 and 120 mm, respectively. As these dimensions are of the same order as those seen on automotive oil pans, these basic dimensions were used for the work done here. For these dimensions, Equation 5.1 shows that sloshing modes are present from about 1 Hz upwards indicating that significant excitation can be expected even for the lowest frequency structural resonances. As a result, attention was focused on one of the lowest-frequency structural modes. This involved the side-to-side swinging of the entire tank and was selected because it would be one of the most challenging for a polymer-only solution from a vibration control perspective. Also, a wall thickness of 7 mm was used for the structure in order to maintain consistency with the work in earlier chapters.

5.3 Finite element model

Finite element (FE) models were constructed using ANSYS and comprised 3-D, 20-node quadratic hexahedral elements. Two meshes were used: in one, the polymer and platelets were modelled individually (in the same way as was done in Chapters 3 and 4) while in the other, homogenised properties from the EBMM method were used. The length of the edge of each element was approximately 1 mm. As the swinging mode only involved motion in one plane, for efficiency the model used only one element in the length direction of the tank. This resulted in a model length of 1 mm as opposed to the true length of 400 mm. The composite was represented using linear elastic material properties with Poisson's ratios of 0.3 for the steel platelets and 0.488 for epoxy. The viscoelastic material properties used in the composite was based on the experimental results obtained from Chapter 4. The density for steel was 7889 kg/m^3 , and for the epoxy was 1130 kg/m^3 .

5.4 Natural frequencies and mode shape

In this section, the natural frequencies and mode shapes were obtained from the numerical models of the tank.

5.4.1 Boundary conditions

Predictions were made for the swinging mode using the full composite and the equivalent homogeneous properties for different temperatures. For both models, results were obtained at temperatures of 25 and 40 °C. Mechanical properties for the polymer and composite were obtained from the experimental results presented in Sections 4.7 and 4.9. The tank was designed with the upper two edges clamped at the top by a fixed support boundary condition, as shown in Figure 5.1a. This was considered appropriate because in the oil pan is open at the top but fixed firmly to the base of the engine block, which in itself is very rigid.

The effect of the liquid was represented using distributed point mass elements. These were connected to the sides and base of the tank. The point mass values for the fluid were calculated to be equivalent to the total mass of fluid. The total value of point masses was 0.048 kg and the total mass of the composite model was 0.0215 kg. Along the base, each point mass value was 0.000012 kg. The interval between each points mass was 1 mm. The point mass value on the sides varied with a linear distribution between 0 to 0.000012 kg depending on the height from the free surface. The deformation shape for the first swinging mode is shown in Figure5.1b.

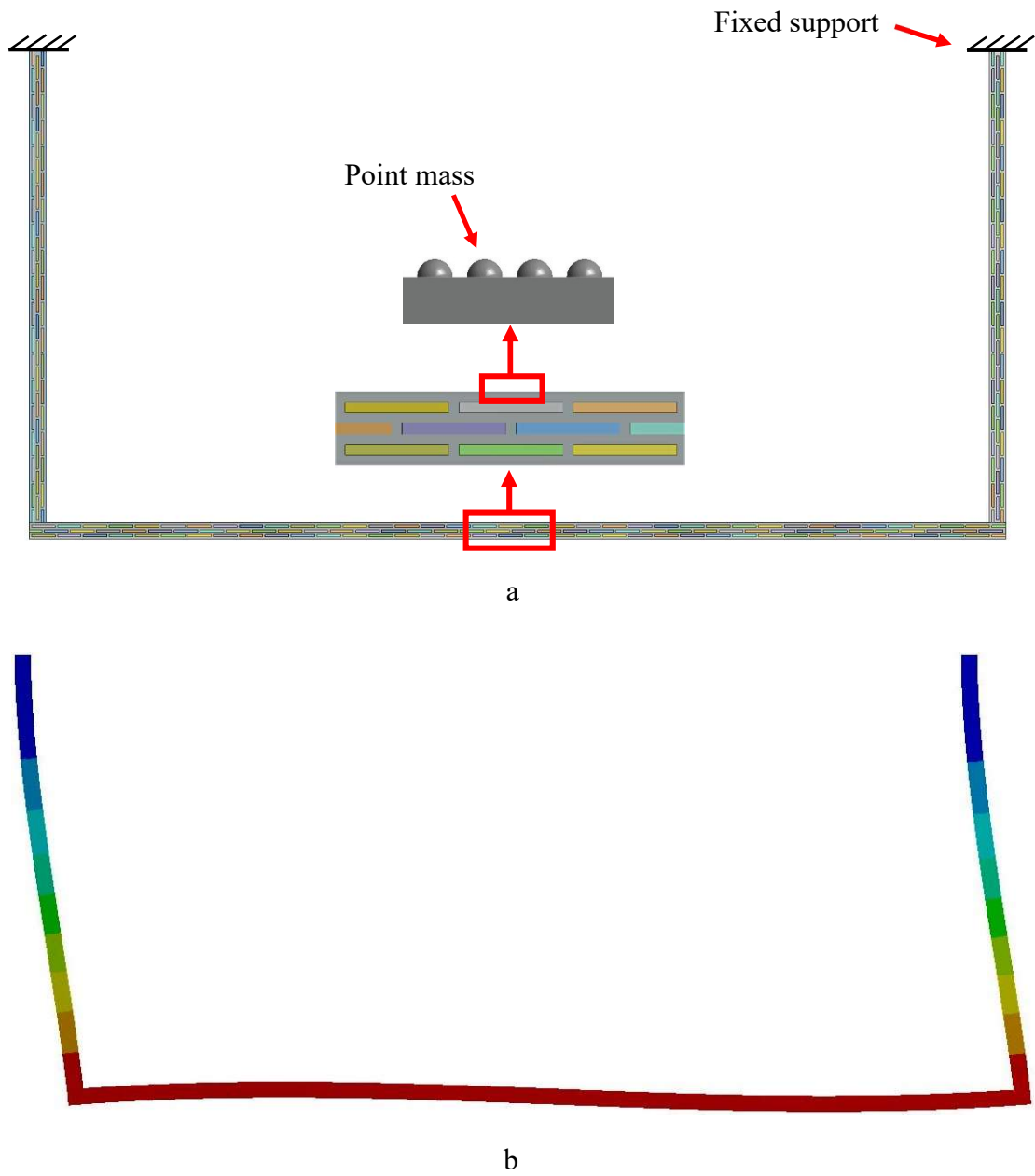


Figure 5.1: FE model for tank (a) undeformed model mesh (b) shape mode of the lateral swinging

5.4.2 Numerical results

The natural frequency was obtained from the numerical models for the matrix, composite and equivalent homogeneous material. The numerical results of the frequency with and without fluid loading are shown in Table 5.1. The results show that the natural frequency is reduced dramatically by the fluid load. Consequently, it can avoid the swing resonance with distribution load in the tank at different temperatures. Also, it can be seen that the equivalent homogenous FE model predicts similar natural frequency values to the fully defined composite. The slightly different natural frequencies (around 15%) between the two approaches are partially due to the modelling around the lower corners of the tank. Close inspection of Figure 5.1a shows that no reinforcing plates bend around the corners. On the contrary, the homogenised model assumes constant properties all the way around the bend.

Table 5.1: Natural frequency of tank swing

Material	T °C	E MPa	Without fluid load f_l Hz	With fluid load f_l Hz
Epoxy	25	114.9	6.0	1.9
	40	15.4	2.6	1.1
Composite	25	363.9	16.6	7.3
	40	63.9	4.8	3.0
Equivalent homogeneous	25	363.9	18.5	8.5
	40	63.9	4.3	3.3

5.5 Harmonic response numerical analysis

The amplitude of response to harmonic forcing was obtained using the numerical model of the tank. The damping ratio was provided to the numerical analysis depending on the loss factor and modulus at each temperature (see Figure 4.4) as,

$$\zeta = \frac{\eta}{2} \quad 5.2$$

Generally, the loss factor of the composite is less than the epoxy. However, the elastic modulus is significantly higher and therefore compensates for the reduction in damping. Also, the two temperatures considered were on the glassy side of the transition zone so an increase in frequency resulted in a movement away from transition and, therefore, a reduction in loss factor.

Forced response results for the configuration involving unreinforced polymer are shown in Figure 5.2. Response levels were calculated at 5 Hz intervals up to 40 Hz and also at the natural frequency itself. The swing applied force was 1 N. The amplitudes were obtained along a large coordinate range up to 100 mm or 450 mm. However, when the thickness increases to greater than 1 mm, the amplitude decreases 1/thickness times lower. As overall damping levels were relatively low, this approach ensured that the highest response was captured in each analysis run.

It can be seen that for the polymer alone, resonant response levels are high, and natural frequencies are low. Operation at the elevated temperature (approaching the glass transition for the epoxy) results in considerably higher peak responses. The increase in loss factor is not of any benefit as the reduction in stiffness is much more dramatic.

In comparison, results for the platelet-reinforcement composite are shown in Figure 5.3. It can be seen that response levels with the composite are much lower: by more than a factor of 10 at 25 °C and around a factor of 4 at 40 °C. It is noticeable that an increase in temperature does reduce performance.

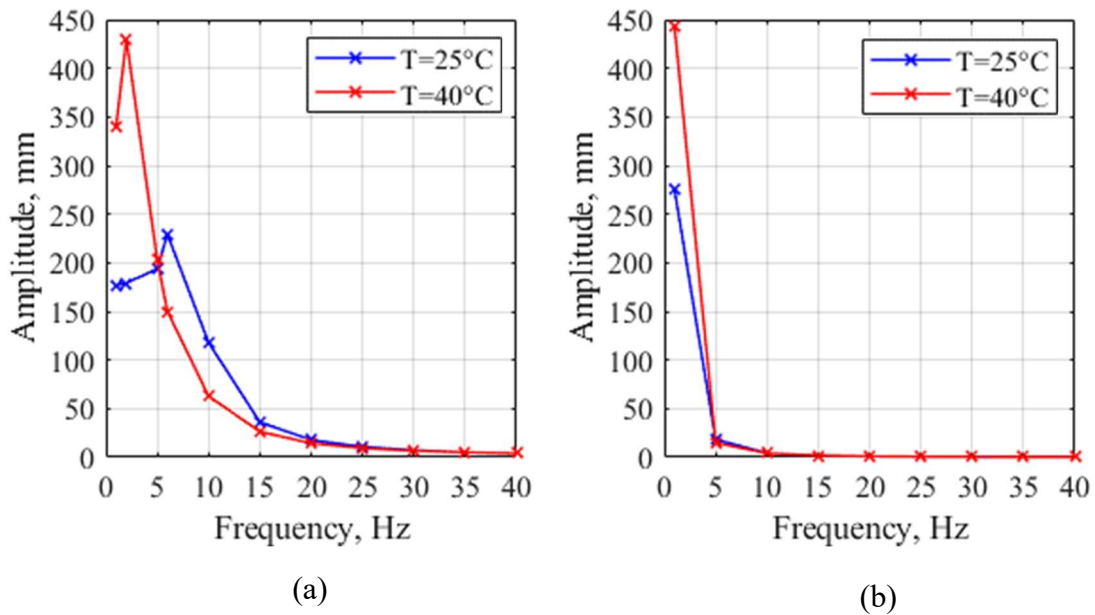


Figure 5.2: Frequency-Amplitude response for the epoxy model (a) without fluid load (b) with fluid load

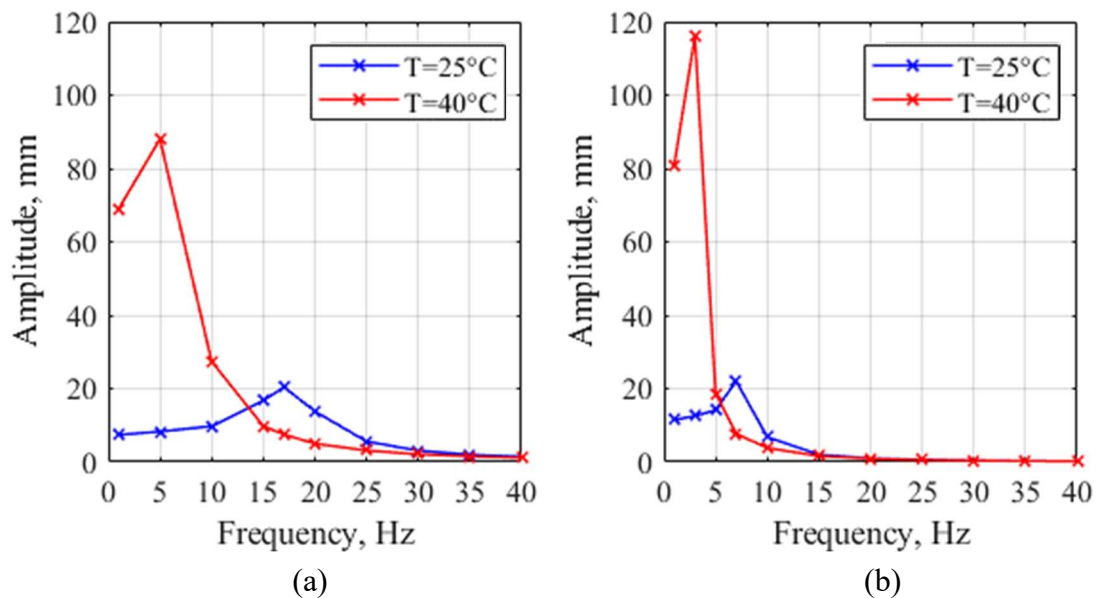


Figure 5.3: Frequency-Amplitude response for the staggered composite (a) without fluid load (b) with fluid load

Figure 5.4 shows the frequency responses for the full composite model and the model using homogenised properties.

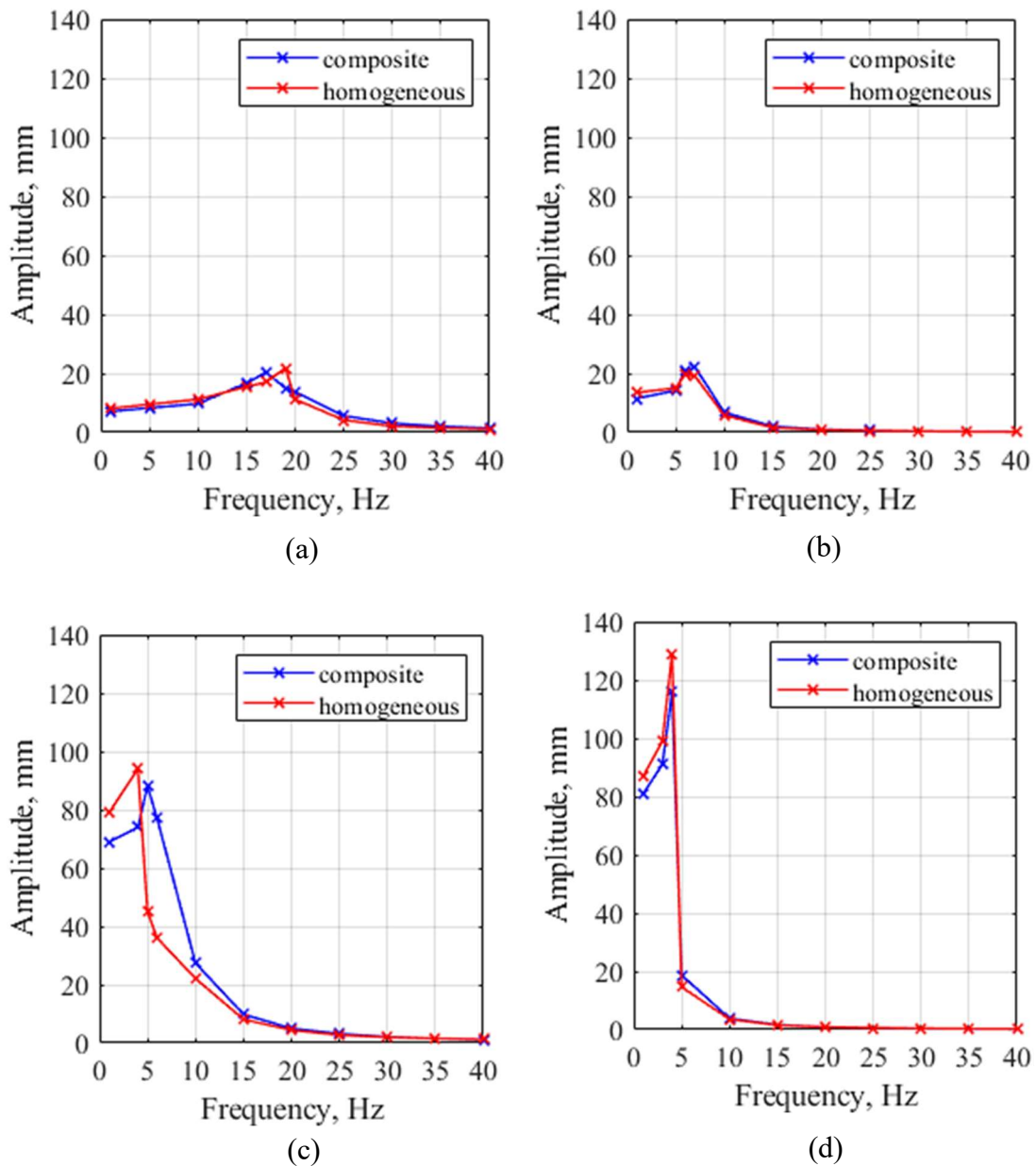


Figure 5.4: Amplitude-Frequency response for the composite and homogeneous model (a) $T=25^\circ\text{C}$ without fluid load (b) $T=25^\circ\text{C}$ with fluid load (c) $T=40^\circ\text{C}$ without fluid load (d) $T=40^\circ\text{C}$ with fluid load

The equivalent density and Poisson's ratio were calculated according to the formulas as,

$$\rho_h = r_p \rho_p + r_v \rho_v \quad 5.3$$

where ρ_h , ρ_p , ρ_v , and r_p are homogeneous density, platelet density, matrix density and platelet volume fraction, respectively.

$$v_h = r_p v_p + r_v v_v \quad 5.4$$

where v_h , v_p , v_v , and r_v are homogeneous Poisson's ratio, platelet Poisson's ratio, matrix Poisson's ratio and matrix volume fraction, respectively.

As mentioned earlier, the slight difference in stiffness is thought to arise from the platelet arrangement at each corner – see Figure 5.1a. In the full composite model, the arrangement of platelets diverges from the expected staggered arrangement and instead, a clear discontinuity is present. As a result, the homogenised property would overestimate the flexural stiffness of the corners, resulting in higher frequencies for this mode.

5.6 FE results and discussion

The frequency response obtained from FE for the staggered composite and equivalent homogeneous were compared together at 25 °C and 40 °C without and with fluid loading. Generally, there was an agreement in the response behaviour described by the different load and temperature conditions. As shown in Figure 5.4, the slight difference was due to inconsistent deformation at the corner of the tank for the staggered composite materials.

The frequency response for the staggered composite and equivalent homogeneous at 25 °C with and without fluid loading are shown in Figure 5.4a and 5.4b. Also, the equivalent frequency responses at 40 °C are shown in Figure 5.4c and 5.4d. Results for the heterogeneous and homogenised properties were in good agreement for the above conditions. This demonstrates that the FE homogeneous model is an adequate way to represent the staggered composite material properties.

Furthermore, the computational time cost are 2 seconds, 65 seconds and 360 seconds for the analytical, FE homogeneous and FE composite model, respectively. It can be seen that the MatLab analytical model decreases $2/360$ (0.55%) times lower, and the FE homogeneous model decreases $65/360$ (18%) times lower. Depending on the homogenised model, the FE design is not limited as the real composite. It can represent the structure as a single material allowing the use of efficient meshing including the use of shell or plate elements.

5.7 Conclusions from the case study

The conclusions that can be drawn from the numerical work considering the performance of the staggered composite in this chapter are listed below,

- The polymer alone provides reasonable vibration levels only when the system is cold, and there is no fluid load. It is inadequate as soon as fluid loads are considered.
- Adding the staggered platelets significantly increases stiffness without dramatically altering the loss factor, which results in a significant reduction in vibration levels. The significance of this finding is that it not only does it increase the vibration suppression ability of a polymer-based design, it allows the system to be operated closer to the transition temperature thereby increasing its operating range.
- The homogenised properties from the model developed in Chapter 3 can be used directly with reasonable accuracy. It opens up the possibility of achieving significant computational cost reductions. For example, a full 3D model of the staggered system would require a huge model (in terms of degrees-of-freedom) when applied to a large, realistic structure making it unattractive for system-level design studies. The homogenised model based on EBMM, however, is not limited in this way as the composite is represented in the structure as a single material, allowing the use of efficient meshing strategies including the use of shell or plate elements.

Chapter 6

Conclusions and future work

The aim of this thesis was to investigate the vibration behaviour of a sub-structured composite comprising stiff platelets arranged in a staggered formation within a viscoelastic matrix. The intended use of this composite was as a local reinforcement for a polymeric structure to combat flexural vibrations. The analytical solution that was developed provides the equivalent properties to estimate the flexural vibration response and provide a huge reduction in computational cost. The model has been shown to be accurate, and the sub-structured damper has been shown to be effective.

6.1 Findings by chapter

Chapter 2 showed that previous publications on laminated and staggered composites do not study the staggered composite under flexural or dynamic conditions. In this work, the polymer normal strain deformation effect between the platelets during flexural loading has been analysed in addition to its consequences for the composite stiffness.

The analytical models presented in Chapter 3 were formulated to estimate the equivalent mechanical properties. The analytical model is able to predict the resultant bending angle value of the soft-stiff composite that has zigzag strain behaviour. Three regions for strain behaviour with respect to the modulus ratio have been identified. First, the equivalent modulus can be obtained by the classic method of parallel and series springs that represent the parts of the unit cell. Second, the strain has a higher interlaminar slope as a zigzag behaviour. Third, the ratio of bending moment in the polymer to the bending moment in platelets is constant at a very low modulus ratio.

The analytical formulation solved the zigzag strain behaviour in the third region. Also, the Effective Bending Moment Method targeted the mechanism of resultant bending angle by locating the effective parts that give the resultant angle.

In Chapter 4, the behaviour of the staggered composite was studied experimentally. Free vibration and static loading tests were used to validate the analytical and numerical models at room temperature. Additionally, comparisons were also carried out at various temperatures and the models were shown to be accurate while the temperature remained in the glassy and transition zones.

Up to this point, a cantilever beam and three bending point tests had been employed to study the effective damping using staggered composite materials. In Chapter 5, the obtained effective properties from a simple cantilever were applied in a practical design for a particular application: to suppress lateral swinging vibrations in a liquid-filled tank with similar dimensions to an automotive oil pan. This is because it considers the most significant contributions to the resulting zigzag strain field that occurs across the thickness of such a structure. This was because equivalent stiffness could be increased dramatically at the cost of a slight reduction in loss factor. This work also showed that the equivalent properties obtained from the analytic model could be used directly in a homogeneous finite element model, significantly reducing computational costs.

6.2 Main conclusions of the research

The principal conclusions of this research are summarised below.

- The new analytical model (using EBMM) is able to predict the dynamic flexural modulus of a structure reinforced using staggered platelets at a modulus ratio less than 0.125 because the zigzag strain behaviour. This approach has been validated using finite element analysis and experiments.
- When subjected to flexure, the bending angle (and hence the deflection) is described by the zone between the ends of the outer platelets.

- When the modulus ratio for the staggered structure exceeds 0.125, the effective flexural modulus can be predicted by using a parallel/series spring approach. This is because the strain through the thickness is nearly linear.
- The flexural modulus and damping of the staggered composite when subjected to different conditions of free and excited vibration were investigated numerically and experimentally. It was shown that the flexural modulus was strongly affected by the staggered platelets, while the damping however, it was relatively affected.
- The increase in flexural stiffness caused by the addition of platelets is about ten times at temperature 25 °C, while it is about three times at temperature 45 °C because of the difference in modulus ratio.
- In the models analytical, numerical and experimental, the unit cell is under Timoshenko beam theory at effective matrix region between the external platelets ends.
- The composite stiffness depends on the frequency value (strain rate) in addition to the Poisson's ratio of the matrix material see (Table 3.2), (Table 3.3) and (Table 3.4).

6.3 Limitations of the work

This work in the thesis has several limitations that can be summarised as follows:

- The analytical model ignored the slight strain variation in the effective parts over the unit cell length.
- The boundary conditions applied for this work were three-point bending and cantilever configurations. However, the concept of effective flexural rigidity is independent of boundary conditions. Therefore, differences are expected to be slight.
- The accuracy of the analytical and numerical models was tested only up to the limit of matrix gap distance equal to the height of the platelets.
- The analytical model was designed for a very small modulus ratio and staggered composite.

6.4 Novelty

The principal contribution of this work was the analysis of flexural damping in a staggered unit cell to achieve simultaneously high stiffness and damping. This is the first study of a damping material that targets flexural vibrations and is constructed using staggered platelets that reinforce a polymer matrix. The model uses a unit cell that was divided into two categories of deformation, namely tension and shear. The equivalent modulus was constructed by considering both deformations, thereby estimating the bending angle that results from a) tension at matrix gaps between the outside platelets ends, and b) shear transfer between the central and outside platelets using the RKU approach. It was mentioned that the mechanism of the resultant bending angle comes from effective parts in the heterogenous staggered composite. These effective parts provide a new understanding for estimating equivalent properties under bending condition.

6.5 Recommendations for future work

The work in this thesis considered the reinforcement of a viscoelastic damping material with a stiff staggered configuration of steel platelets. Analytical models were introduced to describe and evaluate the equivalent rigidity in the unit cell composite. For future work, there are several recommendations listed below.

1. The end platelets in this study were rectangular. Extending the study in the future to include circular edges can be of interest to investigate the effect of this shape on the strain zigzag behaviour and equivalent composite properties.
2. The materials used in this study were epoxy matrix and steel platelets for convenience. Practically, there is no reason not to replace the steel with high-stiffness, lightweight platelets made from a material like carbon fibre. Such a change would not invalidate the assumptions in the modelling. Additionally, the matrix could be made from an entirely different material. For example, a practical

alternative would be to make the matrix from a thermoplastic which would offer interesting options for manufacture.

3. The success of the equivalent modulus estimation means that studies involving local reinforcement in areas of high dynamic strain can be carried out for relatively low computational cost. The advantages of such configurations would be that the heavier platelets would only need to be used where they were essential.
4. The EBMM represents a staggered unit cell. This method can be extended to the hierarchical composite made from a staggered pattern unit cell core (see Figure 2.11).
5. The study used symmetric staggered platelets to construct the sub-structure. Instead, asymmetric platelets could be used to construct one side staggered composite to investigate the equivalent mechanical properties and resulting damping levels. This configuration can change the composite response, which in turn would result in different damping levels and different analytical models addressing zigzag strain behaviour.
6. The model currently considers platelets that are bonded to the matrix. An interesting adaptation of this design would be to allow some slip. This could be achieved either by reducing adhesion between the platelets and the matrix or removing some of the matrix altogether. The advantage of introducing slip damping in addition to viscoelastic damping is that it is less sensitive to temperature, increasing the potential operating range of such a design.

Bibliography

- [1] J. Gryzagoridis, G. Oliver, and D. Findeis, “On the equivalent flexural rigidity of sandwich composite panels,” *Insight Non-Destructive Test. Cond. Monit.*, vol. 57, no. 3, pp. 140–143, 2015.
- [2] M. Hajianmaleki and M. S. Qatatu, “Mechanics of Composite Beams,” in *Advances in Composite Materials - Analysis of Natural and Man-Made Materials*, InTech, 2011, pp. 527–546.
- [3] M. Flores-Dominguez, “Modeling of the bending stiffness of a bimaterial beam by the approximation of one-dimensional of laminated theory,” *J. Eng. Res. Appl.*, vol. 4, no. 3, pp. 492–497, 2014.
- [4] A. S. Sayyad, Y. M. Ghugal, and N. S. Naik, “Bending analysis of laminated composite and sandwich beams according to refined trigonometric beam theory,” *Curved Layer. Struct.*, vol. 2, no. 1, pp. 279–289, 2015.
- [5] T. A. Vest and M. S. Darlow, “Dynamic modeling of linear beam-like structures using the equivalent beam stiffness method part I: Development and benchmarking,” *Mech. Syst. Signal Process.*, vol. 5, pp. 279–289, 1991.
- [6] S. Lenci and F. Clementi, “Effects of shear stiffness, rotatory and axial inertia, and interface stiffness on free vibrations of a two-layer beam,” *J. Sound Vib.*, vol. 331, no. 24, pp. 5247–5267, 2012.
- [7] S. Lenci, F. Clementi, and C. E. N. Mazzilli, “Simple formulas for the natural frequencies of non-uniform cables and beams,” *Int. J. Mech. Sci.*, vol. 77, pp. 155–163, 2013.
- [8] C. P. Chen and R. S. Lakes, “Analysis of high-loss viscoelastic composites,” *J. Mater. Sci.*, vol. 28, no. 16, pp. 4299–4304, 1993.
- [9] B. D. Agarwal, J. M. Lifshitz, and L. J. Broutman, “Elastic-plastic finite element analysis of short fibre composite,” no. 7, pp. 45–62, 1973.

- [10] Y. -S Chou and D. J. Green, "Silicon carbide platelet/alumina composites: III, toughening mechanisms," *J. Am. Ceram. Soc.*, vol. 76, no. 8, pp. 1985–1992, 1993.
- [11] C.-H. Hsueh, "A two-dimensional stress transfer model for platelet reinforcement," *Compos. Eng.*, vol. 4, no. 10, pp. 1033–1043, 1994, doi: 10.1016/s0961-9526(09)80005-1.
- [12] C. H. Hsueh, E. R. Fuller, S. A. Langer, and W. C. Carter, "Analytical and numerical analyses for two-dimensional stress transfer," *Mater. Sci. Eng. A*, vol. 268, no. 1–2, pp. 1–7, 1999, doi: 10.1016/s0921-5093(99)00129-x.
- [13] A. M. Fattahi and M. Mondali, "Theoretical study of stress transfer in platelet reinforced composites," *J. Theor. Appl. Mech.*, vol. 52, no. 1, pp. 3–14, 2014.
- [14] A. N. Norris, "The mechanical properties of platelet reinforced composites," *Int. J. Solids Struct.*, vol. 26, no. 5–6, pp. 663–674, 1990.
- [15] B. Glavinchevski and M. Piggott, "Steel disc reinforced polycarbonate," *J. Mater. Sci.*, vol. 8, no. 10, pp. 1373–1382, 1973.
- [16] M. Brodt and R. S. Lakes, "Composite materials which exhibit high stiffness and high viscoelastic damping," *J. Compos. Mater.*, vol. 29, pp. 1823–1833, 1995.
- [17] C. J. R. Verbeek and W. W. Focke, "Modelling the Young's modulus of platelet reinforced thermoplastic sheet composites," *Compos. Part A Appl. Sci. Manuf.*, vol. 33, no. 12, pp. 1697–1704, 2002.
- [18] S. P. Kotha, S. Kotha, and N. Guzelsu, "A shear-lag model to account for interaction effects between inclusions in composites reinforced with rectangular platelets," *Compos. Sci. Technol.*, vol. 60, no. 11, pp. 2147–2158, 2000.
- [19] P. Zhang and A. C. To, "Highly enhanced damping figure of merit in biomimetic hierarchical staggered composites," *J. Appl. Mech. Trans. ASME*, vol. 81, no. 5, pp. 3–7, 2014.
- [20] R. Lakes, "Materials with structural hierarchy," *Nat. J.*, vol. 361, pp. 511–515,

1993.

- [21] I. Jager and P. Fratzl, “Mineralized collagen fibrils: A mechanical model with a staggered arrangement of mineral particles,” *Biophys. J.*, vol. 79, pp. 1737–1746, 2000.
- [22] E. Carrera, “Historical review of zig-zag theories for multilayered plates and shells,” *Appl. Mech. Rev.*, vol. 56, no. 3, pp. 287–308, 2003.
- [23] H. Murakami, “Laminated composite plate theory with improved in-plane responses,” *J. Appl. Mech. Trans. ASME*, vol. 53, no. 3, pp. 661–666, 1986.
- [24] A. Toledano and H. Murakami, “A high-order laminated plate theory with improved in-plane responses,” *Int. J. Solids Struct.*, vol. 23, no. 1, pp. 111–131, 1987.
- [25] E. Carrera, “On the use of the Murakami’s zig-zag function in the modeling of layered plates and shells,” *Comput. Struct.*, vol. 82, no. 7–8, pp. 541–554, 2004.
- [26] T. Kant and K. Swaminathan, “Analytical solutions for the static analysis of laminated composite and sandwich plates based on a higher order refined theory,” *Compos. Struct.*, vol. 56, no. 4, pp. 329–344, 2002.
- [27] P. Vidal and O. Polit, “A sine finite element using a zig-zag function for the analysis of laminated composite beams,” *Compos. Part B Eng.*, vol. 42, no. 6, pp. 1671–1682, 2011.
- [28] L. Demasi, “Mixed plate theories based on the generalized unified formulation. Part I: Governing equations,” *Compos. Struct.*, vol. 87, no. 1, pp. 1–11, 2009.
- [29] L. Demasi, “Mixed plate theories based on the generalized unified formulation. Part II: Layerwise theories,” *Compos. Struct.*, vol. 87, no. 1, pp. 12–22, 2009.
- [30] L. Demasi, “Mixed plate theories based on the generalized unified formulation. Part III: Advanced mixed high order shear deformation theories,” *Compos. Struct.*, vol. 87, no. 3, pp. 183–194, 2009.
- [31] L. Demasi, “Mixed plate theories based on the generalized unified formulation.

- Part IV: Zig-zag theories,” *Compos. Struct.*, vol. 87, no. 3, pp. 195–205, 2009.
- [32] E. Santarpia and L. Demasi, “Large displacement models for composites based on Murakami’s zig-zag function, Green-Lagrange strain tensor, and generalized unified formulation,” *Thin-Walled Struct.*, vol. 150, no. 106460, pp. 1–18, 2020.
- [33] U. Icardi and A. Urraci, “Free and forced vibration of laminated and sandwich plates by zig-zag theories differently accounting for transverse shear and normal deformability,” *Aerospace*, vol. 5, no. 4, p. 108, 2018.
- [34] U. Icardi and A. Urraci, “Free vibration of flexible soft-core sandwiches according to layerwise theories differently accounting for the transverse normal deformability,” *Lat. Am. J. Solids Struct.*, vol. 16, no. 8, pp. 1–35, 2019.
- [35] U. Icardi, “Higher-order zig-zag model for analysis of thick composite beams with inclusion of transverse normal stress and sublaminates approximations,” *Compos. Part B Eng.*, vol. 32, pp. 343–354, 2001.
- [36] S. Kapuria, P. C. Dumir, and N. K. Jain, “Assessment of zigzag theory for static loading, buckling, free and forced response of composite and sandwich beams,” *Compos. Struct.*, vol. 64, no. 3–4, pp. 317–327, 2004.
- [37] M. di Sciuva, “Bending, vibration and buckling of simply supported thick multilayered orthotropic plates: An evaluation of a new displacement model,” *J. Sound Vib.*, vol. 105, no. 3, pp. 425–442, 1986.
- [38] R. C. Averill, “Static and dynamic response of moderately thick laminated beams with damage,” *Compos. Eng.*, vol. 4, no. 4, pp. 381–395, 1994.
- [39] R. C. Averill and Y. C. Yip, “Thick beam theory and finite element model with zig-zag sublaminates approximations,” *AIAA J.*, vol. 34, no. 8, pp. 1627–1632, 1996.
- [40] H. B. Coda, R. R. Paccola, and R. Carrazedo, “Zig-zag effect without degrees of freedom in linear and non linear analysis of laminated plates and shells,” *Compos. Struct.*, vol. 161, pp. 32–50, 2017.

- [41] A. Tessler, M. Di Sciuva, and M. Gherlone, “Refinement of Timoshenko beam theory for composite and sandwich beams using zigzag kinematics,” *Natl. Aeronaut. Sp. Adm.*, no. 215086, pp. 1–45, 2007.
- [42] A. Tessler, M. Di Sciuva, and M. Gherlone, “A refined linear zigzag theory for composite beams: reformulation of zigzag function and shear stress constraints,” in *VI International Symposium on Advanced Composites and Applications for the New Millennium, Corfu, Greece, 16-17 May, 2007*.
- [43] S. P. Timoshenko, “On the correction for shear of differential equations for transverse vibrations of prismatic bars,” *Philos. Mag. Ser.*, no. 41, pp. 744–746, 1921.
- [44] R. D. Mindlin, “Influence of rotatory inertia and shear deformation on flexural motions of isotropic elastic plates,” no. 18, pp. 31–38, 1951.
- [45] E. Reissner, “The effect of transverse shear deformation on the bending of elastic plates,” *ASME J. Appl. Mech.*, no. 12, pp. 69–77, 1945.
- [46] A. Tessler, M. Di Sciuva, and M. Gherlone, “A shear-deformation theory for composite and sandwich plates using improved zigzag kinematics,” in *Ninth International Conference on Computational Structures Technology*, 2008.
- [47] A. Tessler, M. Di Sciuva, and M. Gherlone, “A refined zigzag beam theory for composite and sandwich beams,” *J. Compos. Mater.*, vol. 43, no. 9, pp. 1051–1081, 2009.
- [48] A. Tessler, M. Di Sciuva, and M. Gherlone, “Refined Zigzag Theory for homogeneous, laminated composite, and sandwich plates: A Homogeneous limit methodology for zigzag function selection,” *Natl. Aeronaut. Sp. Adm.*, no. 216214, 2010.
- [49] A. Pagani, A. G. de Miguel, M. Petrolo, and E. Carrera, “Analysis of laminated beams via Unified Formulation and Legendre polynomial expansions,” *Compos. Struct.*, vol. 156, pp. 78–92, 2016.

- [50] L. Iurlaro, M. Gherlone, and M. Di Sciuva, “The (3,2)-Mixed Refined Zigzag Theory for generally laminated beams: Theoretical development and C0 finite element formulation,” *Int. J. Solids Struct.*, vol. 73–74, pp. 1–19, 2015.
- [51] M. Patni, S. Minera, R. M. J. Groh, A. Pirrera, and P. M. Weaver, “Efficient 3D Stress capture of variable-Stiffness and sandwich beam structures,” in *AIAA Scitech Forum*, 2019, no. 1763.
- [52] D. Versino, M. Gherlone, M. Mattone, M. Di Sciuva, and A. Tessler, “C0 triangular elements based on the Refined Zigzag Theory for multilayer composite and sandwich plates,” *Compos. Part B Eng.*, vol. 44, no. 1, pp. 218–230, 2013.
- [53] A. D. Nashif, D. I. G. Jones, and J. P. Henderson, *Vibration Damping*. New York: John Wiley and Sons, 1985.
- [54] D. Ross, E. E. Ungar, and E. M. Kerwin, “Damping of plate flexural vibrations by means of viscoelastic laminae,” *Struct. Damping, Am. Soc. Mech. Eng.*, pp. 49–87, 1959.
- [55] Michael J. Bateman, “Constrained viscoelastic layer damping of thick aluminium plates: design analysis, and testing,” United States Naval Academy, 1990.
- [56] B. D. Runyon, “The influence of boundary conditions and aspect ratio on approximate solutions for constrained layer damping treatments on beams and plates,” Wright State University, 2004.
- [57] S. Nakanishi, “Study on an estimation method for the loss factor of a dry laminated panel,” in *20th International Congress on Acoustics ICA*, 2010, pp. 1456–1463.
- [58] P. J. Torvik and B. D. Runyon, “Estimating the loss factors of plates with constrained layer damping treatments,” *AIAA J.*, vol. 45, no. 7, pp. 1492–1500, 2007.
- [59] K. S. K. Sasikumar, “Vibration control of beam with composite constrained layer treatment,” vol. 5, no. 2, pp. 176–184, 2015.

- [60] P. Y. H. Huang, P. G. Reinhall, I. Y. Shen, and J. M. Yellin, “Thickness deformation of constrained layer damping: An experimental and theoretical evaluation,” *J. Vib. Acoust.*, vol. 123, no. 2, pp. 213–221, 2002.
- [61] E. R. Marsh, “An integrated approach to structural damping,” Massachusetts Institute of Technology, 1994.
- [62] P. M. G. Belbute, “Study on the bending behavior of sandwich composite beams,” Instituto Superior Técnico, 2011.
- [63] R. A. DiTaranto, “Theory of vibratory bending for elastic and viscoelastic layered finite-length beams,” *J. Appl. Mech.*, pp. 881–886, 1965.
- [64] D. J. Mead and S. Markus, “The forced vibration of a three-layer, damped sandwich beam with arbitrary boundary conditions,” *Sound Vib.*, vol. 10, no. 2, pp. 163–175, 1969.
- [65] D. J. Mead and S. Markus, “Loss factors and resonant frequencies of encastré damped sandwich beams,” *J. Sound Vib.*, vol. 12, no. 1, pp. 99–112, 1970.
- [66] D. K. Rao, “Frequency and loss factors of sandwich beams under various boundary conditions,” *J. Mech. Eng. Sci.*, vol. 20, no. 5, pp. 271–282, 1978.
- [67] S. Uppal, “Discontinuous constrained-layer damping treatments applied to free-free beam,” Iowa State University, 1996.
- [68] J. M. Lifshitz and M. Leibowitz, “Optimal sandwich beam design for maximum viscoelastic damping,” *Int. J. Solids Struct.*, vol. 23, no. 7, pp. 1027–1034, 1987.
- [69] M. Hamdaoui, G. Robin, M. Jrad, and E. M. Daya, “Optimal design of frequency dependent three-layered rectangular composite beams for low mass and high damping,” *Compos. Struct.*, vol. 120, pp. 174–182, 2015.
- [70] K. K. Kumar, Y. Krishna, and P. Bangarubabu, “Estimation of loss factors of a constrained layer plate using viscoelastic layer,” *J. Mater. Des. Appl.*, vol. 229, no. 6, pp. 481–492, 2014.
- [71] Y. V. K. S. Rao and B. C. Nakra, “Vibrations of unsymmetrical sandwich beams

- and plates with viscoelastic cores,” *Journal Sound Vib.*, vol. 34, no. 3, pp. 309–326, 1974.
- [72] M. D. Rao, “Recent applications of viscoelastic damping for noise control in automobiles and commercial airplanes,” *J. Sound Vib.*, vol. 262, no. 3, pp. 457–474, 2003.
- [73] R. Lewandowski, A. Bartkowiak, and H. Maciejewski, “Dynamic analysis of frames with viscoelastic dampers: A comparison of damper models,” *Struct. Eng. Mech.*, vol. 41, no. 1, pp. 113–137, 2012.
- [74] R. U. H. Syed, M. I. Sabir, J. Wei, and D. Y. Shi, “Effect of viscoelastic material thickness of damping treatment behavior on gearbox,” *Res. J. Appl. Sci. Eng. Technol.*, vol. 4, no. 17, pp. 3130–3136, 2012.
- [75] F. Cortes and M. J. Elejabarrieta, “Structural vibration of flexural beams with thick unconstrained layer damping,” *Int. J. Solids Struct.*, vol. 45, no. 22–23, pp. 5805–5813, 2008.
- [76] S. A. Nayfeh, “Damping of flexural vibration in the plane of lamination of elastic-viscoelastic sandwich beams,” *J. Sound Vib.*, vol. 276, no. 3–5, pp. 689–711, 2004.
- [77] J. Meaud, T. Sain, G. M. Hulbert, and A. M. Waas, “Analysis and optimal design of layered composites with high stiffness and high damping,” *Int. J. Solids Struct.*, vol. 50, no. 9, pp. 1342–1353, 2013.
- [78] P. Grootenhuis, “The control of vibrations with viscoelastic materials,” *J. Sound Vib.*, vol. 11, no. 4, pp. 421–433, 1970.
- [79] M. Carfagni, E. Lenzi, and M. Pierini, “The loss factor as a measure of mechanical damping,” in *Proceedings of the International Modal Analysis Conference - IMAC*, 1998, vol. 3243, no. 1, pp. 580–584.
- [80] S. H. Crandall, “The role of damping in vibration theory,” *J. Sound Vib.*, vol. 11, no. 1, pp. 3–18, 1970.

- [81] J. C. Heine, "The stress and frequency dependence of material damping in some engineering alloys," Massachusetts Institute of Technology, 1966.
- [82] W. E. Baker, W. E. Woolam, and D. Young, "Air and internal damping of thin cantilever beams," *Int. J. Meek. Sci. Pergamon*, vol. 9, pp. 743-766., 1967.
- [83] R. Cherif, J. D. Chazot, and N. Atalla, "Damping loss factor estimation of two-dimensional orthotropic structures from a displacement field measurement," *J. Sound Vib.*, vol. 356, pp. 61–71, 2015.
- [84] K. F. De Lima, N. Barbieri, R. Barbieri, and L. C. Winniques, "Young's modulus and loss factor estimation of sandwich beam with three optimization methods by FEM," *Int. J. Comput. Appl.*, vol. 128, no. 3, pp. 35–43, 2015.
- [85] N. K. Mandal, R. A. Rahman, and M. S. Leong, "Experimental study on loss factor for corrugated plates by bandwidth method," *Ocean Eng.*, vol. 31, no. 10, pp. 1313–1323, 2004.
- [86] C. T. Sun, B. V. Sankar, and V. S. Rao, "Damping and vibration control of unidirectional composite laminates using add-on viscoelastic materials," *J. Sound Vib.*, vol. 139, no. 2, pp. 277–287, 1990.
- [87] J. M. Berthelot, M. Assarar, Y. Sefrani, and A. El Mahi, "Damping analysis of composite materials and structures," *Compos. Struct.*, vol. 85, no. 3, pp. 189–204, 2008.
- [88] K. M. Apalak, R. Ekici, M. Yildirim, and S. Erkaya, "Determination of structural damping and optimal vibration control of an adhesively-bonded double containment cantilever joint," *J. Adhes. Sci. Technol.*, vol. 23, no. 2, pp. 339–359, 2009.
- [89] M. S. Ewing, H. Dande, and K. Vatti, "Validation of panel damping loss factor estimation algorithms using a computational model," *AIAA J.*, pp. 1–30, 2009.
- [90] C. D. Johnson and D. A. Kienholz, "Finite element prediction of damping in structures with constrained viscoelastic layers," *AIAA J.*, vol. 20, no. 9, pp. 1284–

1290, 1982.

- [91] M. H. Tsai and K. C. Chang, “A study of the modal strain energy method for viscoelastically damped structures,” *J. Chinese Inst. Eng. Trans. Chinese Inst. Eng. A/Chung-kuo K. Ch’eng Hsueh K’an*, vol. 24, no. 3, pp. 311–320, 2001.
- [92] N. E. Kim and J. H. Griffin, “A special element approach for calculating the vibration response of adhesively bonded and composite structures,” *J. Sound Vib.*, vol. 170, no. 3, pp. 377–395, 1994.
- [93] J. A. Rongong, “Reducing vibration levels using ‘Smart Joint’ concepts,” in *Proceedings of IMSA 25, Noise and Vibration Engineering*, 2000, pp. 817–824.
- [94] G. Lepoittevin and G. Kress, “Optimization of segmented constrained layer damping with mathematical programming using strain energy analysis and modal data,” *Mater. Des.*, vol. 31, no. 1, pp. 14–24, 2010, doi: 10.1016/j.matdes.2009.07.026.
- [95] H. Koruk and K. Y. Sanliturk, “Optimisation of damping treatments based on big bang-big crunch and modal strain energy methods,” *J. Sound Vib.*, vol. 333, no. 5, pp. 1319–1330, 2014.
- [96] D. Lisitano, J. Slavič, E. Bonisoli, and M. Boltežar, “Strain proportional damping in Bernoulli-Euler beam theory,” *Mech. Syst. Signal Process.*, vol. 145, no. 106907, 2020.
- [97] L. J. Pan and B. M. Zhang, “A new method for the determination of damping in cocured composite laminates with embedded viscoelastic layer,” *J. Sound Vib.*, vol. 319, no. 3–5, pp. 822–831, 2009.
- [98] S. N. Goyanes, P. G. König, and J. D. Marconi, “Dynamic mechanical analysis of particulate-filled epoxy resin,” *J. Appl. Polym. Sci.*, vol. 88, no. 4, pp. 883–892, 2003.
- [99] A. Shabeer, A. Garg, S. Sundararaman, K. Chandrashekhara, V. Flanigan, and S. Kapila, “Dynamic mechanical characterization of a soy based epoxy resin

- system,” *J. Appl. Polym. Sci.*, vol. 98, no. 4, pp. 1772–1780, 2005.
- [100] S. Saseendran, M. Wysocki, and J. Varna, “Evolution of viscoelastic behavior of a curing LY5052 epoxy resin in the glassy state,” *Adv. Manuf. Polym. Compos. Sci.*, vol. 2, no. 2, pp. 74–82, 2016.
- [101] P. Canamero-Martinez, J. L. de la Fuente, and M. Fernandez-Garcia, “Master Curve and Time–Temperature–Transformation cure diagram of a polyfunctional epoxy acrylic resin,” *J. Appl. Polym. Sci.*, vol. 120, pp. 2166–2172, 2011.
- [102] D. Ratna, N. R. Manoj, L. Chandrasekhar, and B. C. Chakraborty, “Novel epoxy compositions for vibration damping applications,” *Polym. Adv. Technol.*, vol. 15, pp. 583–586, 2004.
- [103] Y. K. Kim and S. R. White, “Stress relaxation behavior of 3501-6 epoxy resin during cure,” *Polym. Eng. Sci.*, vol. 36, no. 23, pp. 2852–2862, 1996.
- [104] K. V Rao, G. N. Dayananda, and G. S. Ananthapadmanabha, “Viscoelastic characterisation of an epoxy based shape memory polymer (SMEP),” *Indian J. Adv. Chem. Sci.*, vol. 2, pp. 64–67, 2014.
- [105] H. Kishi, M. Kuwata, S. Matsuda, T. Asami, and A. Murakami, “Damping properties of thermoplastic-elastomer interleaved carbon fiber-reinforced epoxy composites,” *Compos. Sci. Technol.*, vol. 64, no. 16, pp. 2517–2523, 2004.
- [106] A. Katunin, W. Hufenbach, P. Kostka, and K. Holeczek, “Frequency dependence of the self-heating effect in polymer-based composites,” *J. Achiev. Mater. Manuf. Eng.*, vol. 1, pp. 9–15, 2010.
- [107] E. G. O. Filho, E. M. O. Lopes, and C. A. Bavastri, “Integrated dynamic characterization of thermorheologically simple viscoelastic materials accounting for frequency, temperature, and preload effects,” *Materials (Basel)*, vol. 12, no. 12, pp. 1–17, 2019.
- [108] R. S. Lakes, “The time-dependent Poisson’s ratio of viscoelastic materials can increase or decrease,” *Cell. Polym.*, vol. 11, pp. 466–469, 1992.

- [109] Q. Chen and K. Worden, “A decomposition method for the analysis of viscoelastic structural dynamics with time-dependent Poisson’s ratio,” *An Int. J. Exp. Mech.*, vol. 47, pp. 1–14, 2011.
- [110] S. SIM and K. J. KIM, “A method to determine the complex modulus and Poisson’s ratio of viscoelastic materials for FEM applications,” *J. of Sound Vib.*, vol. 141, no. 1, pp. 71–82, 1990.
- [111] J. Meaud and G. M. Hulbert, “Dependence of the dynamic properties of Voigt and Reuss composites on the Poisson ’ s ratios and bulk loss factors of the constituent materials,” *J. Compos. Mater.*, vol. 47, no. 26, pp. 3237–3247, 2012.
- [112] T. Pritz, “Frequency dependences of complex moduli and complex Poisson’s ratio of real solid materials,” *J. Sound Vib.*, vol. 214, no. 1, pp. 83–104, 1998.
- [113] T. A. Pritz, “Relation of bulk to shear loss factor of solid viscoelastic materials,” *J. Sound Vib.*, vol. 324, no. 3–5, pp. 514–519, 2009.
- [114] T. Pritz, “The Poisson’s loss factor of solid viscoelastic materials,” *J. Sound Vib.*, vol. 306, no. 3–5, pp. 790–802, 2007.
- [115] F. Allou, M. Takarli, F. Dubois, C. Petit, and J. Absi, “Numerical finite element formulation of the 3D linear viscoelastic material model : Complex Poisson ’ s ratio of bituminous mixtures,” *Arch. Civ. Mech. Eng.*, vol. 15, pp. 1138–1148, 2015.
- [116] S. Pandini and A. Pegoretti, “Time, temperature, and strain effects on viscoelastic Poisson’s ratio of epoxy resins,” *Polym. Eng. Sci.*, pp. 1434–1441, 2008.
- [117] S. Pandini and A. Pegoretti, “Time and temperature effects on Poisson’s ratio of poly(butylene terephthalate),” *Express Polym. Lett.*, vol. 5, no. 8, pp. 685–697, 2011.
- [118] B. Godderidge, S. Turnock, M. Tan, and C. Earl, “An investigation of multiphase CFD modelling of a lateral sloshing tank,” *Comput. Fluids*, vol. 38, no. 2, pp. 183–193, 2009.

- [119] B.Rajendraprasad and V. Ravi, "Design and structural optimization of oil Pan," *Int. J. Mag. Eng. Technol. Manag. Res.*, vol. 2, no. 2, pp. 671–677, 2015.
- [120] K. Kamalakar and T. S. Prakash, "Design optimization of oil pan using finite element analysis," *Int. J. Eng. Sci. Res. Technol.*, vol. 3, no. 12, pp. 335–341, 2014.
- [121] S. Ramesh and B. H. Prashanth, "Experimental modal analysis of passenger car engine oil pan using FEM and FFT analyzer," *Int. J. Res. Eng. Technol.*, vol. 06, no. 03, pp. 1–5, 2017.
- [122] A. Q. Liu, S. P. Lim, and S. T. Chow, "Statistical energy analysis on the damping effect of the oil pan on engine vibration," *Appl. Acoust.*, vol. 34, pp. 131–141, 1991.
- [123] S. B. Madake and P. P. Hujare, "Reduction of vibration response and noise of oil pan using constrained layer damping," *Int. Eng. Res. J.*, no. 2, pp. 5117–5119, 2015.